

MODELS OF CORONAVIRUS PATHOGENESIS AND IMMUNITY

Anne Elizabeth Beall

A dissertation submitted to the faculty of the University of North Carolina at Chapel Hill in partial fulfillment of the requirements for the degree of Doctor of Philosophy in the Department of Microbiology and Immunology.

Chapel Hill
2019

Approved by:

Ralph S. Baric

Mark T. Heise

Nat Moorman

Martin Ferris

Melinda Beck

Jason Whitmire

© 2019
Anne Elizabeth Beall
ALL RIGHTS RESERVED

ABSTRACT

Anne E. Beall: Models of Coronavirus Pathogenesis and Immunity
(Under the direction of Ralph Baric)

Coronaviruses, including Severe Acute Respiratory Syndrome Coronavirus (SARS-CoV), Middle East Respiratory Syndrome Coronavirus (MERS-CoV), and Porcine Epidemic Diarrhea Virus (PEDV) are important emerging viruses that are capable of producing sudden pandemic disease outbreaks with high morbidity, mortality, and economic losses in both animal and human populations. In this study, we aim to identify and understand cofactors of severe disease and immune response to infection, including physiological and genetic mechanisms that contribute to pathogenesis.

-

Porcine epidemic diarrhea virus is a highly pathogenic alphacoronavirus. To study the genetic factors that regulate pathogenesis and transmission, we developed a molecular clone of PEDV strain PC22A. Our data describe the development of a robust reverse genetic platform for identifying genetic factors that regulate pathogenic outcomes and transmission efficiency *in vivo*, providing key infrastructural developments for developing and evaluating the efficacy of live attenuated vaccines and therapeutics in a clinical setting.

-

Severe acute respiratory syndrome (SARS) is a highly lethal human respiratory disease caused by SARS-coronavirus (SARS-CoV), a virus family marked by increasingly frequent outbreaks, pre-emergent zoonotic viruses, and high mortality rates. Though immune responses to

SARS-CoV have been well studied, the role of B cells and antibody in early viral clearance and disease control is unclear. Our findings demonstrate an important role for B cell immunity in SARS-CoV clearance and support the use of early serum transfer and antibody treatment during future coronavirus outbreaks.

-

Obesity is a known risk factor for severe outcomes from respiratory virus infection. Increasing rates of obesity globally and ongoing CoV outbreaks demonstrate the need for investigation into the relationship between obesity and CoV disease. This study evaluates a diet induced obesity model of SARS-CoV infection in the conventional B6 diet induced obesity model. Additionally, diet induced obesity concurrent with SARS-CoV infection is evaluated in a recombinant inbred collaborative cross mouse model to compare the relative impacts of diet and genetics on SARS-CoV pathogenesis. Our findings underline the importance of host health and genetic variability on infectious disease pathogenesis, and point toward a need for increased research into complex host models of infectious disease.

DEDICATION

Dedicated to my parents, John and Heather Beall, the most supportive, loving, and estimable people that I have ever met.

ACKNOWLEDGEMENTS

First, I would like to acknowledge my lab - the Baric Lab - and the wonderful people that I had the pleasure of meeting there. Ralph was the best advisor that anyone could ask for, and patient beyond anything one could deserve. He gave me the freedom to explore and grow that has been invaluable to me in this work and in learning to be a scientist. At this moment, I am especially appreciative of his patience and kind heart. Boyd is the heart of the lab- none of this work, and none of my training, would be possible without him. Vineet mentored me and took me under his wing, for which I will always be thankful. He's also managed to keep in touch and send weekly emails to keep me on my toes, for which I am grateful, though he wouldn't know it. As mentors, Vineet taught me to be tough and honest with myself, Adam taught me confidence, and Tim taught me humility. Jake, Kara, and Jes are my best friends and kept me going every day, and I love them like family. They were my drive and strength whenever I needed them.

Heather has been my best friend and virology sister since the beginning of grad school, and I can't begin to say thank you enough to her. Heather is the best friend, coworker, and motivator that I could have ever asked for. I'm so excited to see what she'll do with her work. I would not have finished this document without her.

Matt loved me and had some strange kind of unwavering confidence in me for three years, and I love him so much for being with me through graduate school. And for everything else.

Kevin is my brother, my sounding board, and my calm at the end of the day. I am so lucky that I got to spend grad school with him.

Ray, Chris, Raulie, Charlie, Sarah, James, Duncan, Blake, Amelia – I don't think they know how much their involvement and friendship meant, but they were the ones that made my best days and evenings during graduate school. I would write so much more if this weren't already a deeply personal and embarrassing process. I love them all.

Andy, Kyle, and Peter back home, have, for over a decade, been my best friends and supports. They keep me sane. I will be lucky if I can keep them as my closest friends and confidants for the rest of my life. I plan to.

Lastly, I am beyond grateful to have my family. My dad is the person I relate the most closely to in the world, and is one of the most generous, kind, encyclopedically intelligent people that I've ever met. I'm so thankful for his advice and love. My mom is the person that I hope I can model after as I grow up – she is driven, compassionate, witty, and doesn't suffer fools. My sister is supportive and loving, and understands my inner world better than anyone. I have the great benefit of learning from her experience, and I am indebted to her for that. My brother is a wellspring of quiet, deep devotion and love that always surprises me, and who is always there when I don't know I need help. I wouldn't be the person that I am or have the support to pursue these studies without my family – I think they are the best family in the world, and I love them so much.

TABLE OF CONTENTS

CHAPTER 1: INTRODUCTION.....	1
1.1 Coronaviruses.....	1
1.1.1 Coronaviridae.....	1
1.2 Human Respiratory Coronaviruses	3
1.2.1 Severe Acute Respiratory Syndrome Coronavirus (SARS-CoV).....	3
1.2.2 Middle East Respiratory Syndrome Coronavirus (MERS-CoV).....	4
1.3 Zoonotic Coronaviruses	4
1.3.1 Porcine Epidemic Diarrhea Virus (PEDV).....	5
1.4 Pre-Emergent Coronaviruses.....	5
1.5 Models of Coronavirus Pathogenesis.....	7
1.5.1 Virus-side: Mouse-adapted coronavirus	7
1.5.2 Virus-side: Manipulating coronavirus genetics	9
1.5.3 Host side: Immune responses to coronavirus infection <i>in vivo</i>	11
1.5.4 Host-side: Transgenic mouse models	18
1.5.6 Host-side: Genetically diverse mouse lines: Collaborative-Cross.....	21
1.5.7 Host-side: Comorbidities and coronavirus infection	23
1.6 <i>Focus on Obesity as Respiratory Virus Comorbidity</i>	24
CHAPTER 2: CHARACTERIZATION OF A PATHOGENIC FULL LENGTH cDNA CLONE AND TRANSMISSION MODEL OF PORCINE EPIDEMIC DIARRHEA VIRUS STRAIN PC22A.....	27
2.1 Introduction	27
2.2 Results	31
2.2.1 Design of PEDV infectious clone.....	31
2.2.2 Recovery of Recombinant Viruses	33
2.2.3 Characterization of Recombinant Viruses	35
2.2.4 icPEDV replication and pathogenesis in gnotobiotic piglets.....	37
2.3 Discussion	38
2.4 Materials and Methods.....	43

CHAPTER 3: HUMORAL IMMUNITY IS REQUIRED FOR CLEARANCE OF SARS-CoV INFECTION	50
3.1 Introduction	50
3.2 Results	52
3.2.1 Activation of antibody-related networks is decreased during lethal SARS-CoV infection.....	52
3.2.2 B cell deficient mice are not able to clear MA15.....	53
3.2.3 Lack of antigen-specific CD4+ T cell responses results in delayed MA15 clearance.	58
3.2.4 Antigen-specific B cells are not required for SARS-CoV clearance.....	60
3.2.5 Convalescent serum at 7 days post infection can efficiently neutralize MA15 <i>in vitro</i>	62
3.2.6 Prophylactic transfer of early antibody protects from MA15 pathogenicity.....	64
3.3 Discussion	66
3.4 Methods.....	70
CHAPTER 4: RELATIVE IMPACTS OF DIET INDUCED OBESITY AND GENETICS ON SUSCEPTIBILITY TO SARS-CoV INFECTION IN THE MOUSE.....	79
4.1 Introduction	79
4.2 Results	83
4.2.1 Obesity Increases morbidity and mortality in the mouse model of SARS-CoV infection.....	83
4.2.2 Obesity impairs lung function and increases lung injury in SARS-CoV infection.....	86
4.2.3 Obesity impacts immune responses to SARS-CoV infection.....	86
4.2.4 Differential response in recombinant outbred mouse lines to high fat diet and SARS-CoV infection.....	87
4.3 Discussion	91
4.4 Methods.....	99
CHAPTER 5: SUMMARY AND FUTURE DIRECTIONS.....	106
5.1 The icPEDV system	106
5.2 Humoral Immunity in primary SARS-CoV infections	109
5.3 Diet Induced Obesity in the SARS-CoV mouse model and collaborative cross	115
5.4 Conclusion.....	118

REFERENCES 120

LIST OF TABLES

Table 1.1: Pathogenic Coronaviruses	6
Table 2.2: Description of Mouse lines used in Chapters 2 and 3	20
Table 2.1: Summary of PEDV replication and pathogenesis in Gn pigs	48
Table 2.2: Summary of IHC staining in infected pigs.....	49
Supplementary Table 3.1. Heat map genes in order of display in Figure 1	75

LIST OF FIGURES

Fig 1.0 Coronavirus Structure	2
Fig 1.1 SARS-CoV and MA15 infectious clone genome	11
Fig 1.2 Collaborative Cross Breeding Strategy and Genetic Variation of 9 Strains	22
Fig 2.1. Schematic of full length PEDV genome and construction of PEDV cDNA infectious clone and mutants	30
Fig 2.2 Growth of icPEDV clones isolated from <i>in vivo</i> small intestine samples	32
Fig 2.3 Confirmatory Studies of infectious clone PEDV virus.....	34
Fig 2.4 icPEDV mimics wtPEDV infection in gnotobiotic piglets	35
Fig 2.5 Histology and IHC staining of icPEDV infected pig intestine.	36
Fig 3.1 Bioinformatics points to an important role for B cells.....	53
Fig 3.2 B cells are required to clear SARS-CoV	57
Fig 3.3 B cell and antibody responses do not correlate with pathogenesis	59
Fig 3.4 Lack of antigen-specific CD4+T cell responses results in delayed SARS-CoV clearance	62
Fig 3.5 Prophylactic transfer of early antibody protects from MA15 pathogenicity	64
Fig 3.6 Prophylactic transfer of early antibody prevents mortality during lethal SARS-CoV infection through viral neutralization	65
Fig 4.1 Obesity increases morbidity and mortality in SARS-CoV infection	83
Fig 4.2 Obesity impairs lung function and increases lung injury in SARS-CoV infection	84
Fig 4.3 Chemokine and monocyte markers in the lung after SARS-CoV infection.....	85
Fig 4.4 SARS-CoV infection outcomes in 9 Collaborative Cross lines comparing high fat and control diets	89
SFig 4.1. Full Bioplex 23-Plex Cytokine and Chemokine Panel Analysis of High Fat and Control Diet MA15 or mock Infected C57BL/6J mice.....	103
SFig 4.2. Bioplex IFN Panel Analysis of High Fat and Control Diet MA15 or mock Infected C57BL/6J mice	104
S4.3. Lymphocyte and Monocyte flow cytometry panels of High Fat and Control Diet MA15 or mock infected C57BL/6J mice	105

LIST OF ABBREVIATIONS

AAM	alternatively activated macrophages
ACE2	angiotensin converting enzyme 2
APN	aminopeptidase N
ARDS	acute respiratory distress syndrome
BALF	bronchial alveolar lavage fluid
BCR	B cell receptor
BF	body fat
BSL	biosafety level
C	caecum
CC	collaborative cross
CD	cluster of differentiation
CD	control diet
CIG5	viperin
CoV	coronavirus
D	duodenum
DIC	dead in cage
DIO	diet-induced obesity
DMEM	Dulbecco's Modified Eagle Medium
DNA	deoxyribonuclease
DPC	days post contact
dpi	days post infection
DPP4	dipeptidyl peptidase 4

ds	double stranded
E	envelope
EC50	half maximal effective concentration
ELISA	enzyme-linked immunosorbence assay
ExoN	exonuclease
FACS	fluorescence activated cell sorting
G-CSF	granulocyte-colony stimulating factor
GM-CSF	granulocyte-macrophage colony-stimulating factor
Gn	gnotobiotic
GWAS	genome-wide association study
H&E	hemotoxalin and eosin
HAE	human airway epithelial cells
HEL	hen egg lysosyme
HFD	high fat diet
I	ilium
ic	infectious clone
IFIT3	Interferon-induced protein with tetratricopeptide repeats 3
IFITM1	Interferon-induced transmembrane protein 1
IFN	interferon
Ig	immunoglobulin
IHC	immunohistochemistry
IL	interleukin
IMM	inflammatory monocyte-macrophage
ip	intraperitoneal

IRF	interferon regulatory factor
ISG	interferon-stimulated gene
J	jejunum
KC	keratinocyte chemoattractant
LCA	leukocyte common antigen
M	membrane
MA15	mouse-adapted SARS-CoV passage 15
MAL	MyD88 adaptor-like
MCP-1	monocyte chemoattractant protein 1
MERS	middle east respiratory syndrome
MHC	major histocompatibility complex
MIP	macrophage inflammatory protein
MRI	Magnetic resonance imaging
MyD88	Myeloid differentiation primary response 88
N	nucleocapsid
Neo	neomycin
NF- κ B	nuclear factor kappa-light-chain-enhancer of activated B cells
nsp	non-structural protein
ORF	open reading frame
OVA	ovalbumin
PCR	polymerase chain reaction
PEDV	porcine epidemic diarrhea virus
PFU	plaque forming units
PRR	pattern recognition receptors

QTL	quantitative trait loci
RANTES	regulated on activation, normal T cell expressed and secreted
RFP	red fluorescent protein
RI	recombinant inbred
RIG-I	retinoic acid-inducible gene I
RLR	RIG-I like receptor
RNA	ribonuclease
RT	room temperature
rtPCR	real time PCR
S	spike
SARS	severe acute respiratory syndrome coronavirus
SDCV	swine delta coronavirus
SNP	single nucleotide polymorphism
SOCS	suppressor of cytokine signaling
ss	single stranded
STAT1	Signal transducer and activator of transcription 1
TBST	TRIS-buffered saline with Triton-X
TC	tissue culture
TCR	T cell receptor
TGEV	transmissible gastroenteritis virus
TLR	toll-like receptor
TNF	tumor necrosis factor
TRAM	translocating chain-associated membrane
TRIF	TIR Domain-containing Adaptor-inducing Interferon-B

UTR	untranslated region
VEE	Venezuelan equine encephalitis
VH:CD	jejunum villous height to crypt depth ratio
VRP	vaccine strain replicon particle

CHAPTER 1: INTRODUCTION

1.1 Coronaviruses

1.1.1 Coronaviridae

Coronaviruses are a species of virus belonging to the family *Coronaviridae* in the order *Nidovirales*. Within *Coronaviridae* and subfamily *Coronavirinae* there are 4 genera: *Alphacoronavirus*, including the highly virulent enteric virus, Porcine Epidemic Diarrhea Virus (PEDV); *Betacoronavirus*, including the lethal human respiratory outbreak viruses, Middle East Respiratory Syndrome Coronavirus (MERS-CoV) and Severe Acute Respiratory Syndrome Coronavirus (SARS-CoV); *Deltacoronavirus*, which primarily infects animals such as pigs and birds; and *Gammacoronavirus*, which primarily infects birds and whales (1). Data supports a distinction between the evolution of these genera, with *Alphacoronavirus* and *Betacoronavirus* likely evolving from a bat coronavirus source, while *Deltacoronavirus* and *Gammacoronavirus* likely evolved from an avian coronavirus gene pool (2).

Coronaviruses are enveloped, positive stranded RNA viruses with a large genome of approximately 30kb in length (Fig 1.0). *Coronavirinae* are spherical in shape, approximately 150nm in diameter, and marked by their spike structures extending from the virion; these spikes convey a crown appearance to the virion (hence, *Corona*) and are important in receptor binding during infection. The genome contains a 5' cap structure and a 3' poly (A) tail and can function as mRNA for translation of its replicase polyproteins. The 5' end of the genome contains a leader sequence and untranslated region (UTR) which contain the various stem loop structures required

for replication and transcription (3). Structural proteins common to coronaviruses include the Spike (S), Envelope (E), Nucleocapsid (N), and Membrane (M) proteins. A variety of luxury functions are encoded in Coronavirus genomes, which oftentimes function in innate immune evasion and pathogenesis, but are not essential for virus replication in cell culture. In addition, the 5' end of the genome encodes 2 large open reading frames which encode novel replicase, helicase and RNA modifying enzymes, essential for virus replication. Unique to Coronaviruses, the genome encodes an nsp14 exonuclease replicase protein responsible for increased replication fidelity- likely required for efficient large RNA genome maintenance and replication. Coronavirus replication itself is accomplished via full length and subgenomic negative strand RNA intermediates, which serve as templates for both genomic and sub-genomic, nested mRNA synthesis, which are a distinctive property of the virus order *Nidovirales* (3).

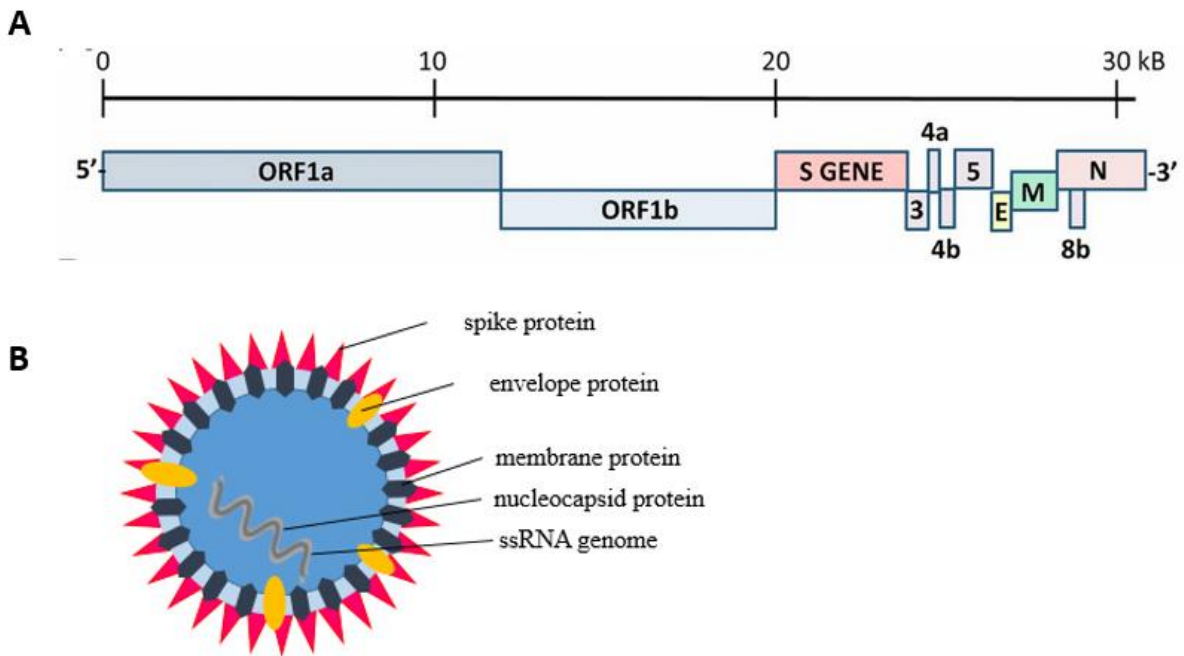


Fig 1.0 Coronavirus structure. Images adapted from *Scobey et al. 2013*. (A) Typical genetic structure of coronavirus, including the Spike (S), Envelope (E), Membrane (M), and Nucleocapsid (N) protein genes. (B) Typical structure of a coronavirus virion.

Coronaviruses infect species ranging from avian to mammalian, and span disease etiologies from a mild gastrointestinal upset to high mortality acute respiratory distress syndrome (ARDS). Many of the highly pathogenic coronaviruses, of note here PEDV, SARS-CoV, and MERS-CoV, are thought to have emerged from bat coronaviruses with or without an intermediate host species (2, 4-7). This is of import because, although coronavirus studies are focused primarily on the most pathogenic human outbreak viruses – namely, SARS-CoV and MERS-CoV – recent research has shown that pre-emergent zoonotic viruses are poised to colonize mammalian species (8, 9). As both population density and human development increase, these coronaviruses may be capable of causing devastating outbreaks in human or animal populations in the future.

1.2 Human Respiratory Coronaviruses

1.2.1 Severe Acute Respiratory Syndrome Coronavirus (SARS-CoV)

SARS-CoV is a highly pathogenic human respiratory virus that emerged in 2002-2003 in southern China, infecting over 8,000 individuals and killing 774. The mortality rate varies by age and comorbidity, but averages 14-15% according to the World Health Organization (10). Initial infection causes flu-like symptoms and may include fever, lethargy, cough, and other symptoms. If disease progresses to a severe state, individuals may develop ARDS, a disease marked by widespread inflammation in the lungs due to diffuse tissue injury to the bronchioles and alveoli (11, 12). ARDS is associated with a 20-50% mortality rate dependent on patient age and underlying medical condition (13). This was the first known large-scale outbreak of a highly virulent coronavirus in a human population. Though no human cases of SARS have been seen

since 2004, research into SARS and human coronaviruses has focused on efforts to better understand the virus, ARDS related pathogenic phenotypes, and possible treatment and vaccine modalities.

1.2.2 Middle East Respiratory Syndrome Coronavirus (MERS-CoV)

MERS is a viral respiratory infection likely spread from bats via a camel intermediary (7, 14). MERS causes a respiratory disease similar to that of SARS in humans, including ground glass opacity in lung scans, diffuse alveoli damage and hyaline membrane formation in lung pathology (15). MERS-CoV first emerged in 2012 and is currently circulating in the Middle East, and causes mortality at a rate of approximately 36% (16, 17). Currently, just over 2,200 human cases have been recorded. Human-to-human transmission has been less common than during the SARS-CoV outbreak, and generally requires close contact with an infected person (18, 19). More alarmingly, asymptomatic spread has been documented and the virus is capable of causing large outbreaks in other countries, like South Korea (20). Various treatments and vaccines are in development, though no MERS-specific treatments are currently available.

1.3 Zoonotic Coronaviruses

Coronaviruses are capable of causing disease in many commercially valuable farm and companion animals, including pigs (porcine epidemic diarrhea virus, transmissible gastroenteritis coronavirus), cows (bovine coronavirus), cats (feline coronavirus), dogs (canine coronavirus), chickens and turkeys (infectious bronchitis virus, turkey coronavirus) and other species (2, 21). For the purposes of this document, we will focus on PEDV and pre-emergent bat coronaviruses.

1.3.1 Porcine Epidemic Diarrhea Virus (PEDV)

PEDV is a porcine coronavirus which has circulated internationally for many decades, first described in Europe in the early 1980's. Though historically PEDV has not been a highly pathogenic agent, highly pathogenic strains emerged in Asia in the early 2,000's and have continued to cause sporadic but virulent outbreaks in present times (22). In 2013, a Hong Kong PEDV strain emerged in the United States when an outbreak occurred in Indiana (23). PEDV quickly spread through livestock herds and killed 10% of United States farm swine population within the first year (22). This strain, known as PC22A, is particularly virulent in nursing piglets, where up to 100% of piglets succumb to disease. Piglets showed weight loss, diarrhea, and severe lethargy, generally dying within the first week of infection. PC22A proved to be highly transmissible via the fecal-oral route and was quickly transmitted between farms and states (24). *In vivo*, PEDV infects epithelial lining the intestine and stomach of the pigs via the APN receptor (25). The outbreak proved to be highly lethal and devastating for the pork industry in the United States (26). Currently, three PEDV vaccines are available, two of which convey lactogenic immunity by passing on maternal antibodies from inoculated sows. These vaccines show significantly improved survival amongst piglets (27, 28). However, outbreaks are an ongoing issue, specifically in winter months or with naive generations of sows (29).

1.4 Pre-Emergent Coronaviruses

Recent studies have found SARS-like viruses isolated from bats that are “poised for human emergence.” In multiple studies, Menachery et. al. describe a cluster of bat coronaviruses, including SHC014-CoV and WIV-1-CoV, which are capable of binding, infecting, and

replicating in human cells (8, 9). In particular, SHC014-CoV binds the same angiotensin converting enzyme 2 (ACE2) receptor as SARS-CoV in human, civet, mouse and bat cells, replicates efficiently in primary human airway epithelial cells (HAE), and fails to be neutralized by anti-SARS monoclonal antibodies. These studies were the first to investigate the prepandemic potential of novel bat coronaviruses to infect primary human airway cells, and as such have increased awareness of possible zoonotic clusters of coronavirus pools capable of jumping into human populations (8, 9, 30, 31). These viruses also resist existing human monoclonal antibody treatments and experiment vaccines targeting epidemic SARS-CoV. Since this time, other pre-emergent SARS-like bat coronaviruses like WIV-1 and WIV-16 have been identified in bats, enforcing the concept of a readily available pool of bat coronaviruses that are capable of efficient replication in human lung tissues. These coronaviruses caution us of potential human outbreaks and show us the necessity of research into treatments for not only past, but pre-emergent coronaviruses.

Table 1.1: Pathogenic Coronaviruses

Coronavirus	Host	Model Organism	Receptor	Outbreak Year	Mortality	Symptoms
SARS-CoV	Human	Mouse	Ace2	2002	14-15%	Mild: flu-like symptoms, fever, cough, malaise. Severe: ARDS, severe lung damage, death.
MERS-CoV	Human	288-330 mouse, or other DPP4 mouse models	DPP4	2012	36%	Mild: flu-like symptoms, fever, cough, malaise. Severe: ARDS, severe lung damage, death.
PEDV	Pig	Gnotobiotic pigs	APN	2013 in U.S.	100% in piglets	Severe dehydration, diarrhea, weight loss, death.
SHC014-CoV, WIV-1	Bat	-	Ace2	<i>the future</i>	Unknown	Unknown

1.5 Models of Coronavirus Pathogenesis

1.5.1 Virus-side: Mouse-adapted coronavirus

Developing an appropriate animal model that replicates human disease is a first priority in researching viral pathogenesis. Small animal models, specifically, allow for reproducibility, statistically appropriate cohorts, and improved understanding of virus-host interactions and anti-viral treatments on a whole-organism scale. Small animal models of infectious disease have been invaluable to research and medical advancements. In the case of SARS-CoV and MERS-CoV, the response of the host immune system to infection is thought to be responsible for severe disease and death, as RAG1 and SCID mice do not develop lethal disease (32). An overactive immune response, infiltration of pro-inflammatory cells, and an influx of inflammatory cytokines and chemokines can lead to damage in the lung, prolonged disease, ARDS, and death (33, 34). The impact of immunity on CoV pathogenesis is further evidenced via human cases during the 2015 Korean MERS-CoV outbreak, wherein three immunocompromised patients exhibited atypical presentations of MERS resulting in prolonged viremia and disease (35). In one patient who had, previous to MERS infection, undergone autologous peripheral blood stem cell transplantation for B cell lymphoma, did not show symptoms of infection until 20 days after exposure, but succumbed to disease. A second patient who had undergone the same stem cell transplantation for T cell lymphoma survived disease, but, likely due to a suppressed immune system and use of corticosteroids, continued to shed virus a month after infection, even after symptomology had resolved. Because of the complexity of the anti-CoV immune response, it is important to study these respiratory viruses within a medically relevant host, ideally, a small animal model. A small animal model allows for nuanced understanding of an intact immune

system response to CoV infection, as well as targeted immune pathway manipulation, such as transgenic mouse models, in order to better study human disease.

In the years following the SARS-CoV outbreak, various mouse models were developed in transgenic, senescent, or otherwise immune compromised mice, which were capable of producing disease similar to human SARS infection. Importantly, in 2007, multiple mouse models of SARS-CoV infection were published, including a mouse-adapted SARS-CoV strain, MA15 (36-39). This strain was propagated by serial passaging SARS-CoV in mouse lungs 15 times, during which time the virus accumulated 6 coding mutations associated with adaptation and increased virulence (Fig 1.1). When these six mutations were then introduced into a SARS-CoV backbone using reverse genetics, the resultant MA15 recombinant virus was highly virulent and lethal in BALB/c mice, replicating human disease in an age-dependent manner. The importance of this development for the SARS coronavirus field is difficult to understate. Mouse adapted SARS-CoV allowed for the infection of fully immune competent, outbred, and transgenic mice of any genetic backbone; in-depth studies of host response in an immune competent host; and the ease, reproducibility, and access to reagents that comes with mouse research (40, 41). MA15s importance is further emphasized by the difficulties in generating a similar mouse-adapted virus for MERS-CoV infection.

Though several models have been generated for MERS-CoV, including camels, primates, and mice, early on most had failed to reproduce human disease symptoms (40-42). After the discovery and evaluation of human DPP4 as the MERS-CoV receptor and the failure of viral passage experiments to create an acceptable mouse adapted MERS-CoV strain, it became clear that defined mutations in the mouse DPP4 receptor prevented MERS-CoV receptor binding, entry and infection (43, 44). Consequently, researchers focused on altering the host DPP4

receptor in order to generate an appropriate mouse model, using transgenics or knockin strategies (44). In 2016, Cockrell et. al. successfully generated a CRISPR/Cas9 modified mouse that incorporated human DPP4 residues at position 288 and 330, allowing for successful MERS-CoV receptor binding and entry (45). These mice, when infected with an adapted MERS-CoV, develop a pathogenic MERS-CoV infection that accurately replicates human infection and disease pathologies. The development of new models has allowed for *in vivo* testing of anti-virals and vaccines, as well as fundamental insights into viral pathogenesis (46, 47). However, the requirement of a transgenic mouse model and adapted virus, as well as the relatively recent introduction of a pathogenic disease model, adds difficulty, time, and expense to MERS-CoV research. Therefore, the chapters of this document dealing with human coronavirus models are focused on SARS-CoV.

1.5.2 Virus-side: Manipulating coronavirus genetics

Virus-host interactions are traditionally studied via gene knockouts of either the host or viral genome. Though there are various methods for generating genetically modified virus, Boyd Yount was the first to segment the coronavirus genome into assembly plasmids for relatively easy generation and manipulation of transgenic SARS virus (48-55). Building infectious CoV requires surmounting obstacles inherent to the CoV genome including the large genome size (~30kb), regions of chromosomal instability, poor sequence stability in bacterial vectors, and the generation of stable genome-length RNA transcripts. To overcome these issues, in 2000 Yount et. al. described a method for breaking down the large CoV into smaller DNA segments subcloned into bacterial plasmid vectors (53). Each subclone could be manipulated and grown separately, allowing for decreased spurious mutations during cloning. Segments were flanked by unique class II restriction sites, which recognize a symmetrical sequence but leave a random 1-4

nucleotide “sticky end” (ie: BglII recognizes GCCnnnn_nGGC, with “n” denoting random nucleotides) (Fig 1.1). These unique restriction sites allow for seamless and directional joining of subgenomic fragments into a full-length DNA construct via simple enzyme digestion and ligation reactions (Fig 1.1) (53, 56). Additional alterations to the infectious clone include identification and ablation of fragment instability sites, addition of cytidine to agarose gels in order to reduce UV damage to genome fragments, and removal of putative T7 polymerase stop signals from the genome. These changes were necessary to build a full length DNA genome, and to successfully transcribe the full length RNA genome (53). Yount developed this method prior to the SARS-CoV outbreak in viruses such as TGEV and MHV, and was able to quickly convert the SARS-CoV, MA15, and MERS-CoV genomes into infectious clone systems used to generate recombinant viruses. This allowed for in-depth study of coronavirus genetics and the impact of coronavirus ORFs on replication and pathogenesis *in vivo* (8, 9, 45, 49-53, 55, 57-67). Additionally, Yount and Beall et. al. worked to create an infectious clone system for PEDV shortly after the U.S. outbreak, described here in Chapter 2 (48). The PEDV infectious clone is replication competent in gnotobiotic piglets and can be used as a resource for PEDV research and testing, as well as a genetic platform for studying PEDV virulence and transmissibility.

1.5.3 Host side: Immune responses to coronavirus infection *in vivo*

During the initial stages of CoV infection, virus is sensed as non-self via Pattern Recognition Receptors (PRRs), such as the Toll-Like Receptors (TLRs) and RIG-I-like receptors (RLRs), on the outer, endosomal, and cytosolic membranes of somatic cells (33). PRRs recognize immunogenic components of the virus itself or its replication intermediates. RLRs such as RIG-I and MDA5 recognize short nucleotide length viral motifs of dsRNA or ssRNA containing primarily 5'ppp-RNA or longer viral RNA motifs, respectively (61, 68, 69). TLRs recognize a wide variety of microbial and viral pathogen-associated molecular patterns (PAMPS) and signal through common pathways intermediates including MyD88, TRAM, TRIF, and MAL in order to induce IFN and antiviral responses (70). It is not known whether CoV signals through many of the TLRs, however, the use of transgenic mouse models has allowed for a better

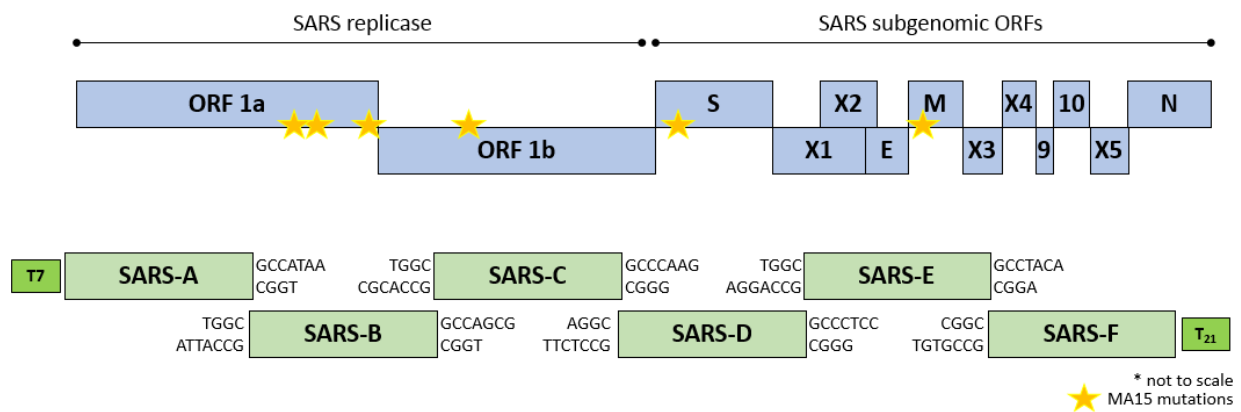


Figure 1.1. SARS-CoV and MA15 infectious clone genome. Images adapted from Yount, *J. Virol.* 2000 and Roberts, *PLoS Pathog.* 2007. Subcloning genome segments into bacterial plasmids allows for easy manipulation, including the addition of mouse-adaptation sites within the SARS-CoV genome (yellow stars). Fragmentation also reduces mutations and breaks up unstable genome segments. With the use of unique type II restriction *BglI* enzymes to generate overlaps, subgenomic fragments can be ligated seamlessly and directionally.

understanding of this viral recognition pathway. Sheahan et al. found that MyD88 was necessary for successful immune response to SARS-CoV infection – 90% of infected MyD88^{-/-} mice succumbed to MA15 infection when compared to B6 (immune intact) and Rag^{-/-} (lymphocyte

deficient) mice (71). MyD88 deficient mice also showed impaired interferon stimulated gene (ISG) transcription and cellular immune responses during infection, indicating that MyD88 is vital in the CoV recognition signal cascade. MyD88 is an intermediate for many TLRs, indicating a putative recognition of CoV by one or more TLRs. Totura et. al. expounded on this finding, using transgenic TLR3, TLR4, TRAM, and TRIF mouse models (72). Totura found that TLR3^{-/-}, TLR4^{-/-}, and TRAM^{-/-} mice all displayed increased weight loss and pathogenesis during MA15 infection, though none displayed the same robust increase in mortality seen in the MyD88^{-/-}. However, TRIF^{-/-} mice exhibited increased morbidity, mortality, and proinflammatory cytokine and immune cell populations in the lung during infection, indicating a definitive TLR involvement in SARS-CoV recognition, and a vital role for the TRIF intermediate in the CoV recognition and interferon induction pathway.

The initial activation of PRRs begins a signaling cascade, initiating the innate immune response to CoV infection. PRR signaling in infection leads to the activation of transcription factors IRF3, IRF7, and NF-κB (33). IRF3 and 7 initiate transcription of IFN α and IFN β , both of which are potent CoV antivirals (33). NF-κB alternately mediates transcription of proinflammatory cytokines such as IL-6 and IL-8. Interestingly, despite the importance of IFN signaling pathways in CoV pathogenesis, the IFN Type I, II, or III receptors are not required for survival of infection (73). Both IFN α /b receptor knockout and IFN γ receptor knockout mice lost weight and recovered similarly to wildtype mice during MA15 infection, indicating, surprisingly, that these receptors likely play a minor role in SARS-CoV pathogenesis individually (63). However, the use of a triple IFN receptor knockout would better confirm these findings. Each of these IFN receptors signals through STAT1 as an important intermediary in the IFN signaling pathway. MA15 infected STAT1^{-/-} mice succumbed to infection and showed high viral titer,

severe lung damage, and 100% mortality. STAT1^{-/-} mice also showed dissemination of virus beyond the lung into the liver, spleen and other tissues after day 9, indicating a role for STAT1 in the prevention of viral dissemination throughout the host. This finding may provide insight into the mechanisms of systemic viral dissemination in human SARS-CoV patients - a study of 19 fatal SARS-CoV patients used histological staining and rtPCR to identify SARS-CoV throughout patients' bodies, including in the lung, intestine, lymph nodes, spleen, liver, and other organs (74).

Some roles of IFN in CoV infection have already been stated – however, the reality of IFN as an inflammation-modulating signaling protein is more complex. SARS-CoV both hides from and inhibits IFN signaling early in infection (63, 75), presumably to defend itself from IFN's potent anti-CoV characteristics. IFN will readily inhibit CoV replication *in vitro*, and will prevent disease when administered *in vivo*, resulting in rapid loss of viral titer and reduction of disease (76). However, IFN can also be a strong stimulator of pathogenesis in CoV infection. Cameron et al. analyzed SARS-CoV patient IFN and ISG expression data, finding that abnormal adaptive and innate immune responses in severe SARS patients correlated with IFN-mediated immunopathology (77). Patients at the peak of illness showed a signature of high IFN and ISG expression – patients with good outcomes resolved IFN responses at this time and switched to an adaptive immune gene expression profile. However, patients with poor outcomes continued to express high IFN, ISG, and proinflammatory cytokine gene expression levels. This finding is similar to Rockx et. al., wherein lethal and non-lethal models of SARS-CoV infection in young and aged mouse models were used to compare inflammatory gene expression markers and identify early markers of lethal disease (78). Proinflammatory markers strongly upregulated in lethal, as opposed to non-lethal, infection and included IL6 and SOCS1/3, as well as a panel of

interferon-signaling related transcripts. Both Cameron and Rockx point to a strong association of IFN upregulation and increased SARS-CoV pathogenesis.

The dual protective and pathogenic roles of IFN in SARS-CoV infection are perhaps best explained by Channappanavar et.al., wherein relative pathogenicity of IFN is temporal (76). Channappanavar finds that a robust early IFN response or early IFN treatment reduces viral titer, reduces immune inflammation, and results in mild clinical disease *in vivo*. Antithetically, preventing all IFN signaling via an IFNAR^{-/-} mouse infection has the same effect – no IFN response means that no overactive immune response occurs, immunopathology is prevented, and disease is mild. However, a delayed IFN response, as is often seen in SARS-CoV infections, leads directly to enhanced disease, lung immunopathology, lethal pneumonia, and a dysregulated inflammatory monocyte-macrophage (IMM) response. Channappanavar finds that in severe infection, dendritic cell derived IFN stimulates IMMs recruited to the lung, where they release inflammatory mediators resulting in a feedforward loop of increased IMM influx to the lung, overactive inflammation, and severe lung immunopathology. IMM additionally reduce effector T cell responses via IFN-mediated T cell apoptosis, further preventing viral clearance and disease resolution. Depletion of IFN or IMM both function to abrogate disease. In this model, IFN contributes to an overactive and pathogenic M1, or inflammatory, polarized monocyte population (76).

Page et al. argues that instead it is a M2, or Th2 skewed, pathogenic monocyte population that causes SARS-CoV immune pathology. In a follow up STAT1 publication, Page et. al. found that alternatively activated macrophages (AAM) and Th2 cytokines (IL-4, IL-13) are upregulated in the lung during MA15 infection of STAT1^{-/-} mice (79). Using a bone marrow chimera to generate STAT1^{-/-} specific to macrophage and monocyte lineages, Page found that this selective

knockout produced similar disease to STAT1^{-/-} mice in pathology, but not in weight loss and mortality. This phenotype was complemented, in that severe lung disease is eliminated when AAMs are inhibited. However, both the presence of pathogenic AAMs and the elimination of lung disease seen with inhibition of AAMs are within a STAT1^{-/-} deficient mouse or monocyte population and a Th2 skewed immune environment. Page et. al. notes that the pathogenic nature of AAMs may not be in their dysfunctional IFN signaling, but in their role in an alternate STAT1-dependent host protection pathway, with a deficiency leading to increased lung injury and fibrosis. It is likely, based on the sum of these studies, that it is the ability to effectively signal and transition from anti-viral pro-inflammatory state to an anti-inflammatory wound healing state that is vital for control of immune pathogenesis in the lung.

The cellular immune response to SARS-CoV infection has been characterized through many thorough studies. Studies of human data have focused on patient outcomes, disease progression, and viral clearance (11, 12, 80-82). Patients develop ARDS associated with neutrophilia, lymphopenia, and prolonged proinflammatory cytokine expression. Using the MA15 model of infection, these patient symptoms and disease outcomes are mirrored in the mouse model (33, 37, 63, 76, 78, 79, 83-91). Innate immune cells such as macrophages and dendritic cells are often the first responders to viral infection, where they are able to sequester viral antigen, activate immune cells, phagocytose dead and dying cells, or secrete inflammation-regulating cytokines and chemokines (86, 92).

Lymphocytes are also vital during primary SARS-CoV infection. Comprehensive and methodical studies into the role of T cells in primary SARS-CoV infection have been published by the Perlman lab as well as others (76, 85, 86, 88-90, 93). T cells are shown to activate the pro-inflammatory state of the lung post-infection by secreting antiviral cytokines, chemokines, and

cytotoxic molecules (86). In a study of 1 year-post infected SARS-CoV patients, CD8+, or effector, T cells, primarily excreted of IFN γ , TNF α , MIP1a, and MIP1b when activated by SARS peptides. CD4+T cells tended to secrete IFN γ , TNF α , and IL-2 (94, 95). Notably, the frequency of “polyfunctional” CD4+T cells, or T cells secreting multiple cytokines, were more common in patients who had experienced severe disease (94, 95). This phenomenon is also seen in MERS-CoV infection, in which patients with severe disease exhibit a more highly active CD4+T but not CD8+T cell response (96).

During acute infection, the initial anti-viral T cell response triggers subsequent cellular responses such as increased antigen presentation, inhibition of viral replication, and direct killing of SARS-CoV infected cells; in this way, T cells directly contribute to viral clearance and control (86, 88, 90). T cells and dendritic cells also excrete IFN in response to CoV infection, which both directly inhibits CoV replication and initiates the transcription of ISGs. ISGs function in regulating the innate immune response to infection and can act as antivirals, but may also function as part of the pathogenic immune hyper-responsiveness seen in severe CoV patients (e.g. ISGs CIG5, MXA, IFITM1, and IFIT3, are induced during infection and persist at high levels in patients who succumbed to SARS infection) (33).

B cells are primarily studied in secondary viral infections for their role in antibody development and secretion. In SARS-CoV infections, patients generate high titers of anti-SARS immunoglobulin G (IgG) antibody in the months following infection, indicative of a protective adaptive B cell response (81, 97-99). However, antibody responses are highly variable in both SARS and MERS patients. During initial infection, a cohort of SARS patients were tested for anti-SARS-CoV neutralizing antibody titer after hospitalization. Interestingly, patients who mounted a strong neutralizing antibody response against SARS-CoV within the first two weeks

of infection were far more likely to be severe SARS cases when compared to those patients who did not generate a neutralizing antibody response until 3 or more weeks after infection (98). Similarly, in a cohort of MERS-CoV patients, high anti-MERS-CoV antibody neutralization titers following infection correlated directly with severe MERS cases. CD4+T cells, the helper T cells tasked with activating B and other immune cells, from these patients were also hyperactive and polymorphic (96). In both of these cases, a highly active humoral immune response correlated with severe disease, pointing to either a general hyper-stimulation of immune cell responses, or, a possible compensatory mechanism for viral control in the case of severe coronavirus infection.

While potent infection leads to a robust antibody response in patients, mild or moderate infections can result in a loss of CoV- specific circulating antibody. SARS-CoV patients tested 1 year post infection still showed virus-specific antibodies, but IgG titers were waning, and the majority of patients showed no anti-SARS-CoV antibody titers 6 years after infection (81, 97). In a study of confirmed South Korean MERS-CoV patients 1 year after infection, memory T cell responses were still functional against MERS-CoV, but antibody response varied depending on the severity of infection –severe disease correlated with retaining anti-MERS-CoV after 1 year, whereas mild disease correlated with a total loss of MERS-CoV specific antibodies. Patients who had experienced severe infection all had some level of MERS-CoV serum antibodies (100). However, patients who had experienced mild or moderate disease often retained no notable serum antibody against MERS-CoV. Though early B cell activation in CoV has not been studied, it is apparent that B cell activation and subsequent antibody secretion is dependent on disease severity or viral titer. Understanding whether hyper antibody responsiveness is a side effect of or compensatory mechanism for severe CoV infection would be valuable to better understand anti-

CoV immune responses. These low or non-existent antibody responses also allow for the possibility that traditional antibody-screening for potential CoV-infected patients may vastly underestimate the total number of CoV cases, missing patients with mild to moderate CoV pathology. Additionally, this may leave patients at risk for a secondary CoV infection. Understanding, and possibly strengthening, the humoral immune response in CoV patients may lead to better protection against subsequent CoV infections.

During acute infection, the role of B cell and antibody responses to SARS-CoV has not been exhaustively researched. In Chapter 3, we explore the role of early B cell and antibody responses in MA15 infected mice. Herein, we describe a vital role for antibody in timely viral clearance from the lung, as well as a protective role of early serum antibody against mortality.

1.5.4 Host-side: Transgenic mouse models

With any pathogenic virus, the genetics and lifecycle of the virus itself only partially accounts for disease outcomes. Host dynamics also impact disease outcomes, via cellular factors, innate immunity, and immune cells that contribute to prevent injury and clear virus. In the case of coronaviruses, the host response is thought responsible for the disease state, and so it is necessary to study the role of host factors that contribute to severe disease outcomes (76, 77, 101).

Since the advent of transgenic mouse models, knockouts and transgenic mice have become a common and robust tool in disease research (102, 103) as evidenced by the many transgenic lines used in the findings of the previous section. In the context of coronavirus-host interactions, gene knockouts have been vital in researching coronavirus pathogenesis as well as the host immune response to coronavirus infection. The findings in this document make use of a mixture of transgenic, knockout, and wild-type mice in order to investigate the role of anti-viral

lymphocytes and antibody in SARS-CoV clearance and recovery within the first week of infection. All mouse models used in this thesis are described Table 2.2 below.

Table 2.2: Description of Mouse lines used in Chapters 2 and 3

Mouse Line	Background	Description	Literature Reference
C57BL/6J	C57BL/6J	Most widely used inbred strain of mouse.	(104)
muMT	C57BL/6J	<i>Ighm</i> null. Homozygous mutant mice lack mature B cells. There is no expression of membrane-bound IgM, although some B cells may be produced using a C gene other than <i>mu</i> .	(105)
OTI	C57BL/6J	Transgenic inserts for mouse Tcr α -V2 and Tcr β -V5 genes. The transgenic T cell receptor was designed to recognize ovalbumin peptide residues 257-264 (OVA257-264) in the context of H2Kb (CD8 co-receptor interaction with MHC class I). This results in MHC class I-restricted, ovalbumin-specific, CD8 ⁺ T cells (OT-I cells). That is, the CD8 T cells of this mouse primarily recognize OVA257-264 when presented by the MHC I molecule.	(106)
OTII	C57BL/6J	Mice express the mouse alpha-chain and beta-chain T cell receptor that pairs with the CD4 co-receptor and is specific for chicken ovalbumin 323-339 peptide in the context of I-Ab (CD4 co-receptor interaction with MHC class II). This results in CD4 ⁺ T cells that primarily recognize ovalbumin peptide residues 323-339 when presented by the MHC class II molecule.	(107)
Rag ^{-/-}	C57BL/6J	A 1356 bp genomic fragment of the Rag1 gene was replaced by a Neo cassette. RAG-1-deficient mice have small lymphoid organs that do not contain mature B and T lymphocytes. The arrest of B and T cell differentiation occurs at an early stage and correlates with the inability to perform V(D)J recombination.	(108)
HELMET	C57BL/6J	Mice carrying the IghelMD4 transgene recognize HEL - B cells are specific for HEL and the mice fail to produce virus-specific antibody responses. More than 90% of B-cells in the spleen are derived from the transgene and are predominantly IgM and IgD	(109, 110)
Diet Induced Obesity C57BL/6J	C57BL/6J	Normal genetic background. Susceptible to obesity through high fat diet.	(111)
CC012, CC061, CC041, CC030, CC003, CC001, CC035, CC046, CC010	Mixed recombinant inbred lines	Recombinant inbred strains derived from outbreeding parental strains: A/J, C57BL/6J, 129S1/SvImJ, NOD/ShiLtJ, NZO/HiLtJ, CAST/EiJ, PWK/PhJ, and WSB/EiJ.	(112)

1.5.6 Host-side: Genetically diverse mouse lines: Collaborative-Cross

The response to infectious disease in humans is largely dependent on a complex set of traits and genetics inherent to the individual infected. However, when studying viral infections, science is limited to the resources that are readily available to study *in vivo* disease – namely, inbred mouse lines. These inbred mice are ideal for reproducibility and understanding the bases of disease progression and pathogenesis, as well the aspects of pathogenesis unique to each virus species. However, these inbred lines lack the genetic complexity and diversity seen in human populations that account for variation in disease susceptibility within a population (112, 113).

To this end, the Complex Trait Consortium generated the Collaborative Cross (CC), a large panel of recombinant inbred (RI) mouse strains designed to mimic the genetic variability seen in humans (112, 113). To generate this panel, 8 founder lines of mice (A/J, C57BL/6J, 129S1/SvImJ, NOD/LtJ, NZO/HILtJ, CAST/EiJ, PWK/PhJ, and WSB/EiJ) were crossed to each other in a funnel design through multiple generations in order to create a genetically outbred series of mouse lines, containing various genome admixtures of each parent (~13%)(Fig 1.2). Once the susceptibility alleles of the 8 founders were scrambled in each funnel, mice were backcrossed through 20 generations to create ~80+ inbred mouse lines derived from these 8 founder strains. The recombinant inbred (RI) lines allow for fully sequenced inbred lines, but still offer high genetic variability between lines. CC mice can be used in the study of complex traits or diseases in order to study phenotypes across genetically disparate lineages of mice, or to map quantitative trait loci (QTLs) associated with a given phenotype (114, 115). The CC is therefore an ideal resource for understanding and mapping the impact of genetics on disease severity, and in this case, the relative impact of comorbidity and genetics on SARS-CoV pathogenesis. In recent authoritative papers, Gralinski et. al. mapped SARS-CoV susceptibility

alleles in the CC lines, elucidating the mechanism of one such susceptibility allele, *Ticam2*, that regulated weight loss and disease severity (116, 117). These studies serve as an example of the possibilities of viral pathogenesis studies in the CC, as well as the future of research in viral-host dynamics.

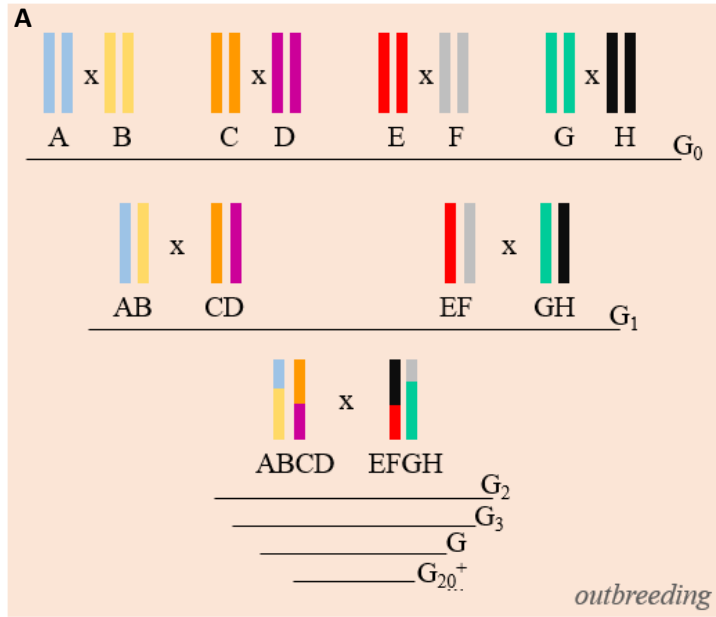
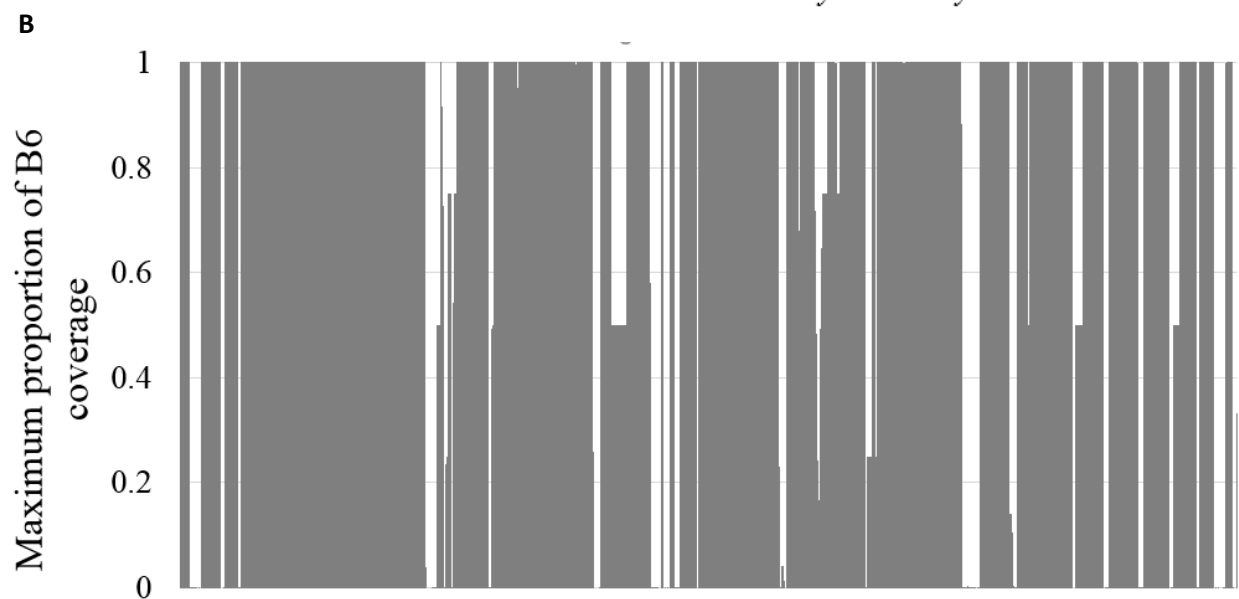
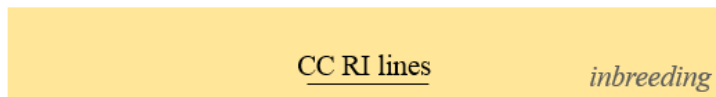


Fig 1.2. Collaborative Cross Breeding Strategy and Genetic Variation of 9 Strains. (A)

Breeding strategy for CC lines. Eight founder lines were bred via “funnel breeding” through >20 generations to develop >100 recombinant mouse lines. These lines were then sibling bred through multiple generations to develop recombinant inbred lines (<100 lines due to failure to thrive in many inbred lines). (B) Image of genome coverage of B6 haplotypes based on haplotype mapping by the 9 CC strains used in this study. 1=full B6 genome coverage amongst the CC 9 lines. 0= no genome coverage amongst the CC 9 lines. *Haplotype analysis done by Dr. Martin Ferris.*



1.5.7 Host-side: Comorbidities and coronavirus infection

The host influence on viral pathogenesis is not limited to genetic variability. Just as the complexity of human genetics is a determinant of disease outcome, an individual's personal health and disease state can impact viral pathogenesis and patient outcomes. In the case of SARS-CoV, increasing age is one of the primary predictors of disease severity and mortality. Mortality rates approach 50% in individuals over 65 years old (11, 12, 80, 85, 118-121). Age-correlated disease severity has been documented in studies of human patients and has been replicated in the MA15 mouse model of infection. Immune senescence is a well-documented phenomenon. The drivers of immune senescence are in debate, and may include chronic CMV infection, increased adiposity with age, or decreased production of sex steroids (122, 123). No matter the cause, immune senescence is marked by tissue damage, production of reactive oxygen species, and release of cytokines that result in a chronic pro-inflammatory state. This chronic inflammation leads to suppression of the immune response during acute viral infection.

In the respiratory tract, immune senescence is marked by aberrant functioning of neutrophils, monocytes, and dendritic cells. Additionally, T cells show a higher ratio of memory to naïve T cell populations, leading to poor responsiveness to new antigens. T cells also show dysfunction in proliferation, cytokine production, and cytotoxicity during acute infections (124). Studies of SARS-CoV in the context of host age have revealed that immune transcripts, cytokine and chemokine responses, and oxidative stress responses all vary with age and impact host disease progression. By studying age as a comorbidity of infection, possible treatments of SARS-CoV infected patients have been discovered, such as the inhibition of phospholipase A2 (85); contrastingly, the aged model proved previously proposed treatments to be detrimental, such as

finding that the doubly inactivated SARS-CoV vaccine strain increased disease susceptibility in the aged population (64, 85, 125).

Other comorbidities, such as type II diabetes and sex have also been identified in SARS patients (12, 126). In the case of MERS-CoV, comorbidities are proving to be an even more important determinant of disease outcomes (127, 128). In patients presenting with MERS, 86% of fatal cases had a comorbid illness, while just 42% of recovered or asymptomatic patients had a comorbidity. Comorbidities important for MERS patient outcomes include diabetes, chronic kidney or heart disease, and obesity (19, 129-131). Despite patient data, very few models exist to study the impact of comorbidities on CoV pathogenesis. Understanding viral infections in a medically relevant context will likely require a better understanding of the interactions between comorbidities, viral pathogenesis, and patient outcomes.

1.6 *Focus on Obesity as Respiratory Virus Comorbidity*

Obesity is a promising candidate for coronavirus comorbidity studies. First, >30 body mass index, metabolic syndrome, type II diabetes, and other obesity-related conditions significantly increase the risk of mortality in human coronavirus patients (19, 129-131). Secondly, around the world, and in the Middle East particularly, obesity rates are increasing; in 2017 in Saudi Arabia, 52% of adults are considered obese (132). Lastly, obesity causes chronic inflammation, impaired respiration, insulin resistance, and dysfunctional immune regulation, all of which can exacerbate a respiratory viral infection and have been shown to increase severity and mortality in ARDS patients (133).

Recent studies into obesity as a comorbidity have informed influenza pathogenesis research (134-136). In human influenza infections, obesity is a risk factor for prolonged hospital stays and poor outcomes in severe infection (137, 138). *In vivo* studies of influenza pathogenesis

in the high fat diet mouse model have replicated this phenotype. O'Brien et. al. found that obesity predisposed mice to impaired wound healing during influenza infection, with increases in bronchial alveolar lavage fluid (BALF) and protein concentration in BALF increased in obese infected mice (139). These findings are evidence of increased fluid permeability in the lungs – in essence, a more severe ARDS phenotype - and lack of lung repair after influenza injury. Additionally, infiltrating immune cells such as neutrophils, monocytes, T cells, and NK cells remained in the lung for more days after infection in obese mice suggesting that obesity impaired recovery and elongated the proinflammatory phase of infection.

Milner et. al. compared the lung metabolome during influenza infection between lean and obese mice, and reported glucose, insulin, adiponectin, and leptin levels in mice (135, 140). The study determined that obesity was directly linked to increased morbidity and mortality when accounting for diet, and determined large differences in metabolomics profiles in the lungs of lean versus obese mice. These and other studies have begun to elucidate the relationship of respiratory virus infections and obesity as a comorbidity in the context of influenza infection. Obesity-associated respiratory damage phenotypes are likely to apply in the context of other respiratory infections.

In Chapter 4, we focus on new animal models of emerging CoV disease, developing the diet-induced obesity model in conjunction with SARS-CoV infection in both inbred mice and CC mice. Obesity does significantly increase mortality in the MA15 model of infection and contributes to reduced respiratory function. However, in the context of genetically diverse RI lines, the impact of genetic line on fat gain during the high fat diet was significantly varied, as was the impact of genetic line on MA15 susceptibility. These findings develop a new mouse

model for severe SARS-CoV pathogenesis and offer insight onto the dynamic and complex relationship between viral susceptibility, host genetics, and comorbidity.

**CHAPTER 2: CHARACTERIZATION OF A PATHOGENIC FULL LENGTH cDNA
CLONE AND TRANSMISSION MODEL OF PORCINE EPIDEMIC DIARRHEA VIRUS
STRAIN PC22A**

Published - Beall, Anne, Boyd Yount, Chun-Ming Lin, Yixuan Hou, Qihong Wang, Linda Saif, and Ralph Baric. “Characterization of a Pathogenic Full-Length CDNA Clone and Transmission Model for Porcine Epidemic Diarrhea Virus Strain PC22A.” *MBio* 7, no. 1 (January 5, 2016). <https://doi.org/10.1128/mBio.01451-15>.

2.1 Introduction

Coronaviruses are important emerging viruses that are capable of producing sudden pandemic disease outbreaks with high morbidity, mortality, and economic losses in animal and human populations(141). Porcine epidemic diarrhea virus (PEDV) is an alpha coronavirus that has recently emerged in the United States, since killing >8 million piglets, nearly 10% of all United States farm piglets in 2014 (142). In the United States, newly emerged strains of PEDV are highly virulent and cause mortality rates in suckling piglets between 80-100% (142). Clinically, pigs infected with PEDV have severe diarrhea and vomiting, leading to death by dehydration within a few days of infection (143, 144) (142). PEDV readily spreads by fecal-oral

transmission routes between swine, in swine feed, and through contaminated farming and transport equipment (39). A second newly discovered swine coronavirus in the United States, designated swine delta coronavirus (SDCV) was discovered in Ohio and found to be closely related to coronaviruses detected in Hong Kong in 2012 (145). Porcine orthoreoviruses, similar to strains identified in South East Asia, have also been detected in US herds (146). It is clear that new approaches are desperately needed to control pandemic outbreaks of swine respiratory and enteric viruses.

Although the origins of PEDV remain obscure and early sequence studies had suggested similarity to human coronavirus NL63, more recent studies argue that PEDV is more closely related to several bat alphacoronaviruses identified in the US, South America and Eurasia (25, 147). PEDV first emerged in Europe in the 1970s and spread across Europe and into Asia (148). However, it was not until late 2010 that extremely virulent forms emerged in China (149). In the United States, phylogenetic studies suggest that PEDV is most closely related to Chinese strain AH2012*, although its transmission route to the US still remains uncertain (25, 142, 150). Since the first United States outbreak of PEDV in April 2013, PEDV has rapidly spread across 34 states, Canada, Central America, and has returned to devastate the swine industry in Asia (151, 152). In the advent of this ongoing outbreak, new strategies are desperately needed to understand pathogenic mechanisms, the functions of viral genes, and to provide new technologies to combat this disease.

PEDV appears to recognize CD13, an aminopeptidase N protein as receptor for entry into pig cells, as well as a sugar co-receptors heparan sulfate and/or N-acetylneuraminic acid (153, 154). PEDV can infect multiple cell types *in vitro* including swine, human, primate, and bat, suggesting the possibility of adaptation and spread to other species (153). The PEDV genome is

composed of 28k nucleotides encoding seven known open reading frames (ORFs) expressed from both genomic and sub-genomic mRNAs (155). Subgenomic mRNAs are arranged in a nested fashion from the 3' end of the genome. PEDV encodes the traditional coronavirus structural proteins – a receptor-binding spike glycoprotein (S), the envelope protein (E), membrane glycoprotein (M), and nucleocapsid protein (N). The spike glycoprotein is a type I membrane glycoprotein composed of S1 and S2 external domains, a transmembrane domain, C terminal cytoplasmic domain, and signal peptide. The S protein plays a role in virulence, growth adaptation, receptor binding, and virus-cell membrane fusion (156, 157). The PEDV envelope protein (E) upregulates stress pathways in the host cell, induces anti-apoptotic factors, and is important for viral budding (158). The PEDV nucleocapsid protein (N) induces cell stress and prevents apoptosis through similar pathways and additionally prolongs the host cell's S-phase (159). Additionally, PEDV encodes at least three additional ORFs- ORF1a, ORF1b, and ORF3. ORF1a/b encodes two viral proteases that process these large precursor polyproteins into 16 nonstructural proteins including the viral replicase and associated RNA modifying enzymes that are critical for full length and sub-genomic positive and negative strand RNA synthesis (160). ORF3 regulates virus production and encodes an ion channel important for viral fitness, but is not required for viral replication *in vitro* (161, 162).

In this manuscript, we generate the first infectious cDNA clone of a North American virulent PEDV strain, PC22A (163). Parental genomic and ORF3 deleted recombinant viruses were generated using the infectious cDNA clone system; the latter mutant was also engineered to express red fluorescent protein. Both recombinant viruses are replication competent *in vitro* and pathogenic in neonatal gnotobiotic piglets. Parental and recombinant viruses were efficiently transmitted to uninoculated pigs via indirect contact, allowing for genetic studies into the

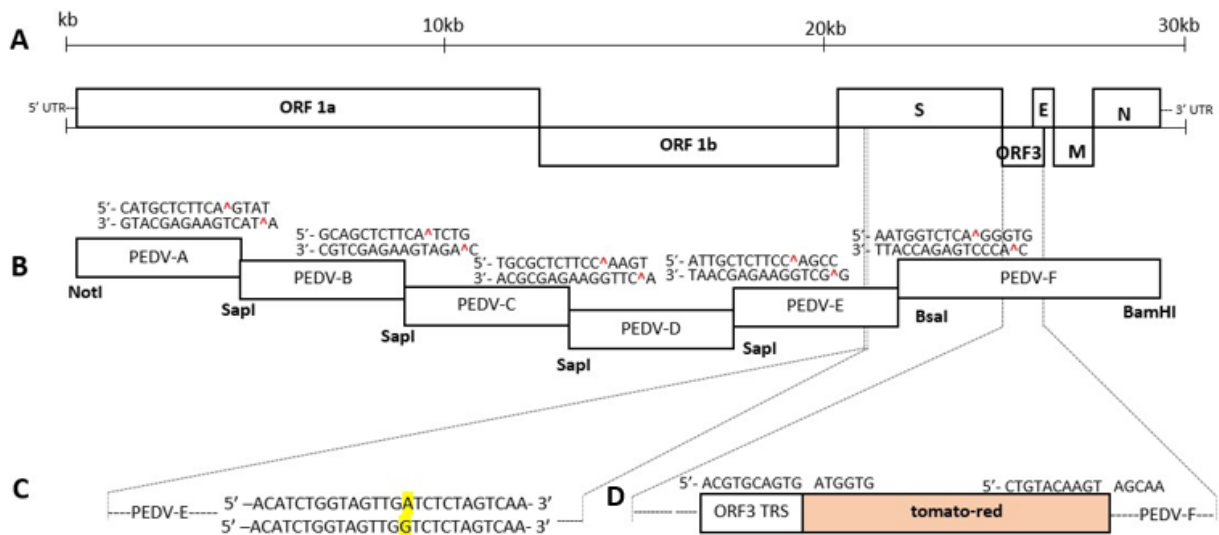


Figure 1. Schematic of full length PEDV genome and construction of PEDV cDNA infectious clone and mutants. (A) PEDV genome, including ORF1a, ORF1b, spike (S), ORF3, envelope (E), membrane (M), and nucleocapsid (N). (B) cDNA fragments comprising icPEDV. Restriction sites joining fragments are noted. (C) icPEDV: BsaI site removed in icPEDV. (D) PEDV- Δ ORF3-RFP: Restriction sites used to replace ORF3 with tomato-red and ORF3 transcription regulatory sequence (TRS).

molecular mechanisms regulating virus transmission and pathogenesis. The availability of an infectious clone for PEDV will allow for further opportunities to understand gene function and genetic variants in PEDV pathogenesis and transmission, leading to better informed design of vaccines and therapeutics.

2.2 Results

2.2.1 Design of PEDV infectious clone

We have developed molecular clones for several highly pathogenic swine and human coronaviruses, using class II restriction endonucleases to directionally assemble a full length cDNA viral genome from a set of sequentially designed smaller cDNAs (49-53, 56). To develop a molecular clone for PEDV, the highly virulent PC22A (*Fig 1A*) strain was sequenced and synthesized as six contiguous PEDV subclones designated A-F (*Fig 1B*). Subclones A/B, B/C, C/D, and D/E are joined by unique SapI restriction endonuclease cleavage sites (at nucleotide positions 4071, 8287, 12016, and 16941, respectively) that allow for directional assembly into a full length cDNA without alteration of the viral amino acid sequence. Subclones E and F are joined at a unique BsaI site at nucleotide position 22504. In subclone F, a single BsaI restriction site in PEDV-PC22A was removed by introducing a silent mutation at position 24337, effectively marking the recombinant genome (*Fig 1C*). Thus, each fragment contains a unique set of class II restriction enzyme sites flanking the genomic sequence that allow for unique 3-nt overhangs between each fragment. This specificity allows for systematic, efficient, and directional assembly of the complete PEDV genome by *in vitro* ligation. The PEDV A fragment contains a T7 start site, whereas the F fragment terminates in 22 A residues, allowing for *in vitro* transcription and capping of a polyadenylated full length transcript.

PEDV-ORF3 is an accessory ORF encoding a putative ion channel protein that is oftentimes deleted in some natural isolates or following *in vitro* passage, suggesting that it encodes nonessential functions *in vitro* and/or *in vivo* (162). To generate a fluorescently marked PEDV genome mutant, ORF3 in the PEDV-F fragment was replaced with red fluorescent protein (RFP), tomato-red (Figure 1D). The mutant was created using native restriction enzyme recognition sequences that allowed for the preservation of the ORF3 transcription regulatory sequence (TRS) which regulates subgenomic RNA expression (Figure 1D).

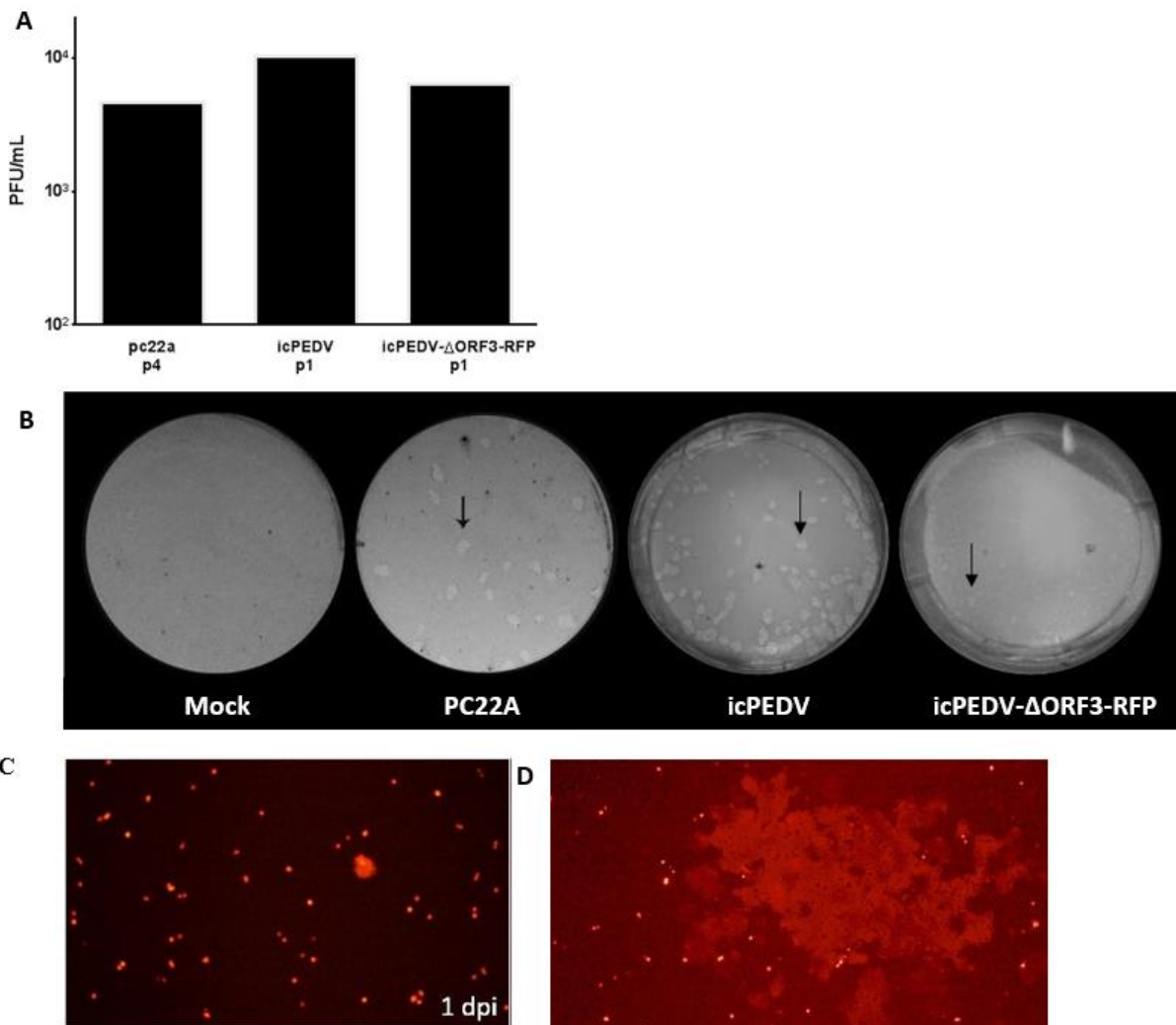


Figure 2.2. Growth of icPEDV clones isolated from *in vivo* small intestine samples. (A) Titers of viral stocks isolated from small intestinal contents at noted passages, harvested 2 dpi. (B) Representative plaques of mock, parental PC22A, icPEDV, and icPEDV-ΔORF3-RFP; from left to right 2 dpi. (C) Fluorescent microscopy of passage 0 icPEDV-ΔORF3-RFP in cell culture at 1dpi. (D) Syncytia formation of p0 icPEDV-ΔORF3-RFP 2 dpi.

2.2.2 Recovery of Recombinant Viruses

To isolate recombinant wildtype and RFP expressing PEDV recombinant viruses, each plasmid fragment was digested with noted restriction enzymes, purified, and ligated to create a full length PEDV cDNA genome. Using the T7 RNA polymerase, full length transcripts were synthesized *in vitro* as previously described by our group (49, 53). As previous swine and human coronavirus infectious clones displayed improved recovery rates and replication efficiency in the presence of supplemented N gene transcript (49, 53), capped PEDV-N gene transcripts were mixed with the full length genomic transcripts prior to electroporation into Vero cells. Within 24-48 hrs post electroporation, recombinant virus subgenomic mRNA could be detected via RT-PCR. After isolating recombinant virus from pig intestinal contents after inoculation, wildtype and recombinant viruses replicated to titers that approached or exceeded 1×10^4 PFU/mL in Vero cells, equivalent to titers commonly reported in the literature (*Fig 2A*). Recombinant icPEDV produced a similar plaque morphology (*Fig 2B*) to the parental strain, and formed syncytia characteristic of PEDV in culture (*Fig 2C*). Notably, icPEDV- Δ ORF3-RFP displayed a reduced plaque size compared to either PC22A or icPEDV (*Fig 2B*), indicative that ORF3 may be important for *in vitro* growth of the virus, and suggestive of a possible attenuation of the ORF3 deletion mutant. At 48 and 72 hrs post electroporation with icPEDV- Δ ORF3-RFP, fluorescent red cells were seen cell culture, both within individual cells as well as within larger syncytia (*Fig 2D*).

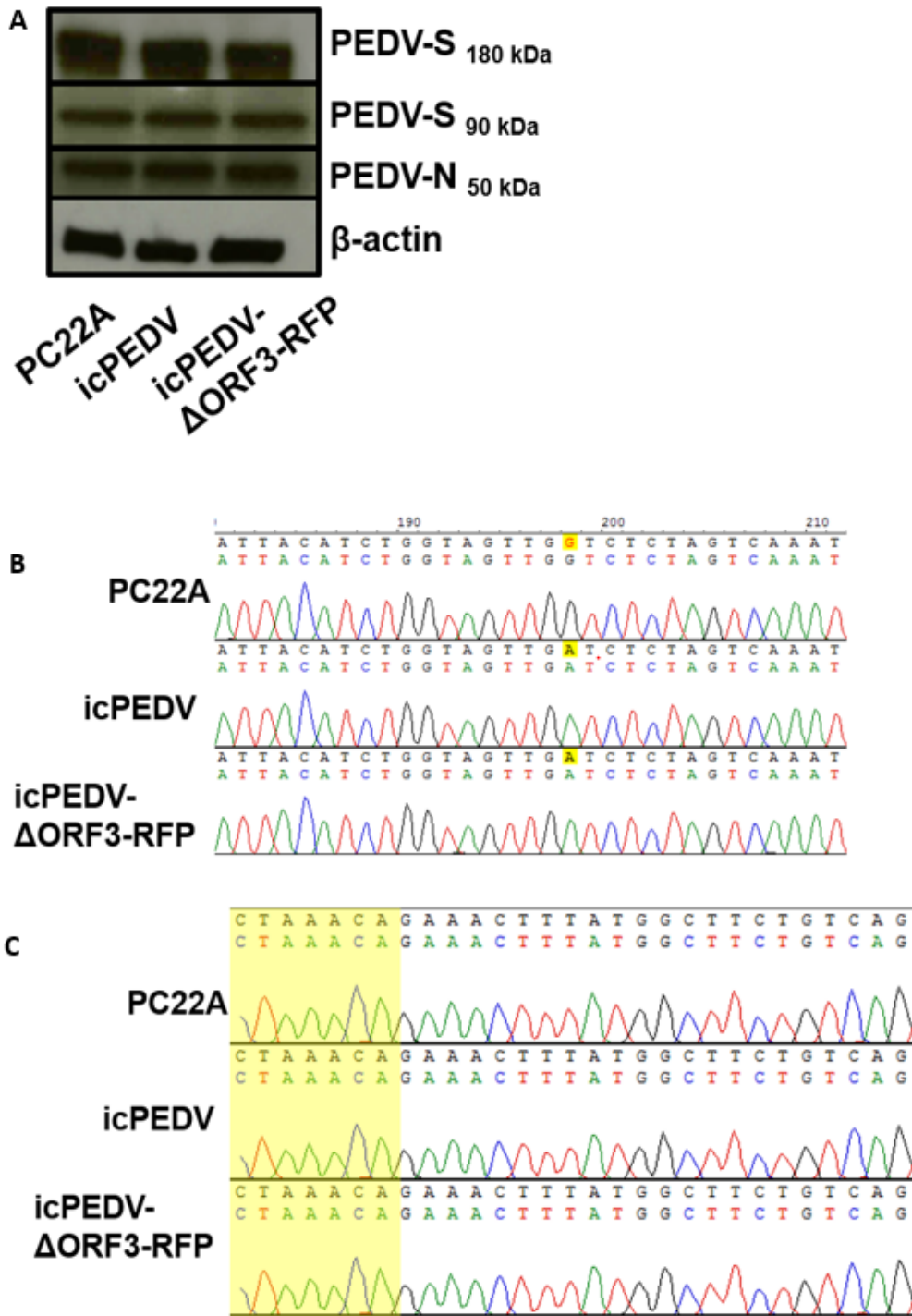


Figure 2.3. Confirmatory studies of infectious clone PEDV virus. (A) Western blot for PEDV spike (PEDV-S) before (180kDa) and after (90kDa) cleavage with trypsin, and nucleocapsid (PEDV-N) protein. Protein isolated from Vero cells infected with PC22A, icPEDV, or icPEDV- Δ ORF3-RFP 2 dpi. (B,C) Sequence of viral RNA isolated from VERO cells infected with p0 parental PC22A, icPEDV, or icPEDV- Δ ORF3-RFP, harvested and sequenced 2dpi. (B) Altered BsaI cloning site is conserved after viral passage in piglets denoted in yellow. (C) Transcription regulatory sequence (TRS) in the leader region of PEDV subgenomic transcripts is conserved between wt and icPEDV; sequence denoted in yellow.

2.2.3 Characterization of Recombinant Viruses

To evaluate protein expression in our recombinant PEDV, we cloned and expressed PEDV-S and PEDV-N into Venezuelan equine encephalitis virus strain 3526 replicon constructs (VRP), and isolated VRP-PEDV-S and VRP-PEDV-N particles. The VRP were inoculated into the footpad of mice, and polyclonal PEDV-N and PEDV-S antisera was collected after a day 21 boost. Using western blot techniques, we confirmed the presence of the 180/90 and ~50kDa PEDV-S and PEDV-N proteins, respectively, in icPEDV, icPEDV- Δ ORF3-RFP, and parental PEDV infections *in vitro* (Fig 3A). Thus, molecularly derived viruses have similar protein expression phenotypes as parental virus.

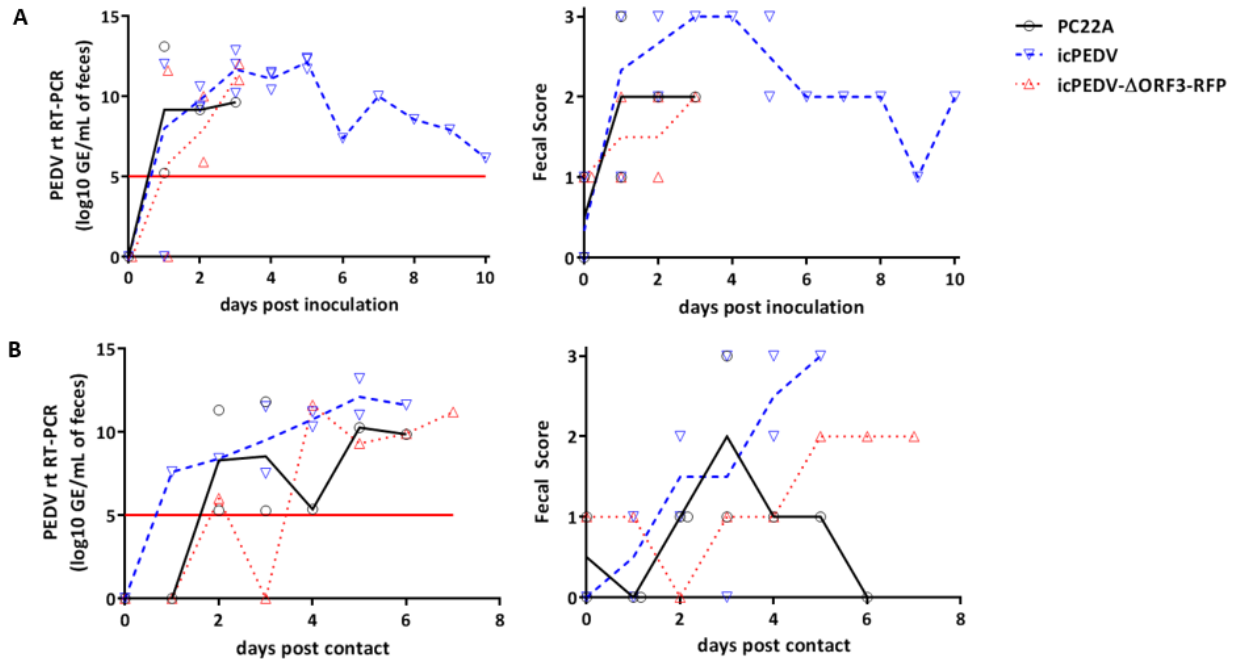


Figure 2.4. icPEDV mimics wtPEDV infection in gnotobiotic piglets. Gnotobiotic piglets were infected orally with 2mL PEDV supernatant with an uninoculated piglet cohoused to determine transmission. All animals succumbed to illness or were euthanized due to illness at their final time point. (A) mean RT-qPCR titer of fecal samples and fecal scores after viral inoculation. Line represents mean values with individual piglet values shown by points. (B) RT-qPCR titer of fecal samples and fecal scores in cohoused transmission control piglets, days after contact with inoculated piglets in A. The limit of detection in rt RT-PCR figures (Ct=37) is represented by a red line.

To further confirm the presence of the recombinant virus post-electroporation, we reverse transcribed genomic RNA from virions in the culture media and then sequenced to demonstrate the presence of the distinguishing BsaI cloning site in infectious clone viruses (Fig 3B). Additionally, we sequenced the leader-containing subgenomic mRNA transcripts to ensure that both our recombinant viruses and their parental strain shared the wildtype transcription

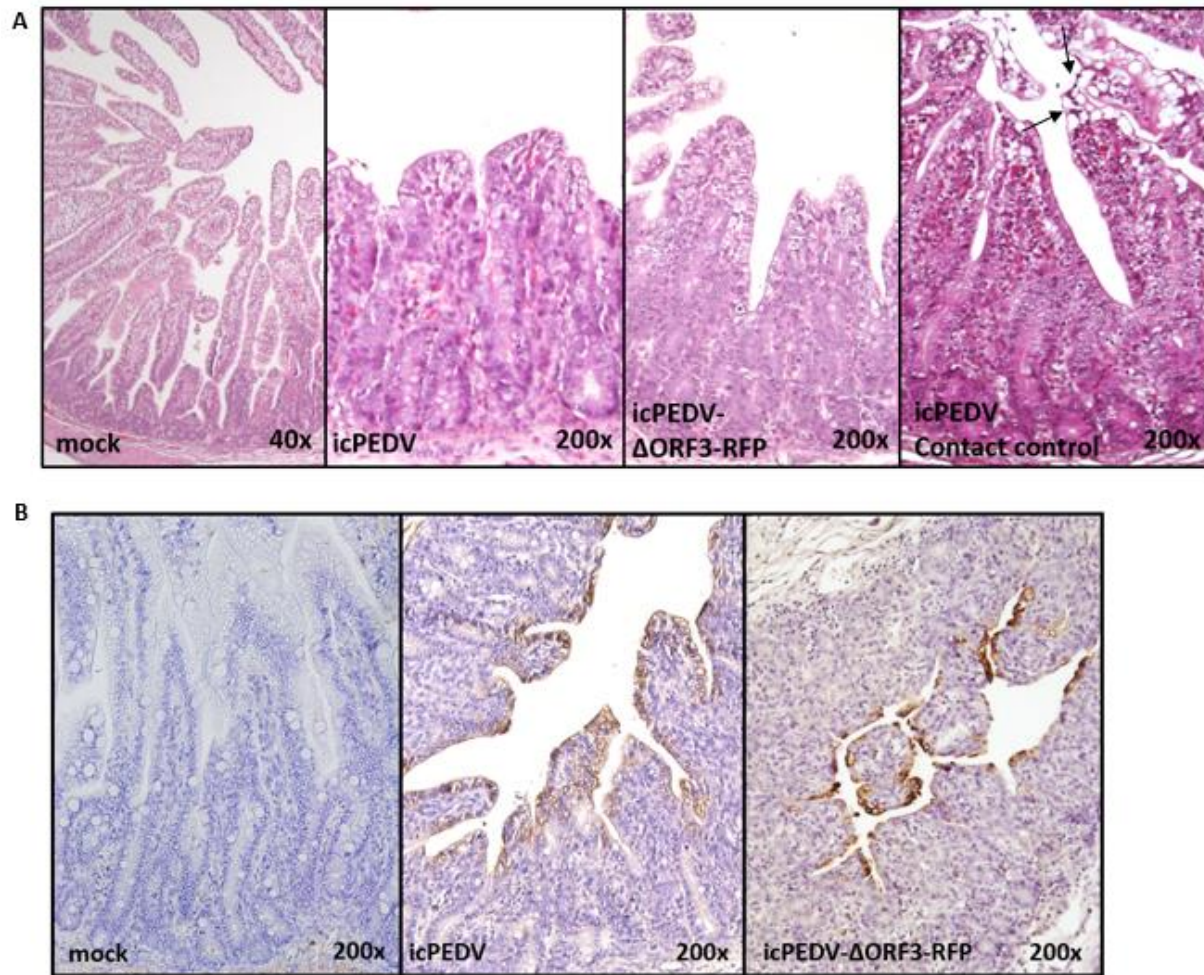


Figure 2.5. Histology and IHC staining of icPEDV infected pig intestine. Gnotobiotic piglets were oral inoculated with 2mL PEDV. A contact control piglet was cohoused with inoculated piglet(s) to determine transmission. All animals succumbed to illness or were euthanized due to illness at their final time point (PEDV 1dpi, icPEDV 4dpi, icPEDV-ΔORF3-RFP 7dpi, contact control 4dpi). (A) Representative histological slides of jejunum infected with mock, parental PC22A, icPEDV, or icPEDV-ΔORF3-RFP. A contact piglet infected by icPEDV is also shown. Cell fusion and vacuolation were noted at the villi tips (arrow). (B) Immunohistochemistry (IHC) staining (brown) for PEDV nucleocapsid (N) protein using mouse anti-PEDV N protein monoclonal antibody (SD6-29). PEDV antigens were detected in the entire villous epithelial cells in jejunum of icPEDV and icPEDV-ΔORF3-RFP inoculated piglets, but not in mock-inoculated piglet.

regulatory sequence (TRS) required for normal coronavirus replication and growth kinetics (*Fig 3C*). Together, these data definitively demonstrate that both recombinant clones generated replicating recombinant virus *in vitro*.

2.2.4 icPEDV replication and pathogenesis in gnotobiotic piglets

PEDV PC22A is highly pathogenic in newborn piglets and is rapidly transmitted to littermates. To determine if icPEDV replicated parental PEDV PC22A *in vivo* pathology and transmission phenotypes, gnotobiotic (Gn) pigs were orally inoculated with icPEDV (P0), icPEDV- Δ ORF3-RFP (P0), or PC22A (P3) and housed with uninfected indirect contact pigs (*Table 1*). Challenged animals demonstrated fecal viral RNA shedding, and diarrhea started 1-3 days post infection (DPI) in all three virus groups (*Fig 4A and Table 1*). Importantly, uninoculated indirect contact pigs within each group demonstrated both robust virus shedding and diarrhea, confirming the transmissibility of both PC22A and recombinant virus (*Fig 4B*). All three viruses replicated to similar peak titers (11-13 log₁₀ GE/mL). However, PC22A- and icPEDV-group pigs had more severe diarrhea (highest fecal scores of 3) than icPEDV- Δ ORF3-RFP-group pigs (highest score of 2). Day of harvest for each piglet was dependent on clinical fecal scores, or occurred upon death of the piglet. Notably, day of harvest varied both between virus types and within virus groups. Because of the animal numbers in each group, and because of the variation within each PEDV group, the day of harvest cannot be used as a reliable indicator of the relative degree viral virulence nor attenuation. The pathogenesis of icPEDV in Gn pigs also replicated the PEDV strain PC21A pathogenic phenotype, which had been collected from the same swine farm on the same day as PC22A (144). Histopathological examination showed severe villous atrophy in PEDV PC22A-, and icPEDV-inoculated pigs, and moderate-to-severe villous atrophy in icPEDV- Δ ORF3-RFP-infected pigs

(Fig 5A). The villous height: crypt depth (VH:CD) ratio of the jejunum of mock inoculated pig was significantly higher than those of PC22A-, icPEDV-, and icPEDV- Δ ORF3-RFP-infected pigs ($P < 0.05$) (Table 1). Immunohistochemistry (IHC) for PEDV-N protein confirmed the presence of recombinant virus throughout the small intestine (duodenum, jejunum, and ilium) in both icPEDV and icPEDV- Δ ORF3-RFP-infected pigs (Fig 5B and Table 2). In addition, icPEDV antigens were also detected in the large intestine (colon).

These results indicate that the cell culture supernatants of icPEDV and icPEDV- Δ ORF3-RFP contained infectious recombinant virus particles that replicated well in gnotobiotic pigs. While the icPEDV recombinant virus replicated the parental PC22A clinical phenotypes *in vivo*, icPEDV- Δ ORF3-RFP infection resulted in a partial attenuation in pigs based on lower diarrhea scores. The rapid infection of contact pigs suggests efficient transmission of icPEDV and icPEDV- Δ ORF3-RFP, replicating both parental PC22A and circulating US strain transmission phenotypes.

2.3 Discussion

Emerging viruses pose a considerable threat to humans and society, by causing morbidity and mortality in human populations, or causing significant losses in important food sources and trade leading to economic instability and loss of critical protein sources, especially in rural poor populations. Porcine epidemic diarrhea virus is a serious live-stock pathogen that is causing significant economic losses in the swine industry internationally. To date, over a billion piglets have died globally. Live vaccine has been used historically to combat PEDV outbreaks in Asia, however, live vaccines available today are ineffective in preventing outbreaks of circulating pandemic strains, including US outbreak strains, and have not significantly reduced the global

disease burden (152). Other important nidovirus infections of swine include transmissible gastroenteritis virus (TGEV) and its related respiratory variant designated porcine respiratory coronavirus (PRCV), and porcine reproductive and respiratory disease virus (PRRSV), which have caused major economic losses to the swine industry since the late 1980s (164-166). In addition to PEDV, another emerging coronavirus, porcine delta coronavirus, has recently been reported in swine, demonstrating the possibility of continued emergent threats to this important food industry (145, 167). Given the apparent increase in the number of new swine viruses identified over the past 30 years, it seems clear that management practices and/or other changes in the ecosystem are providing an environmental setting that promotes the emergence of new viral pathogens for the swine industry. If so, these data document the need for the development of new, rapid response intervention platforms for disease control in critical livestock populations that are centrally linked to human health. In this manuscript, we describe the first molecular clone for a highly pathogenic US strain of PEDV, PC22A strain, isolated from an outbreak in Ohio in June 2013 (163). Both the parental PEDV PC22A strain and its derivative recombinant cloned virus were genetically stable and fully pathogenic in neonatal gnotobiotic pigs, demonstrating that icPEDV not only provides a strategy that allows for the systematic evaluation of the role of viral genes in pathogenesis, tropism and virulence, but a translational platform for the development of rationally attenuated live virus vaccines. In addition, we have constructed a recombinant PEDV that encodes an indicator gene, RFP, which allows for rapid evaluation of antiviral efficacy and neutralizing antibodies levels using high throughput cell culture systems.

Recently, a molecular clone for a high growth tissue culture variant of a 2010 Thai isolate, designated PEDV_{AVCT12}, was reported in the literature (168). In contrast to our findings, full length recombinant PEDV_{AVCT12} virus could not be isolated unless ORF3 expression had

been ablated, either by naturally occurring deletions or by insertion of an indicator gene in this location. Interestingly, naturally occurring deletions also removed 7 amino acids from the c-terminal of the S gene, similar to deletions described with other tissue culture strains like PEDV strain CHM2013 (168). At this time, the discrepancy between the two laboratory results is intriguing and most likely is directly related to the backbone sequence of the two isolates and/or the difficulties associated with culturing clinical isolates of PEDV *in vitro*. Tissue culture PEDV_{AVCT12} replicates 2-3 logs more efficiently than wildtype PEDV PC22A and icPEDV in culture and trypsin is also required to culture these latter isolates *in vitro*. Future studies may well reveal the emergence of similar tissue culture adaptations during serial passage of our highly virulent PEDV PC22A and icPEDV in culture. Importantly, pathogenic outcomes *in vivo* were not evaluated using the heavily tissue culture adapted PEDV_{AVCT12} strain, so the utility of this recombinant virus to evaluate pathogenic outcomes and/or the role of tissue culture adaptive mutations in virulence are uncertain at best. Although an exact infectious dose of our recombinant viruses were not determined from these studies, <1 PFU of PEDV PC22A is sufficient to cause disease in piglets (24).

Little information is available regarding the molecular mechanisms governing efficient coronavirus pathogenesis and transmission between hosts. Importantly, icPEDV and icPEDV- Δ ORF3-RFP are efficiently transmitted to co-housed littermates, providing a potential platform for investigating the genetic mechanisms regulating efficient transmission between hosts. While similar studies using highly pathogenic influenza viruses in ferrets are highly controversial because of potential human pandemic concerns (169), identifying genetic factors that attenuate transmission frequency offer a powerful tool to improve the safety and efficacy of live attenuated coronavirus vaccines, especially given the high animal density manufacturing approaches used in

the swine industry. Such studies may also provide significant insights into the fundamental principles and genetic functions that influence the transmission efficiency of other highly pathogenic human coronaviruses, like Severe Acute Respiratory Syndrome Coronavirus (SARS-CoV) and Middle East Respiratory Syndrome Coronavirus (MERS-CoV).

PEDV infection is most devastating in neonatal and suckling piglets, necessitating vaccines that target lactogenic immunity through the vaccination of pregnant sows and gilts. Piglets do not attain passive immunity pre-parturition, but instead receive IgG and IgA based lactogenic immunity from colostrum and milk, respectively. For both TGEV and PEDV, sows infected with live virulent virus transferred more protective immunity against viral challenge in their nursing piglets than sows infected with attenuated or inactivated virus (170). The USDA has granted conditional licenses to two PEDV manufacturers to date. The Harris Vaccine uses an attenuated Venezuelan Equine Encephalitis (VEE) virus vaccine strain replicon particle (VRP) expressing the PEDV spike protein (171). The second is a parenteral killed virus vaccine made by Zoetis (44). Both are used to immunize pregnant sows and gilts. The efficacy and protective ability against various circulating US strains is still under evaluation. We note that the VRP platform described in our paper was based on a BSL2, non-select agent, Venezuelan equine encephalitis virus strain designated 3526, which has been used in animal and human trials (172-174). In contrast to other VEE replicon platforms, VEE 3526 retains wildtype E1 and E2 glycoproteins that efficiently target dendritic cells (175, 176), but lacks E3 sequences. This deletion of E3 confers an attenuated phenotype *in vivo*. VEE 3526 expressing appropriate S glycoprotein genes provides robust protection against other coronaviruses like SARS-CoV, MERS-CoV and HKU5-S (55, 177, 178). Using VEE 3526 structural genes allows for recovery of high titer VRP encoding PEDV S and/or N proteins under BSL2 conditions. It remains

unclear whether the VRP3526 platform will prove sufficiently robust to induce lactogenic immunity in sows capable of protecting suckling piglets (178). Future experiments will have to be designed and implemented to test the relative efficacy of VRP vaccines, killed whole virus vaccines, or future live attenuated virus vaccine.

Importantly, no live virus vaccine is currently available in the United States, nor have historical live vaccines been effective in combating current US or Asian strains (14). Robust studies using SARS-CoV have identified several viral genes, including the E protein, the ExoN nsp14 RNA proof-reading machinery, and the 2-O-methyltransferase nsp16 replicase, as high priority targets for rational attenuation of coronaviruses (32, 179, 180). Because coronaviruses undergo RNA recombination at high frequency and encode an exonuclease function (181, 182), recombination repair and reversion to wild type virus is a pressing concern when designing live attenuated coronavirus vaccines. However, our laboratory has developed strategies to prevent recombination repair that limit the capacity of rationally designed live attenuated virus to revert to wildtype virus sequence (65). Effective vaccines are increasingly important as new strains are identified in the United States and circulating strains continue to devastate herds. The infectious clone platform allows for rapid construction of genetically modified PEDV variants, to evaluate the function of antigenic variation on neutralization phenotypes, and can be used for the rational design of a live virus vaccine. This platform also allows for incorporation of genetic changes to enhance the replication of the virus *in vitro* for more efficient production of attenuated vaccines. Globally, humans have experienced coronavirus outbreaks with increasing frequency including the identification of two new human coronaviruses in the last fifteen years –notably, SARS-CoV and MERS-CoV (183). Human and animal coronaviruses share similar structural proteins and replication dynamics. Currently, no transmission model is available for these important human

pathogens. The neonatal pig model described in this study can provide a surrogate transmission model for human coronaviruses. Separately, the study of coronavirus transmission in its original host in a BSL2 climate affords the opportunity to safely and accurately research a family of viruses that is devastating animal and human populations. It is possible that genetic manipulation of PEDV recombinant viruses will enable studies that can significantly enhance our understanding of the role of coronavirus genetics in transmission, virulence and pathologies that are central to both animal and human health and disease prevention.

In this manuscript, we describe a reverse genetic platform for a US highly virulent PEDV strain that causes lethal disease in newborn piglets, allowing for the future identification of attenuating mutations and virulence alleles. In parallel, we have developed indicator viruses that can be used for high-throughput neutralization assays or to evaluate the impact of antivirals. This reverse genetics system will allow for quick and robust PEDV genetic manipulation in a clinical North American isolate, allowing for in-depth study of viral replication and pathogenesis, which are essential for the development of a safe and robust live attenuated virus vaccines.

2.4 Materials and Methods

Viruses and Cells

The wild type strain PC22A strain of PEDV, passage 4, was cultured on Vero cells, as described previously (Oka 2014). Cells were grown in growth media containing Dulbecco's Modified Eagle Medium (DMEM) (Life Technologies) supplemented with 5% fetal bovine serum (Life Technologies) and 1% antibiotic-antimycotic (Gibco). Virus was grown in Vero cells in maintenance media, which was DMEM supplemented with 10 ug/mL trypsin (Life

Technologies), 0.3% tryptose phosphate broth (Sigma), and 1% antibiotic-antimycotic (Life Technologies). Cells were kept in a humidified incubator at 37°C and 5% CO₂.

Assembly of Full Length Recombinant PEDV

The icPEDV clone was designed using six separate fragments ordered from Biobasic flanked with unique flanking class II restriction sites that leave non palindromic overhangs. Sequences were ordered based on PC22A passage 4 sequence (Genbank Accession #KM392224.1). All cDNA subclones were grown in the pcXL-TOPO vector. In fragment E, a naturally occurring BsaI site was removed by introducing a silent mutation in order to prevent interference with assembly of the full length infectious clone. All PEDV fragments were sequenced after transfection into bacterial culture to ensure sequence fidelity. The PEDV fragments were digested using restriction sites designated in Figure 1, run on a 1% agarose gel, excised, and purified using a QIAquick Gel Extraction Kit (Qiagen). The PEDV fragments were mixed and ligated overnight at 4°C using T4 DNA ligase (Roche). Ligated fragments were phenol/chloroform extracted, and full length T7 RNA transcripts were generated as described in the mMessage mMachine manufacturer protocol (Ambion), but allowing the reaction to run at 30°C for 3 hrs, then room temperature for 2 hrs. In addition, SP6 PEDV N gene transcripts were generated from PCR purified PEDV N gene sample using a 4:1 ratio of cap to GTP (Ambion).

To generate the ORF3 deleted RFP construct, tdTomato was amplified using PCR with flanking PEDV sequence, then inserted using native restriction sites in the PEDV-F fragment. PEDV-F- Δ ORF3-RFP was cultured and sequenced to ensure seamless replacement of ORF3 with RFP containing the ORF3 TRS.

***In Vitro* Transfection**

Genome length and N RNA transcripts were mixed with 800uL of Vero-BI cells (1×10^7 cells/mL) in PBS, then added to an electroporation cuvette. Three pulses of 450V at 50uF were used to transfect the cells with a Gene Pulser II electroporator (BioRad). The cells were allowed to recover for 10 min at room temperature, and then were transferred to a 75cm² flask in growth medium at 37°C for 2 hr, after which time the cells were washed and incubated in cell culture medium. Trypsin was added to the culture at 5ug/mL 12 hrs post electroporation to assist in virus recovery and spread.

Sequence Analysis Identification of Marker Mutations

Virus harvested from small intestinal contents was grown in Vero-BI cell culture for 48 hrs. Virion RNA was harvested from supernatant using the QIAamp Viral RNA mini kit (Qiagen). After purification, viral cDNA was generated with Superscript II Reverse Transcriptase (Life Technologies) as previously described by our group (49). To demonstrate the presence of the marker mutation, the icPEDV BsaI mutation site was amplified by PCR using primers 5'-tccaagccatttctagttctatt-3' and 5'-TGACACAACAAAGATGAGAACA-3'. PCR amplicons were gel purified and then sequenced using primers 5'-tcaggctagcaggaagtttag-3' and 5'-AGGTCAACTAGTGTGTTGTTGATAT-3'.

Western Blot and Transcript Analysis

Virus from infected animals were cultured in Vero-BI cell culture for 48 hrs, washed with PBS, and intracellular RNA was harvested from cells using NP40 buffer (150mM NaCl, 1% Triton X-100, 50mM Tris pH 8.0) for Western Blots or TRIzol (Life Technologies) for RNA analysis. cDNA from viral RNA transcripts was generated using Superscript II Reverse Transcriptase (Life Technologies) and PCR amplified using primers pairs in the PEDV leader

sequence and nucleocapsid gene. PCR products were separated on a 1% agarose gel and visualized on a DarkReader transilluminator (Clare Chemical Research).

For Western Blot analysis, protein from infected cells was denatured in 4x Lammeli buffer (BioRad) at 95°C for 6 mins, then separated on a gradient 4-15% Mini-PROTEAN precast gels (BioRad) prior to electrophoretic transfer of the proteins to PVDF membranes (BioRad). To detect PEDV antigens, blots were first blocked with 5% milk in TBST and then probed with a polyclonal mouse sera diluted 1:200 from mice which had been immunized with Venezuelan Equine Encephalitis replicon particles (VRP) expressing PEDV nucleocapsid (N) protein or spike (S) glycoprotein. Blots were developed using GE Amersham ECL Western Blotting Detection reagents and exposed to film for imaging.

Animal Studies

Four groups of 2-3-week-old gnotobiotic (Gn) pigs were used to examine the replication and pathogenesis of icPEDV- and icPEDV- Δ ORF3-RFP-derived viruses *in vivo*, and compared with PC22A and mock infected positive and negative controls, respectively (Table 1). Piglets were orally inoculated with 2 mL of icPEDV or icPEDV- Δ ORF3-RFP culture supernatants after transfection (P0)($<1.0 \times 10^2$ PFU/ml), or with tissue culture-adapted (TC) PC22A strain at passage level 3 (P3) with a dose of 5.8 log₁₀ PFU/pig. To investigate transmission, Pig No. 2, 5, 7 and 10 were co-housed in the same isolator as infected pigs but were separated by a stainless steel divider that contained small holes which only allowed indirect contact between the groups. Animals were monitored daily for clinical signs of disease including diarrhea and vomiting. Rectal swabs were collected for scoring fecal denseness (score 0=normal; 1=pasty; 2=semi-liquid, diarrhea; and 3=liquid, diarrhea) and for enumerating fecal viral RNA shedding by RT-qPCR. Except for one pig in icPEDV group, which was kept for long term for the production of

hyperimmune serum, the Gn pigs were euthanized at acute infection phase [within 5 days post-inoculation (DPI) or 7 days post-contact the inoculated pigs (DPC)] for histopathological examinations. At necropsy, small and large intestinal contents were collected and tested by RT-qPCR for viral RNA levels and for infectious virus by plaque assay. The different sections of small intestine [duodenum (D), jejunum (J), ileum (I)] and large intestine [caecum (C) and colon] were collected for histopathological examination and stained by H&E. The derivation and maintenance of Gn pigs, sample collection and testing, and histopathology were performed as previously described (163, 184). All the animal use protocols employed in this study were reviewed and approved by the Agricultural Animal Care and Use Committee, The Ohio State University.

Immunohistochemistry (IHC) Staining

The IHC staining procedure was optimized as described previously (24) using non-biotin polymerized horseradish peroxidase (HRP) system (BioGenex Laboratories, San Ramon, CA). Briefly, intestinal tissue sections from each pig were deparaffinized and rehydrated in graded ethanol to phosphate-buffered saline (PBS, pH 7.4). Antigen retrieval and unmasking were performed by treatment with 0.05 % pronase E (Sigma-Aldrich1, St. Louis, MO) for 20 min. The endogenous peroxidase activity was quenched with 3% hydrogen peroxide (Sigma) for 20 min. Then, the sections were incubated in Power Block™ solution (BioGenex) for 30 min at room temperature (RT). Mouse monoclonal antibody anti-PEDV nucleocapsid (N) protein (SD6-29, a gift from Drs. Nelson E. and Lawson S., South Dakota State University) was applied to each section at 4 °C overnight. After two washes in PBS, commercial Super Sensitive™ IHC Detection System (BioGenex) was used. Finally, these sections were counterstained with Mayer's haematoxylin (BioGenex), dehydrated, and cover-slips added. The IHC signal of PEDV

antigen was scored as 0–3 according to the percentage of villous enterocytes within the section showing a positive signal. Score 0 = no positive cells, score 1 = less than 30%, score 2 = 30 to 60%, score 3 = more than 60% of villous enterocytes showing a positive signal.

Table 2.1: Summary of PEDV replication and pathogenesis in Gn pigs

Group	No of Pigs	Pig No.	Age of inoculation (day)	Inoculation/Contact ^a	Onset of fecal RNA shedding / diarrhea (DPI or DPC)	Highest fecal score ^c / fecal RNA shedding titer (GE/mL)	Age (DPI) of piglet at euthanasia (day)	Jejunum villous height: crypt depth (VH:CD) ratio
icPEDV	5	1	19	Inoculation	2 / 2	3 / 12.9	ND ^b	ND
		2	19	Contact	2 / 4	3 / 13.2	24 (5)	1.2 ± 0.2
		3	16	Inoculation	1 / 2	3 / 11.5	20 (4)	1.4 ± 0.2
		4	16	Inoculation	1 / 2	3 / 12.0	21 (5)	1.3 ± 0.2
		5	16	Contact	1 / 2	3 / 11.5	21 (5)	3.1 ± 1.5
icPEDV- ΔORF3- RFP	3	6	14	Inoculation	1 / 1	2 / 11.6	16 (2)	2.2 ± 0.1
		7	14	Contact	2 / 5	2 / 11.6	21 (7)	1.0 ± 0.0
		8	14	Inoculation	1 / 3	2 / 10.8	17 (3)	2.7 ± 0.4
PC22A	4	9	18	Inoculation	1 / 1	3 / 13.0	19 (1)	1.4 ± 0.3
		10	18	Contact	2 / 3	3 / 11.8	21 (3)	1.3 ± 0.1
		11	26	Inoculation	1 / 1	2 / 11.8	27 (3)	ND
		12	26	Contact	1 / 2	1 / 11.12	21 (7)	ND
Mock	1	11	NA	NA	NA	1 / NA	19	6.8 ± 0.9

^a Pigs No. 2, 5, 7 and 10 were exposed by indirect contact to the pigs which were housed in the same isolator through small holes drilled into the stainless steel divider. Panel located between the 2 pigs in the shared pig tub isolator unit.

^b ND: not done because Pig#1 was used for hyperimmune serum production.

^c fecal score: 0=normal; 1=pasty; 2=semi-liquid, diarrhea; and 3=liquid, diarrhea.

Table 2.2: Summary of IHC staining in infected pigs.

Group	Pig No.	DPI	IHC signal intensity			
			duodenum	jejunum	ileum	colon
icPEDV	2	5	0	3	3	1
	3	4	2	3	3	1
	4	5	1	3	2	2
	5	5	1	3	2	1
icPEDV- Δ ORF3-RFP	6	2	0	1	1	0
	7	7	1	2	3	0
	8	3	0	2	2	0

Note: The IHC signal of PEDV antigen was scored as 0–3 according to the percentage of villous enterocytes within the section showing a positive signal. Score 0 = no positive cells, score 1 = less than 30%, score 2 = 30 to 60%, score 3 = more than 60% of villous enterocytes showing a positive signal.

CHAPTER 3: HUMORAL IMMUNITY IS REQUIRED FOR CLEARANCE OF SARS-CoV INFECTION

3.1 Introduction

Severe acute respiratory syndrome (SARS), caused by a novel coronavirus (SARS-CoV), resulted in over 8,000 cases of respiratory disease with high mortality in 2002 and 2003 (185). Patients with severe pathology developed acute lung injury associated with neutrophilia, lymphopenia, and prolonged proinflammatory cytokine expression (186). In surviving patients, infectious virus was cleared between 1 and 3 weeks after infection (187). Because human isolates of SARS-CoV replicate, but do not produce severe disease in mice, *in vivo* pathogenesis studies have focused on a mouse-adapted SARS-CoV strain designated MA15 to reveal fundamental insights into pathogenesis and immunity (10). Several studies have demonstrated the critical importance of innate immune responses and wound repair pathways in regulating SARS-CoV pathogenesis (16, 72, 73, 75, 188-193); additionally, T cell responses have been found to be critical for virus clearance and protection from clinical disease in mice infected with SARS-CoV. Survival has been associated with robust SARS-CoV specific CD4⁺ and CD8⁺ T cell responses during infection (86, 87, 89, 90). Findings to date have shown critical roles for both innate and T cell-mediated immune functions in virus clearance, however, the role of B cells in primary infection and viral clearance have not yet been characterized.

Serum analysis of SARS-CoV-infected patients and in SARS-CoV mouse models have primarily focused on the development of protective neutralizing IgG antibody responses in the weeks and months after infection (99, 191, 194, 195). The SARS nucleocapsid is an

immunodominant antigen during infection and the vast majority of SARS-CoV reactive antibodies (80-90%) in patients bind to the nucleocapsid protein (N) (99). During the SARS-CoV outbreak, IgG titers against the N protein as well as the spike glycoprotein (S) were initially detected in patients at ~2 weeks post-infection. These IgG titers peaked at approximately 4 weeks post-infection (194). Though anti-SARS-CoV IgG titers were detectable through one year post-infection, IgG antibody titers declined over this period and subsequently became undetectable in many patients six years after infection (81, 196). At approximately two weeks post-infection in human patients, antibody titers skew towards a higher IgG to IgM ratio, suggesting that CD4+ T cells are highly activated after initial infection (81). Taken together, these previous reports indicate that antigen-specific antibody responses are robust in patients that clear virus infection and survive infection.

Passive transfer of SARS-specific monoclonal and polyclonal sera has been shown to be protective in both young and aged mouse models of human disease, as well as in humans during the SARS-CoV outbreak (197). Prophylactic treatment with monoclonal anti-SARS-CoV antibodies reduces viral load in the mouse lung and eases disease burden in mouse models of human coronavirus (CoV) infection (195, 198, 199). During the SARS-CoV outbreak, antibodies from convalescent sera of recovered patients were passively transferred to symptomatic SARS patients who had not responded to other forms of treatment. Patients receiving convalescent sera recovered from infection and rapidly cleared virus (200). Coupled with the above studies of anti-SARS-CoV antibody responses, these results suggest the importance of humoral immunity in virus clearance and convalescent sera transfer as a possible treatment for CoV infection. However, the exact role of B cells and antibodies in the control of primary infection has not yet been critically examined.

In this study, we focus on B cell and antibody responses to MA15 during the first two weeks of infection. Previous studies have shown that *Rag*^{-/-} and SCID mice, both without functional adaptive immune cells, are unable to clear MA15, whereas immunocompetent mice clear virus within 7-10 days post infection (dpi) (71). To investigate the role of lymphocytes and humoral immunity in virus clearance, we infected B cell-deficient (*muMT*^{-/-}), CD4 T cell receptor (TCR) fixed (OTII), and CD8 TCR fixed (OTI) mouse strains with MA15. While both TCR-fixed mouse strains cleared virus by 15 dpi, the *muMT*^{-/-} mice were unable to clear virus from the lung, and maintained high viral titers well past 15 dpi. Because T cells have primarily been implicated as responsible for MA15 clearance, the inability to clear virus in T cell competent, B cell deficient mice was surprising. Furthermore, we show that 7 dpi convalescent serum is capable of neutralizing MA15 *in vitro*. *In vivo*, prophylactically transferred 7 dpi convalescent sera prevented mortality in 12- and 20-week old mice challenged with a lethal dose of MA15. Together, these data indicate a major role for humoral immunity in control of primary SARS-CoV infection and signal a possible new treatment avenue for CoV-mediated disease in the context of future outbreaks.

3.2 Results

3.2.1 Activation of antibody-related networks is decreased during lethal SARS-CoV infection.

Using existing systems biology datasets for SARS-CoV infection (201), network analysis comparing lethal and sublethal MA15 challenge revealed a module eigengene (dark-red), a cluster of coordinately expressed genes regulating immunoglobulin, antibody heavy, and antibody light chain transcript expression (9). Expression of this eigengene cluster was significantly diminished

at 4 and 7 dpi in the lethal model as compared to the sublethal model of MA15 infection (Fig. 1, S. Table 1). Consistent with reports from human studies (186), these data suggest a role for B cell and antibody responses in regulating disease progression following MA15 infection. The role of early humoral immune response to MA15 infection in viral clearance and pathogenesis has yet to be systematically evaluated. Based on these factors, we decided to explore the role of B cells and antibodies within the first 7 dpi of MA15 infection.

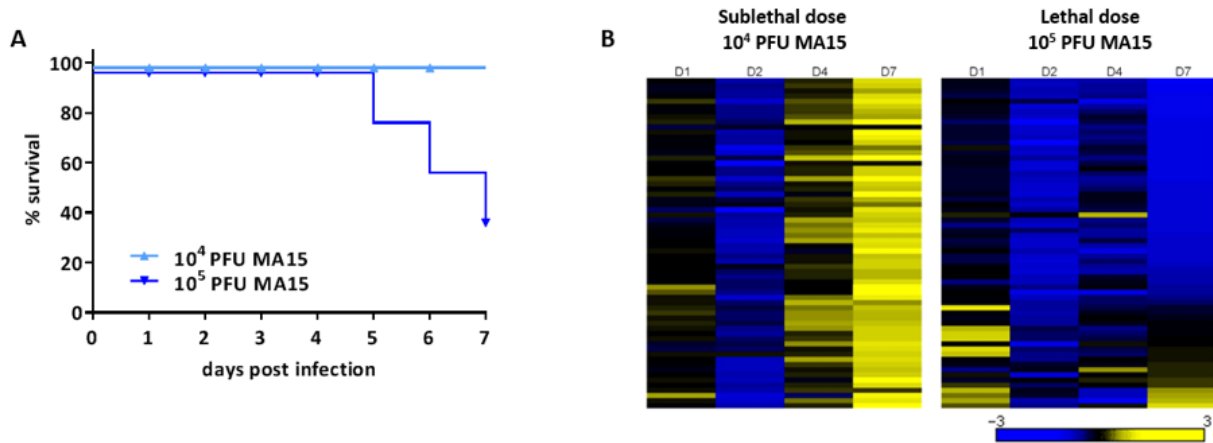


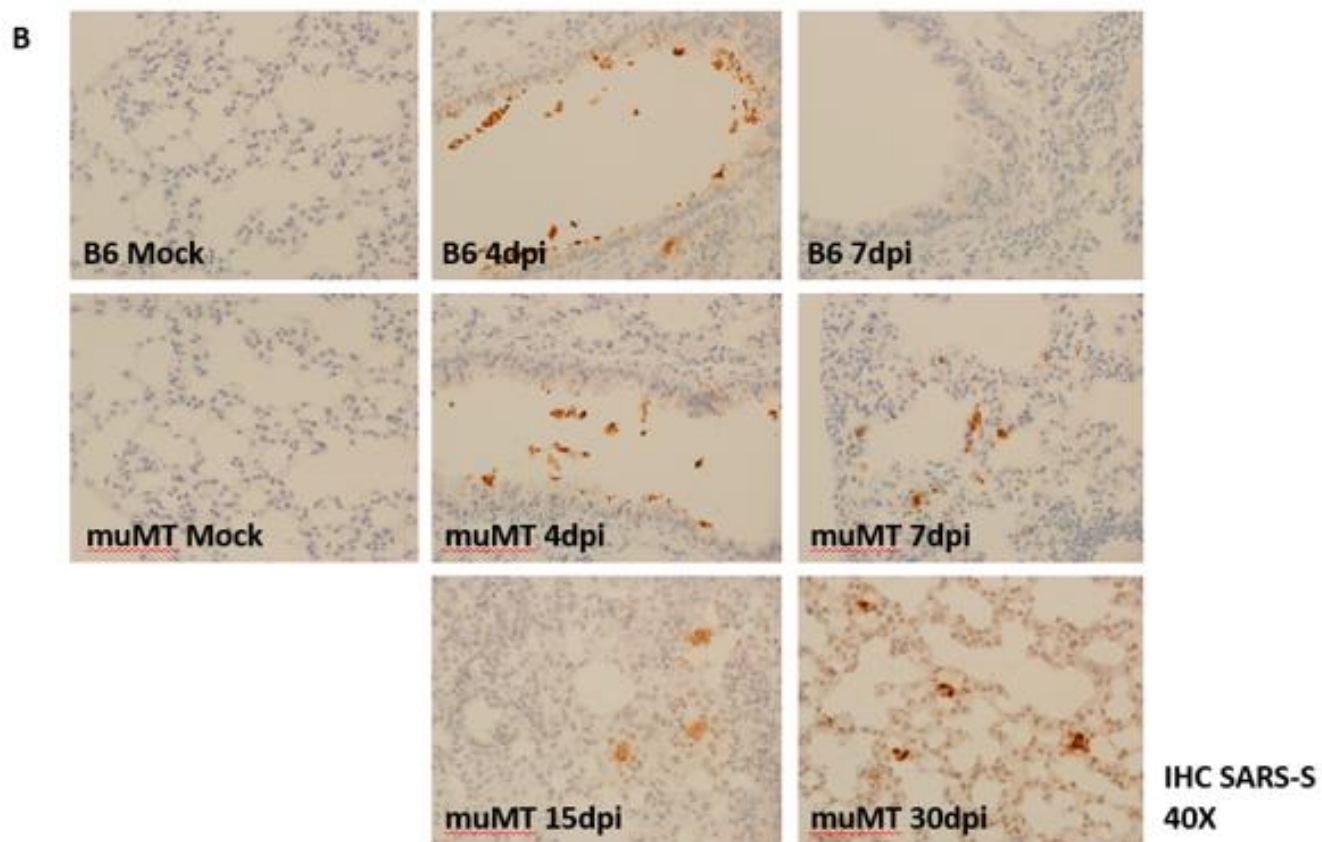
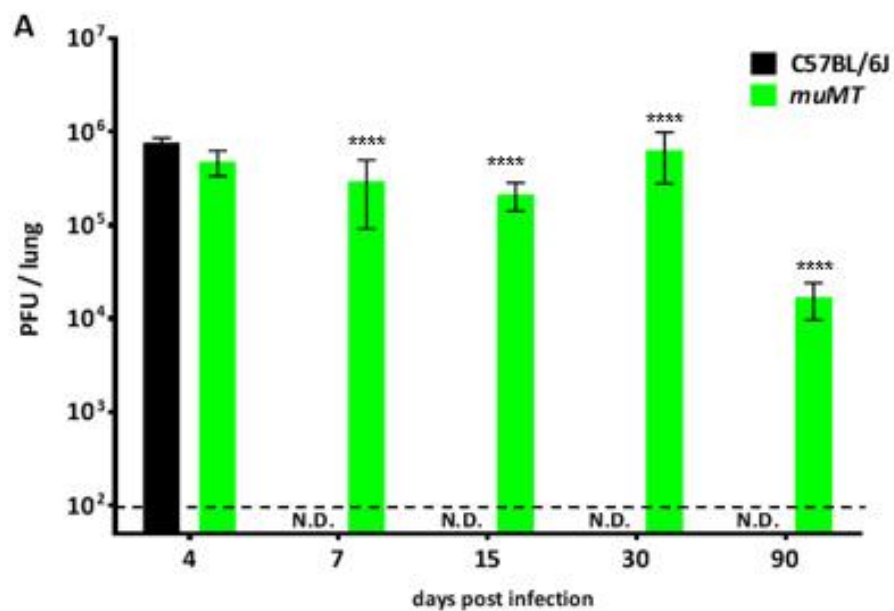
Fig 3.1. Bioinformatics points to an important role for B cells. 20 week old C57BL/6J mice were infected intranasally with a 50 μ L sublethal (10^4 PFU/mouse) or lethal (10^5 PFU/mouse) dose of MA15 SARS-CoV diluted in PBS. (A) Survival curves for infected mice. Mice dropping below 70% weight loss were humanely sacrificed and counted as succumbing to disease for the purposes of the experiment. All mice were sacrificed at 7 dpi. n=5 per group. (B) Log₂ fold change ratio of immunoglobulin family-related gene expression from the lungs of MA15 SARS-CoV-infected C57BL/6J mice after infection compared to mock infected mice. Yellow indicates increased gene expression compared to mock. Blue indicates decreased expression compared to mock. Probe and gene descriptions provided in Fig S1.

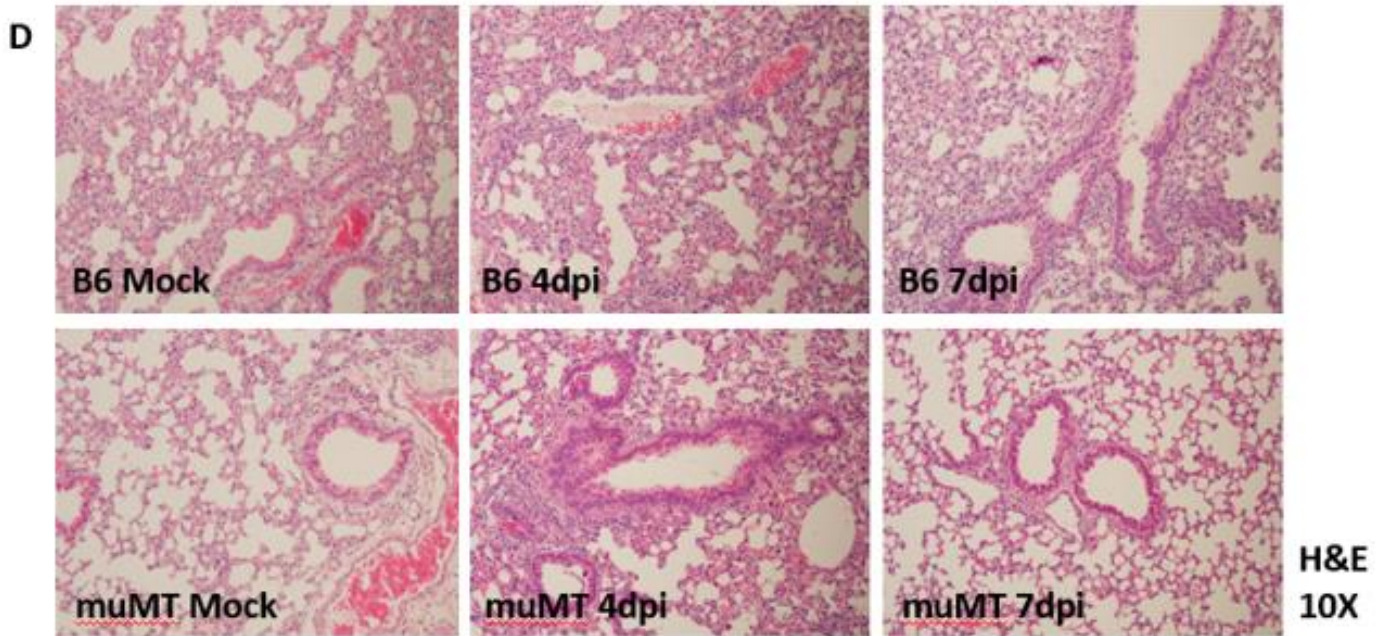
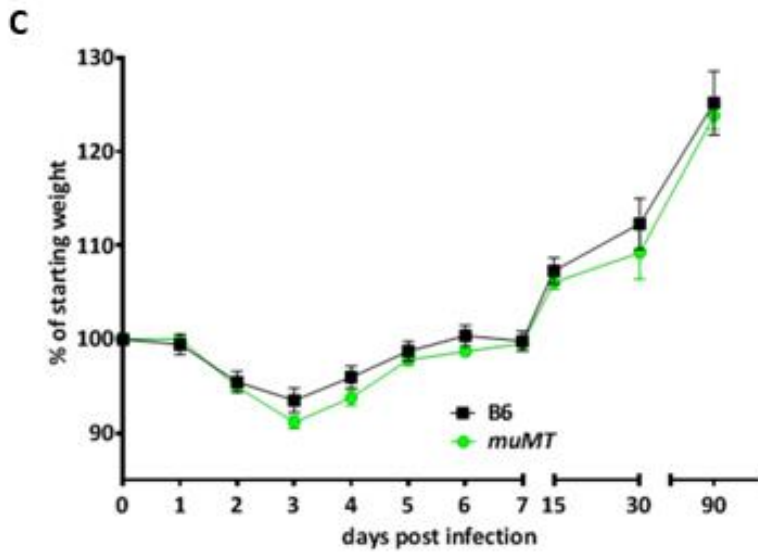
3.2.2 B cell deficient mice are not able to clear MA15.

To determine the role of B cells and antibody in viral clearance, we infected 10-week old B cell-deficient (*muMT^{-/-}*) (105) and immune intact C57BL/6J (B6) control mice with a sublethal dose of MA15, weighed and monitored mice daily, and harvested lung for titer and histology at

timepoints between 4 and 90 dpi (Fig 2) (10). As expected, control mice retained virus at high titer in the lung through 4 dpi, followed by rapid virus clearance to below the limit of detection by 7 dpi. Surprisingly, *muMT*^{-/-} mice retained high viral titers in the lung through 90 dpi despite the presence of an otherwise intact immune system. We stained lung histology sections from later timepoints for SARS N protein. In control animals, we detected no viral antigen, but SARS N antigen staining was clearly evident at late time points in the *muMT*^{-/-} model, consistent with our lung titer data (Fig 2B). Both B6 and *muMT*^{-/-} mice demonstrated equivalent weight loss and recovery, despite *muMT*^{-/-} mice retaining high virus titer in the lungs at later timepoints (Fig. 2C). Additionally, pathology scoring on histological slides showed no significant difference in lung injury or recovery between B6 and *muMT*^{-/-} mice (Fig 2D-E), suggesting that total viral clearance is not required for recovery from SARS disease, consistent with previous findings (71). These data support the hypothesis that B cells are directly or indirectly required for clearance of MA15 infection following primary challenge.

To determine whether B cell or antibody responses to SARS-CoV infection were differential between lethal and sublethal infections, we infected 20 week old B6 mice with a mock, low, sublethal, or lethal dose of MA15 (Fig. 3). We monitored mice and weight daily through 7 dpi (Fig. 3A-B), then harvested mice for lung hemorrhage scoring, flow cytometry analysis of the lung and spleen, and serum antibody titer (Fig. 3C-F). Serum antibody was analyzed by ELISA against purified SARS-S protein for anti-SARS-CoV IgG and IgM. We observed no significant differences in splenic B cell numbers, B cell activation, or serum antibody titer between infectious doses (Fig. 3F). These data together suggest that though B cell and antibody responses impact viral clearance in the lung, the lack of these responses do not impact weight loss and recovery from lung injury in the MA15 model under these treatment conditions.





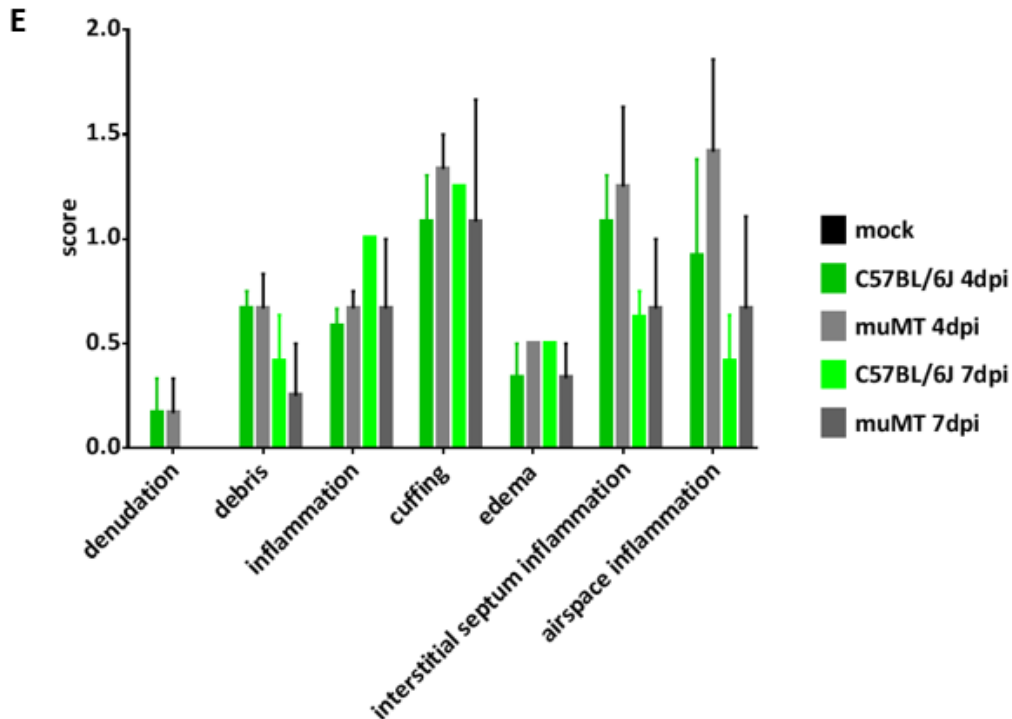
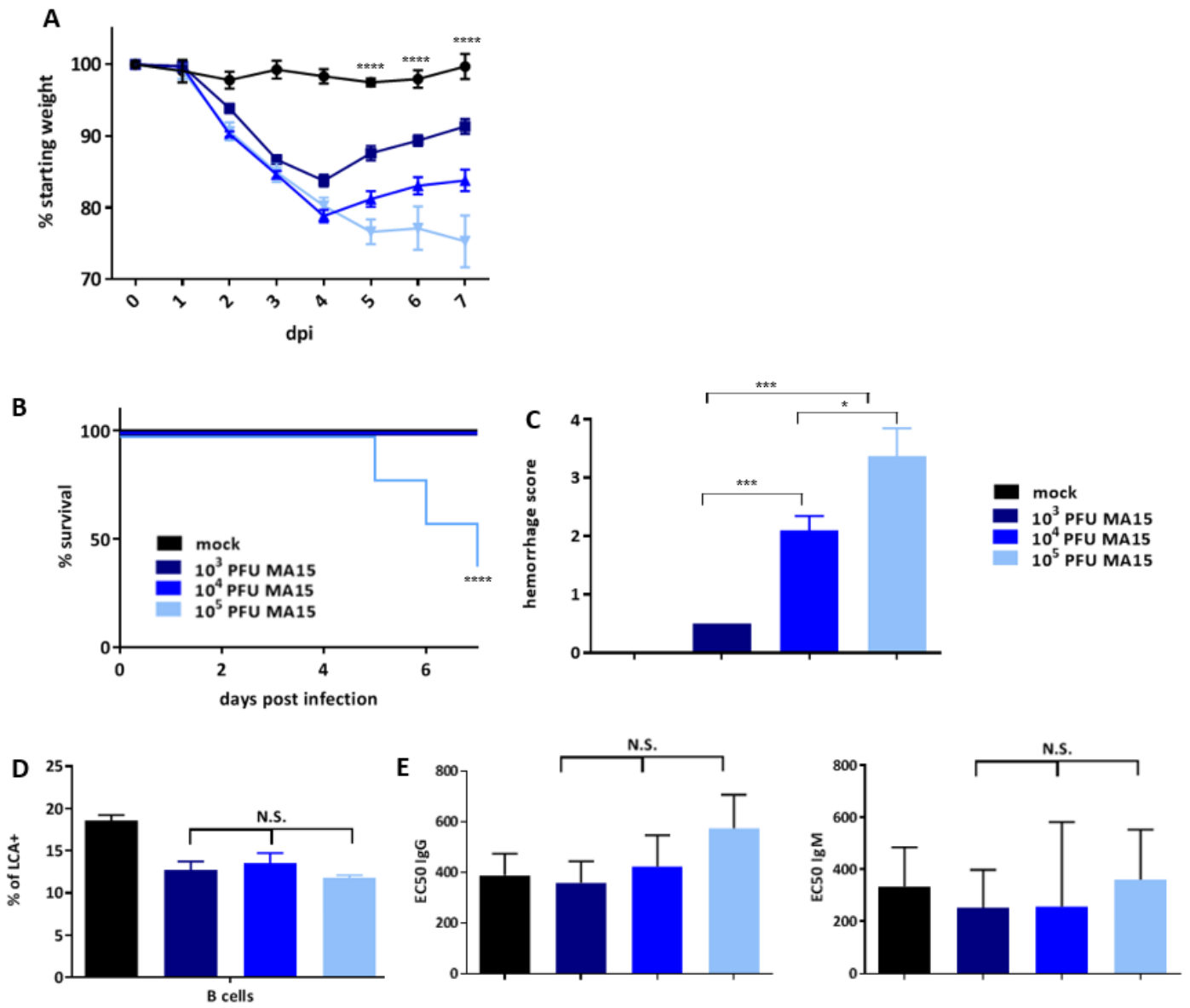


Fig 3.2. B cells are required to clear SARS-CoV. 10 week old C57BL/6J or *muMT* B cell deficient mice were infected with a sublethal dose of MA15 SARS-CoV (10^4 PFU/mouse). *n*=5/group. (A) Lung mean virus load was quantitated by plaque assay. Statistical significance determined using ANOVA analysis, with **** signifying $p < 0.0001$. (B) Representative images of lung sections at indicated timepoints post-infection. SARS-CoV staining was performed via immunohistochemistry using anti-SARS-N and is shown in brown. (C) Mean weight loss per group is represented as a percent of starting weight for each mouse. Mice were weighed daily. (D) Representative images of lung sections at indicated timepoints post-infection. H&E staining is shown. (E) Lung injury scores from mice at indicated times. None show significant differences between C57BL/6J and *muMT* mice at matched timepoints.

3.2.3 Lack of antigen-specific CD4+ T cell responses results in delayed MA15 clearance.

To further characterize interactions that may explain the critical role for B cells, we sought to evaluate the role of T lymphocytes in MA15 clearance by infecting OTI and OTII (fixed CD8 or CD4 TCR, respectively) mice with a sublethal dose of MA15 (Fig. 4) (106, 107, 202). Wild-type B6 mice were used as an immunocompetent control and *Rag*^{-/-} mice were used as an immunodeficient control. All mice displayed similar weight loss and recovery phenotypes during infection, suggesting that neither CD4+T nor CD8+T MA15-specific responses are individually required for recovery from disease (Fig. 4A). At 4 dpi, B6, OTI, OTII, and *Rag*^{-/-} mice retained high titers of MA15 in the lung. However, by 7 dpi, B6 and OTI mice had cleared virus in the lung, suggesting that MA15-specific CD8+T cells are not required for clearance in this model (Fig 3B). However, viral clearance in OTII mice was delayed until 15 dpi. These data suggest that a CD4+T cell response to MA15 infection contributes to, but is not essential for, viral clearance. Because of the importance of CD4+T cell help in B cell activation in response to viral infection (203), this delay in clearance in the OTII model points to a role for CD4+T cell activation of B cells in viral clearance during the first week of infection. Together, these data further support a role for B cell and antibody responses in MA15 clearance early in infection (87)



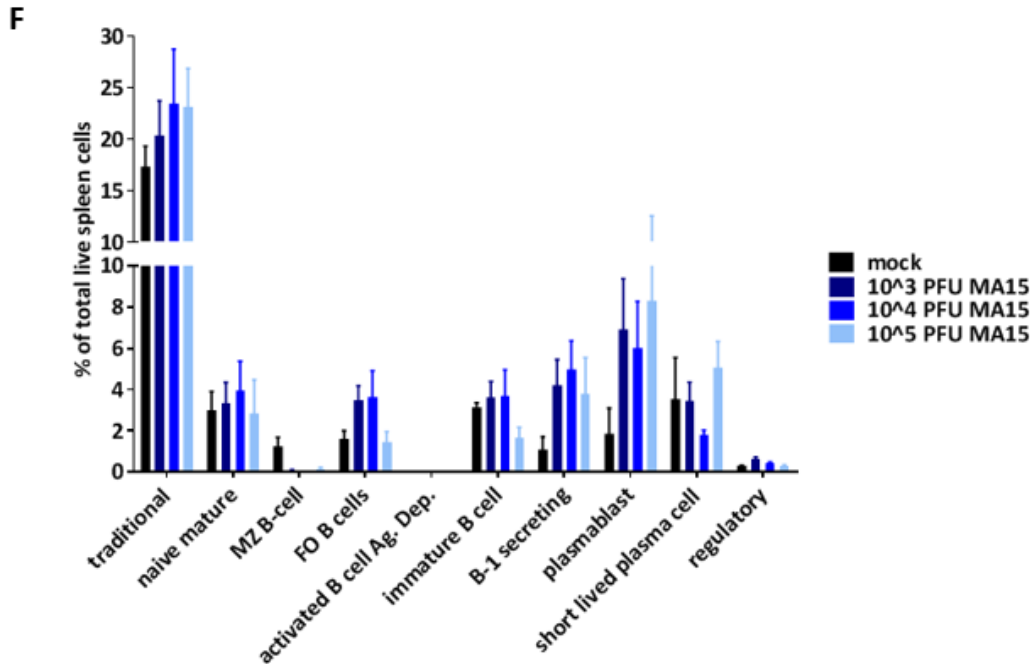


Fig 3.3. B cell and antibody responses do not correlate with pathogenesis. 20 week old mice were infected intranasally with a lethal (10^5 PFU/mouse) or sublethal (10^3 or 10^4 PFU/mouse) dose of MA15 SARS-CoV. *n*=5/group. (A) Mean weight loss per group is represented as a percent of starting weight for each mouse. Weights at each dose significantly differed from each other group at 5, 6, and 7 dpi. (B) Survival curves of infected mice. (C) Mean hemorrhage score of mouse lungs taken during 7 dpi harvest. (D) Mean total B cells as a percent of LCA+ cells. B cells are defined as B220+ and CD20+. (E) Mean SARS-S reactive immunoglobulin levels represented as EC50. (F) Splenic B cell populations after MA15 SARS-CoV infection at mock, sub-lethal, and lethal infection doses in 10 week old C57BL/6J mice – no significant differences were seen in B cell populations. All statistics performed by t test. * $p < 0.01$. *** $p < 0.0001$. **** $p < 0.00001$.

3.2.4 Antigen-specific B cells are not required for SARS-CoV clearance.

We next investigated B cell function and antigen specificity and its impact on virus control and clearance. For these purposes, we used the HELMET mouse strain, wherein B cells are present in normal levels but carry B cell receptors only reactive to HEL, the hen egg lysozyme, rendering them unable to create viral antigen-specific antibodies (109). HELMET mice were infected with a sublethal dose of MA15, as above, and were monitored and weighed daily. HELMET mice showed similar weight loss and recovery to other mouse strains (OTI, OTII, Rag^{-/-}, B6), suggesting that a

fixed BCR did not result in increased pathology during infection (Fig. 4A). However, MA15-infected HELMET mice maintained high virus titers in the lung through 7 dpi, but, eventually cleared virus infection by 15 dpi (Fig 4B). These data suggest an important role for antigen-specific B cells in early viral clearance in the lung, but are also consistent with previous findings outlining the capability of virus-specific T cells to clear virus from the lungs (88, 90, 204). Importantly, the results suggest that B cells or antibody are needed in an antigen-independent capacity to help prime T cell-mediated clearance. Together, the data indicate an overlapping and complementary role for virus-specific B and T cells in MA15 clearance in the lung.

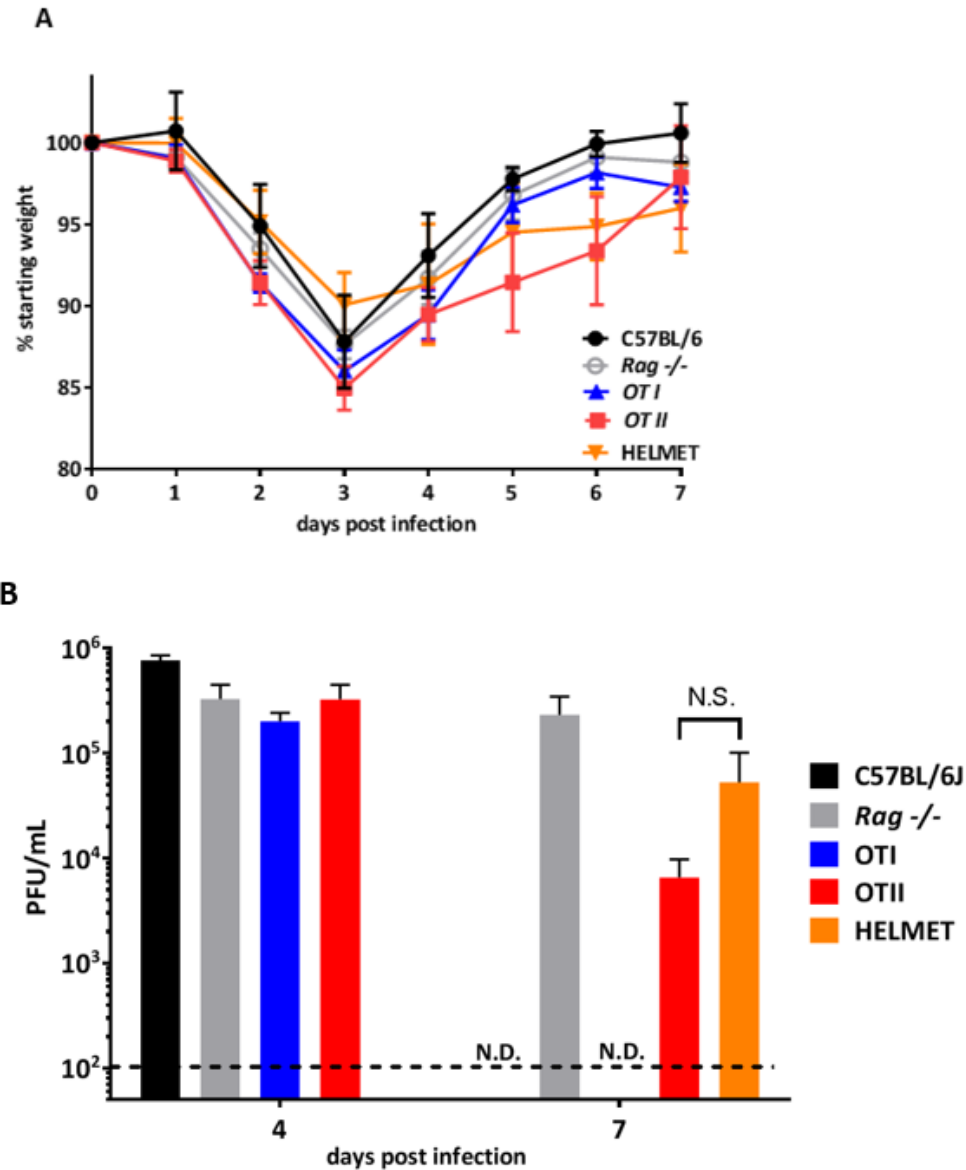


Fig 3.4. Lack of antigen-specific CD4⁺T cell responses results in delayed SARS-CoV clearance. 10 week old mice were infected with a sublethal dose of MA15 SARS-CoV (10^4 PFU/mouse). $n=5$ /group at 4 and 7 dpi. $n=3$ /group at 15 dpi. (A) Mean weight loss per group is represented as a percent of starting weight for each mouse. Mice were weighed daily. No significant difference between weight groups. (B) Lung mean virus load was quantitated by plaque assay. All statistics performed by t test.

3.2.5 Convalescent serum at 7 days post infection can efficiently neutralize MA15 *in vitro*.

In order to analyze serum antibody responses to MA15 infection over time, we infected B6 mice with a sublethal dose of MA15 and harvested sera at 4, 7, and 29 dpi (Fig. 5). We analyzed

sera for IgG and IgM antibody concentration against purified SARS-S glycoprotein. During infection, IgM responses against MA15 were established within the first week, peaked early and remained high through 29dpi (Fig. 5A). IgG responses were evident early infection, but peak titers were evident at 29dpi, which is a common antibody kinetic response to acute viral infection (205) (Fig. 5B). Sera neutralization titers were determined using Vero cell neutralization assays against MA15, with neutralization reported as the 50% effective concentration of antibody (EC50). Serum antibodies at all timepoints showed a time-dependent neutralization of MA15 (Fig 5C-D). Surprisingly, as early as 7 dpi, convalescent sera was able to efficiently neutralize virus *in vitro* and displayed similar neutralization efficiency to 15 dpi convalescent sera. This early neutralization response may explain the requirement for B cells in MA15 clearance during early MA15 infection.

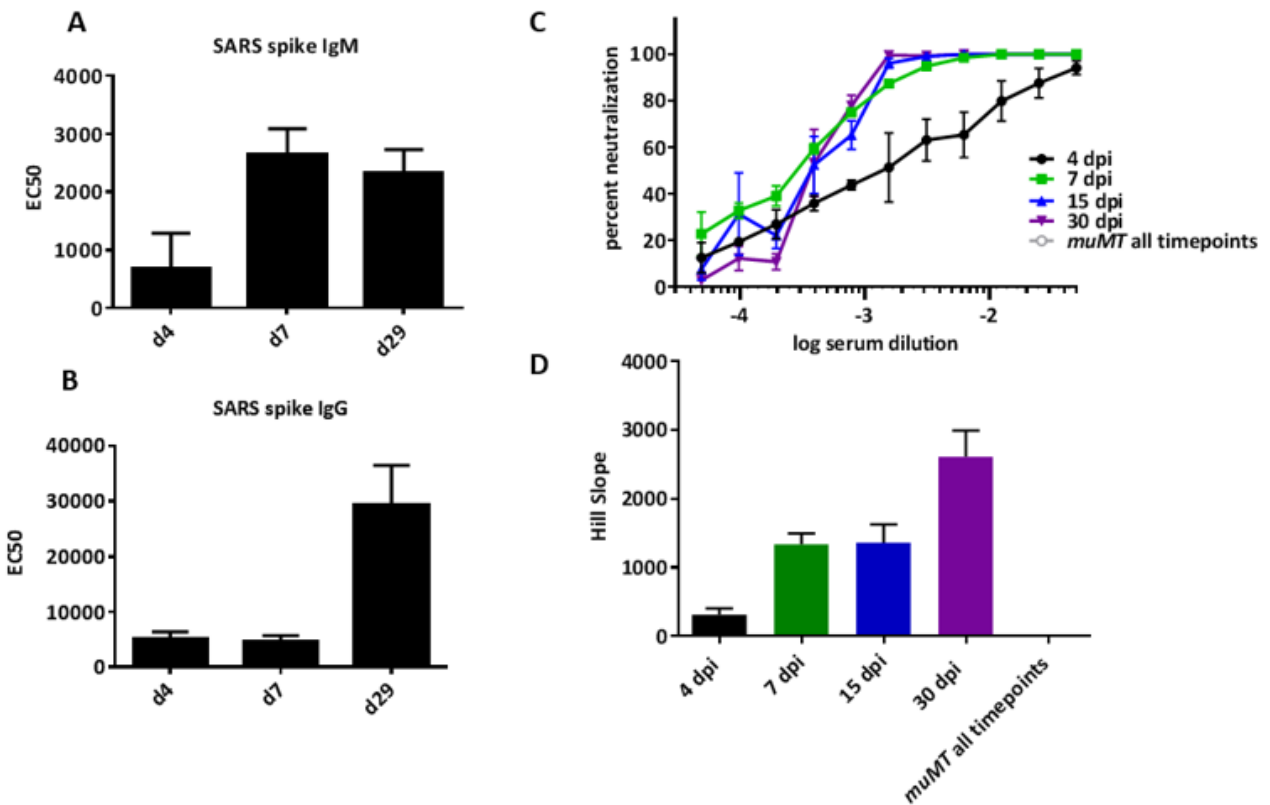


Fig 3.5. Serum antibodies at 7 days post infection can efficiently neutralize SARS-CoV *in vitro*. 10 week old mice were infected intranasally with a sublethal dose of MA15 SARS-CoV (10^4 PFU/mouse). $n=5$ /group. (A-B) Mean serum IgM (A) and IgG (B) EC₅₀ against SARS-CoV spike protein. $n=5$ mice/group. (C) SARS-CoV plaque neutralization and (D) hill slopes of neutralization curves were determined by plaque assay using serum taken from MA15 SARS-infected mice at the indicated timepoints.

3.2.6 Prophylactic transfer of early antibody protects from MA15 pathogenicity.

In order to determine whether inoculation with 7 dpi convalescent sera can protect against lethal MA15 infection, we again purified sera from MA15-infected B6 mice at 7 dpi. Sera from infected mice was pooled then used to intraperitoneally inoculate 20 week old B6 mice prior to receiving a lethal inoculation of MA15 24 hours later (Fig. 6A). We monitored mice for weight loss daily then harvested at 7 dpi or when moribund. Passive transfer of convalescent sera from 7 dpi protected mice following lethal MA15 challenge from severe disease and weight loss (Fig.

6B). These data suggest that early convalescent sera could be used prophylactically to neutralize

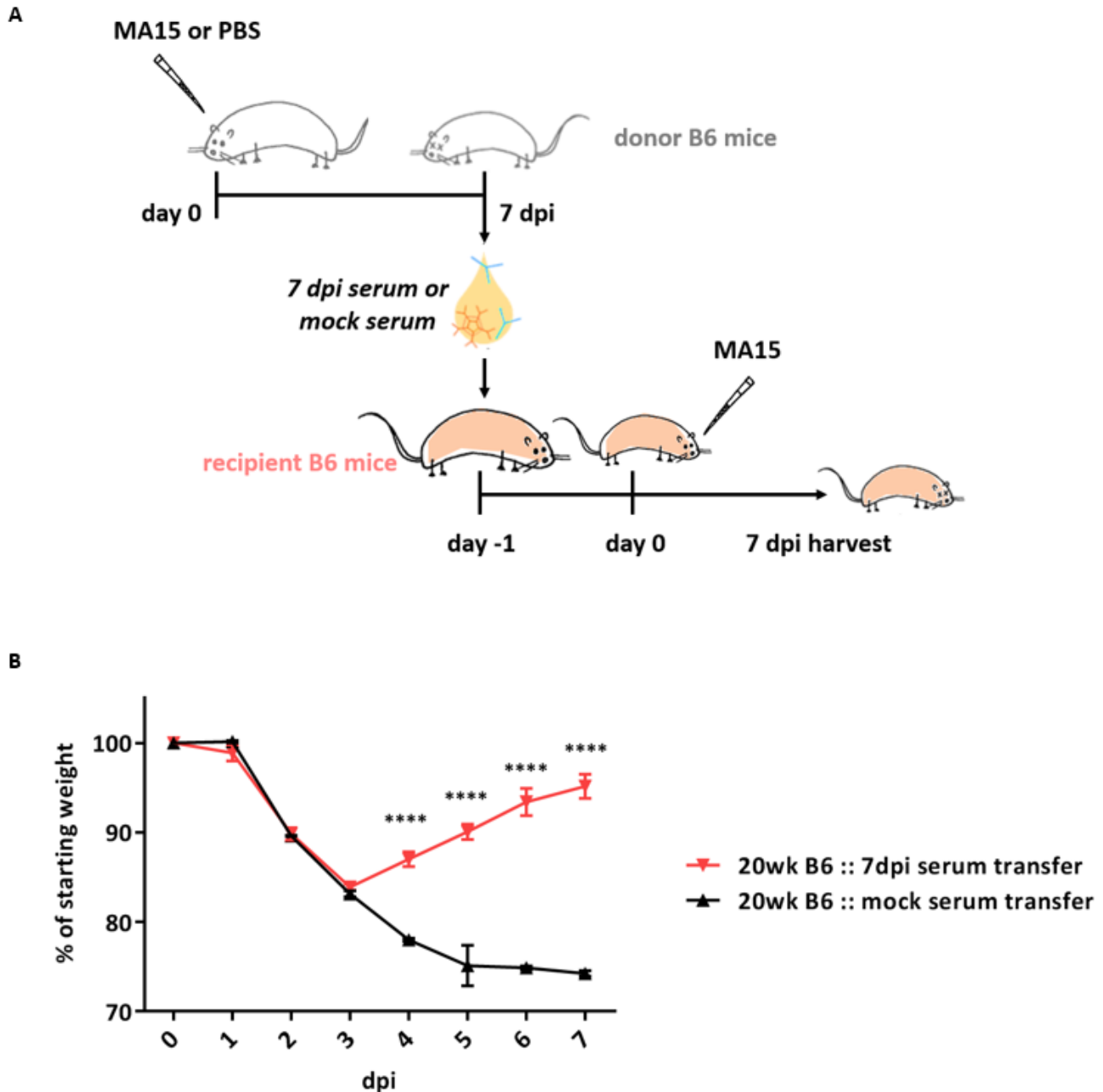


Fig 3.6. Prophylactic transfer of early antibody prevents mortality during lethal SARS-CoV infection through viral neutralization *in vivo*. Experimental set up of serum transfer experiments. C57BL/6J mice were infected with SARS-CoV at a sublethal dose and serum was harvested at the indicated time point after infection. Serum was transferred at a 1:1 ratio *i.p.* to the experimental mouse, which was infected with a lethal dose of SARS-CoV 24 hours later. Mice were weighed daily and harvested 7dpi. (A) Mean weight loss of mock serum of 7dpi serum transfer to 12 week or 20 week old C57BL/6J mice. (B) :: shorthand for received. Statistical significance determined using ANOVA analysis, with **** signifying $p < 0.0001$.

virus and prevent mortality in coronavirus infection.

3.3 Discussion

Lethal SARS-CoV infection causes an immune-mediated disease marked by dysregulated innate immune responses, cytokine levels, and T cell responses, which contribute to severe disease and death (86). Conversely, survival is associated with activation of virus-specific T cells which contribute to early virus clearance and diminish clinical disease (89, 90, 93). In this study, we extend these studies to show that B cell and antibody responses also play a critical role in disease control and virus clearance during MA15 infection in lethal B6 mouse models. Using a systems based approach, we utilized eigengene modules to predict an important role for B cell responses in protection from lethal disease outcomes, then used a panel of genetically immunodeficient mice and convalescent serum transfer experiments to support the hypothesis that early B cell and antibody responses also play an important role in protection from severe MA15 infection and by contributing to virus clearance.

Our systems biology approach applies robust statistical modeling to large expression datasets in order to discover coordinated expression patterns associated with lethal and sublethal viral infections. This has led to the discovery of key signaling and expression pathways in SARS-CoV pathogenesis and disease (72, 201, 206, 207). As in human infections (186), transcriptomic analysis comparing lethal and non-lethal MA15 infection of the mouse lung revealed that B cell activation and antibody production was impaired in lethal, but not sublethal, infection, suggesting a role for humoral immunity in SARS-CoV pathogenesis and clearance. Additionally, previous studies have shown that while MA15 was cleared from the lungs of wild-type mice within 7 dpi, immunodeficient SCID and *Rag*^{-/-} mice retained high titers of virus in the

lung up to three weeks after infection (32, 71). Because SCID and *Rag*^{-/-} mice lack functional lymphocytes, these findings pointed to a critical role for lymphocytes in viral clearance within the first week of infection.

During primary infection, SARS-CoV infects the lung epithelium where dendritic cells are able to sequester viral antigen and migrate to the lymph node in order to activate lymphocytes through direct antigen presentation, MHC activation, and secondary activation signals (101). Consequently, virus-specific T cells act as effectors that activate and recruit subsequent immune cell populations (86). Additionally, virus-specific T cells migrate to the site of infection and secrete antiviral cytokines, chemokines, and cytotoxic molecules which lead to inflammation, increased antigen presentation, inhibition of viral replication, and direct killing of virus-infected cells (86, 101). Based on current studies, SARS-CoV clearance and survival early after infection is thought to be heavily regulated by T cell activities, as opposed to B cell or antibody-mediated processes. After coronavirus infection, T cell responses can be either pathogenic or protective, depending on the virus strain and host species (208). However, Chen et al. determined that depletion of CD4⁺T cells, but not CD8⁺T cells, delayed viral clearance and led to a poor virus-specific antibody response in aged Balb/c mice in response to SARS-CoV Urbani infection, suggesting a role for helper T cell activation of B cells and subsequent antibody-aided viral clearance (87).

Building on this observation, immunocompromised *Rag*^{-/-} mice fail to clear another coronavirus, murine hepatitis virus (MHV-1), instead maintaining high viral titers within the lung for weeks following primary infection (71, 209). Additionally, Chachu et al. determined that *muMT*^{-/-} and HELMET mice did not clear murine norovirus as efficiently as immunocompetent mice due to a lack of virus-specific antibody responses (210). Consonant with

our findings reported with SARS-CoV, adoptive transfer of polyclonal or monoclonal antibodies against murine norovirus led to viral clearance, suggesting a distinct role for antibody in virus clearance (210, 211). In the case of adoptive transfer of virus-neutralizing antibody, various SARS-CoV studies have used exogenous monoclonal SARS-specific IgG to induce sterilizing immunity to primary infection but also to drive virus clearance (197, 199). These data demonstrate that virus-specific antibody will protect animals from lethal disease and clear virus after infection

Based on a number of elegant studies (86, 88, 90, 91), it is clear that T cell responses play a significant role in SARS-CoV clearance and the control of severe disease outcomes (72, 206, 207). In our study, *muMT*^{-/-} mice, lacking mature B cells and membrane-bound IgM, were not able to clear MA15 virus. Our *muMT*^{-/-} findings are novel to the current dogma of the field and support a significant role for B cells in MA15 clearance. Consonant with our findings, influenza, a respiratory (-)ssRNA virus, is not efficiently cleared from the lungs of *muMT*^{-/-} mice (204). However, MA15 failed to be effectively cleared even after 90 dpi, when high viral titers were still present in the lung. These data support the hypothesis that B cell and/or antibody responses are required for MA15 clearance during primary infection. While *muMT*^{-/-} mice lack mature B cells in the B6, but not BALB/c (212) mouse model, we note that *muMT*^{-/-} mice can also use a different pathway to produce some CD19⁺/CD0⁺/IgD⁺ B1 cells and to produce non-specific IgE and IgG antibodies (213). However, our data suggest that these cells and activities do not appear to function in MA15 clearance.

To address the role of T lymphocytes in our MA15 clearance model, we investigated whether mice deficient in virus-specific CD4⁺T cells (OTII) or CD8⁺T cells (OTI) showed the same inability to clear virus that was seen in *Rag*^{-/-}, SCID, and *muMT*^{-/-} mice. OTI mice, which

lack a virus-specific CD8+T cell response, were able to clear virus on the same timescale as B6 mice, while OTII mice, which lack a virus-specific CD4+T cell response, demonstrated delayed viral clearance in the lung. These data corroborate previous findings in which depletions of CD4+T cells and CD8+T cells in senescent Balb/c demonstrated delayed MA15 clearance after infection (87). One of the primary roles of CD4+T cells during a respiratory viral infection is to help in B cell activation (203). After infection, B cells are primed by viral antigen binding the B cell receptor, then activated by CD4+T cells via CD40/CD40L and cytokine signaling (214). Activated B cell can then divide and produce antigen-specific antibodies (215). While other cell types are capable of activating B cells, CD4+T cells are primarily responsible for robust B cell activation during the first days of viral infection (203). It is likely that the observed delay of MA15 viral clearance in OTII mice, or CD4+ T cell depleted mice in Chen et. al. (87), is likely due to impaired B cell activation and therefore delayed or weakened antibody responses. Because HELMET mice eventually clear virus, the data also support the idea that antigen non-specific B cells may play a key role in T cell priming/help and T cell-mediated clearance.

Passive immunotherapy approaches are being developed to prevent and treat several human medical conditions where alternative therapeutic options are absent, including MERS-CoV infection (216, 217). Our data support previous passive transfer experiments in humans, which have appeared to enhance protection from lethal disease after SARS-CoV infection (200). In support of these findings, we showed that 7 dpi convalescent mouse sera was able to efficiently neutralize MA15 in in vitro neutralization assays. Moreover, prophylactic transfer of 7 dpi convalescent sera significantly protected mice in a lethal MA15 challenge. While sera was chosen from patients late after infection and with high antiviral IgG and IgM titers (26), our data suggests that neutralizing sera isolated early from convalescent patients who experienced mild,

but not severe infections could protect from severe disease and mortality. The ongoing MERS-CoV outbreak and discovery of SARS-like CoVs circulating in bats and other wild animals suggest that recurrence of another coronavirus-mediated disease remains a possibility (198, 199, 218, 219) and that passive immunotherapy might serve as a rapid response treatment option (216). Thus, rapid treatment using sera transfer could be an important factor in suppressing viral replication and mortality in the early days of an outbreak.

Our systems based studies clearly demonstrated significant differences in B cell immunoglobulin gene expression responses following lethal infection in mice. In humans, patients with poor outcomes had poor ISG and immunoglobulin gene expression levels, persistent chemokine levels, and deficient anti-SARS spike antibody production as well (186), demonstrating concordant outcomes in mouse and human models. SARS-CoV clearance is a complex phenotype both in humans and in mice and is heavily regulated by both T cell function and early induction of neutralizing antibodies. Future studies focusing of the role of B cell activation and antibody secretion in the initial days of viral infection may provide critical new insights into pathogenic mechanisms of emerging coronaviruses, leading to new therapeutic regimens for disease control and public health preparedness. As several zoonotic SARS-like viruses are poised for reemergence, these data suggest that optimal SARS-CoV vaccines should elicit robust antibody and memory T cell responses.

3.4 Methods

ETHICS STATEMENT AND BIOSAFETY

Mouse studies were carried out in accordance with the recommendations for the care and use of animals by the Office of Laboratory Animal Welfare at the NIH. IACUC at UNC-CH approved the animal studies performed under IACUC protocol 15-155. All virus work was

performed in a certified biosafety level 3 (BSL3) laboratory containing redundant exhaust fans while wearing personal protective equipment including HEPA-filtered powered air purifying respirators, Tyvek suits, hoods, and boots; work was additionally confined to a class II biological safety cabinet.

CELL CULTURE AND VIRUS

Recombinant mouse-adapted SARS-CoV (MA15) was generated, passaged once, and titered on Vero E6 cells. For viral titering, the right bottom lobe of each mouse was homogenized then serially diluted to assess plaque forming units (PFU) in Vero E6 cells, with a detection limit of 100 PFU, as previously described by our group (188).

ANIMALS AND INFECTIONS

Mice were obtained from the Jackson labs (Bar Harbor, ME), housed and bred in pathogen-free conditions in accordance with guidelines established by the Department of Comparative Medicine at UNC-CH. Strains used include C57BL/6J (B6), *muMT*^{-/-}, HELMET (HELMET), *Rag*^{-/-}, OTI, and OTII mice. All mice were female. During infection, mice were maintained in SealSafe ventilated caging system in a BSL3 laboratory, equipped with redundant fans as previously described by our group (5). Before viral infection, mice were anesthetized by administering 50 µl ketamine/xylazine mixture intraperitoneally and then infected intranasally with 50 µl virus solution or control PBS. 10-week old mice were used in sublethal models or 20-week old mice in lethal models. Twenty week aged mice were infected with 10⁴ PFU MA15, a lethal dose and 10-12-week old mice were infected with 10⁵ PFU MA15, a sublethal dose (201). Following sedation and infection, mice were monitored daily for weight loss and survival, as well as for signs that the animals were moribund (including labored breathing, lack of movement and lack of grooming). Mice that reached 20% weight loss were placed under exception and

monitored at least twice daily. Mice deemed moribund or near 30% weight loss were euthanized at the discretion of the researcher. Mice were euthanized with an isoflurane overdose followed by major organ removal, at various time points, to collect lung tissues. Cervical dislocation was used as a secondary euthanasia method. All are approved methods of the Institutional Animal Care and Use Committee (IACUC) at the UNC-CH.

ELISA AND NEUTRALIZATION ASSAYS

ELISA plates were coated in carbonate buffer (0.8ug/mL of SARS-S antigen) overnight and blocked at 4°C, before serum was serially diluted 2-fold 10 times with 3 replicates per sample and added to a 96-well plate. HRP conjugated secondary was used at 1:2000 for 1 hour, then developed in Thermo Scientific Pierce 1-Step Ultra TMB ELISA Substrate then stopped in 0.1M sodium fluoride, and read by plate reader at 450nm.

To perform plaque reduction neutralization assays (PRNT₅₀) serum was serially diluted 2-fold and incubated with 100 PFU of the MA15 for 1 hour at 37°C. The virus and antibodies were then added to a 6-well plate with 1×10^5 Vero E6 cells/well with n=2 replicates per sample. After 1 hour incubation, cells were overlaid with 0.8% agarose in media. Plates were incubated for 48 hours then stained with neutral red for 3 hours, and plaques were counted. The percentage of plaque reduction was calculated as $[1 - (\text{no. of plaques with antibody}/\text{no. of plaques without antibody})] \times 100$.

HISTOLOGICAL ANALYSIS AND LUNG SCORING

Lung samples were fixed in 10% phosphate-buffered formalin for >7 days, then moved to new formalin solution at 4°C before removal from BSL3. Fixed samples were then placed in cassettes, rehydrated, and moved to ethanol solution prior to submission to the Lineberger Comprehensive Cancer Center Animal Histopathology Core for processing and sectioning.

Histopathology tissue sections were boiled in Tris-EDTA buffer for antigen retrieval, then stained using anti-SARS-S antibody and HRP-conjugated secondary antibody. HRP was developed using DAB (Thermo Scientific Metal Enhanced DAB Substrate Kit), then counterstained. Histopathology was scored, blinded to infection and animal status, for airway disease, vascular disease, parenchymal pneumonia, diffuse alveolar damage, eosinophils and immunohistochemistry on a scale of 0–3 (0, none; 1, mild; 2, moderate; 3, severe). Gross hemorrhage of lung tissue was observed during harvest and scored on a scale of 0 (no hemorrhage in any lobe) to 4 (extreme and complete hemorrhage in all lobes of the lung).

FLOW CYTOMETRY

The left lung of each mouse was used for flow cytometric staining of inflammatory cells. Mouse lungs were perfused with PBS before harvest. Tissue was dissected and digested in RPMI (Gibco) supplemented with DNase and Collagenase (Roche) in an incubated shaker. Samples were strained using a 70 micron filter (BD) and any residual red blood cells were lysed using ACK lysis buffer, stained, then fixed in 2% formalin solution. Cells were stained in three separate panels using: (1) FITC anti-Ly-6C clone AL21 (BD), PE anti-SigLecF clone E50-2440 (BD), PETR anti-CD11c clone N418 (MP), PerCP anti-B220 clone RA3-6B2 (MP), PE-Cy7 anti-Gr-1 clone RB6-8C5 (eBio), eF450 anti-CD11b clone M1/70 (eBio), APC anti-LCA clone 30-F11 (eBio), APC-eF780 anti-MHC class II clone M5/114 (eBio) or (2) FITC anti-CD94 clone 18d3 (eBio), PE anti-CD3E clone 145-2C11 (eBio), PETR anti-CD4 clone RM4-5 (MP), PerCP anti-CD8 clone 53–6.7 (BD), PE-Cy7 anti-CD49b clone DX5 (eBio), eF450 anti-LCA clone 30-F11 (eBio), AF647 anti-CD19 clone 6D5 (Biolegend), APC-eF780 anti-B220 clone RA3-6B2 (eBio), (3) BB515 anti-CD19 (BD), APC-R700 CD45R (BD), BV606 anti-IgD (BD), BV421 anti-IgM (BD), PE anti-CD21 (BD), APC anti-CD138 (BD), BV737 anti-CD80 (BD), BV786

anti-CD5 (BD), APC-Cy7 anti-MHCII (BD). Samples were run in the UNC Flow Cytometry Core Facility on a Beckton Dickinson LSR II and analyzed in FlowJo, as previously described by our group (220).

ADOPTIVE SERUM TRANSFER

Whole blood was harvested from infected or mock-infected animals at various timepoints after infection and moved to EDTA serum tubes then centrifuged to remove cells and debris. Serum was collected, measured for volume, and pooled by harvest date and stored at -80°C. A 1:1 volume (500uL) of serum was transferred to uninfected mice intraperitoneally one day prior to intranasal infection. Infection and subsequent mouse handling were performed as described above.

GENE ANALYSIS AND NETWORK MODULES

All infection response networks, network modules, and heat maps were generated and analyzed within our previous publication (28).

Supplementary Table 3.1. Heat map genes in order of display in Figure 1

Probe	Gene	Description
A_51_P1033 64	ENSMUST0000010 3552	Immunoglobulin heavy chain V gene segment [Source:IMGT/GENE_DB;Acc:IGHV1S12] [ENSMUST00000103552]
A_51_P1047 68	ENSMUST0000010 3498	Immunoglobulin heavy chain V gene segment [Source:IMGT/GENE_DB;Acc:IGHV1S55] [ENSMUST00000103498]
A_51_P1282 48	Igh	Mouse IgMk rearranged heavy-chain mRNA variable region (V-D-J) anti-DNA autoantibody [M20831]
A_51_P1507 05	Igj	Mus musculus immunoglobulin joining chain (Igj), mRNA [NM_152839]
A_51_P1507 10	Igj	Mus musculus immunoglobulin joining chain (Igj), mRNA [NM_152839]
A_51_P1835 81	Pou2af1	Mus musculus POU domain, class 2, associating factor 1 (Pou2af1), mRNA [NM_011136]
A_51_P2031 48	AB017433	Mus musculus mRNA for anti-IL-18 IgG heavy chain, clone 125-2H, partial cds. [AB017433]
A_51_P2307 16	Igh-VJ558	K0727F04-5N NIA Mouse Hematopoietic Stem Cell (Lin- [CA578712]
A_51_P2708 07	Tnfrsf17	Mus musculus tumor necrosis factor receptor superfamily, member 17 (Tnfrsf17), mRNA [NM_011608]
A_51_P2723 41	EG211331	BY724721 RIKEN full-length enriched, adult male aorta and vein Mus musculus cDNA clone A530011I23 5'. [BY724721]
A_51_P2882 95	ENSMUST0000010 3496	Immunoglobulin heavy chain V gene segment [Source:IMGT/GENE_DB;Acc:IGHV1-7] [ENSMUST00000103496]
A_51_P2988 02	Bfsp2	Mus musculus beaded filament structural protein 2, phakinin (Bfsp2), mRNA [NM_001002896]
A_51_P3282 75	ENSMUST0000010 3505	Immunoglobulin heavy chain V gene segment [Source:IMGT/GENE_DB;Acc:IGHV1S45] [ENSMUST00000103505]
A_51_P3466 81	A75Y090902	Mus musculus clone GN-2-M1 monoclonal anti-alpha-1,3- galactosyltransferase IgM heavy chain mRNA, partial cds [AY090902]
A_51_P4056 38	LOC544905	601217727F1 NCI_CGAP_Lu29 Mus musculus cDNA clone IMAGE:3586566 5'. [BE371942]
A_51_P4428 89	LOC639988	PREDICTED: Mus musculus similar to Ig heavy chain V region VH558 A1/A4 precursor (LOC639988), mRNA [XM_916675]
A_51_P4521 53	2010001M09Rik	Mus musculus RIKEN cDNA 2010001M09 gene (2010001M09Rik), mRNA [NM_027222]
A_51_P4619 02	L22886	Mus musculus rearranged IgH mRNA, V-region, cell line Cyd- 1. [L22886]
A_51_P4767 57	Igh-VJ558	Mus musculus adult male testis cDNA, RIKEN full-length enriched library, clone:1700110L11 product:immunoglobulin heavy chain, (J558 family), full insert sequence. [AK007163]

A_51_P5037 57	Igl-V1	Mus musculus adult male small intestine cDNA, RIKEN full-length enriched library, clone:2010004G10 product:immunoglobulin lambda chain, variable 1, full insert sequence. [AK008094]
A_51_P5137 70	ENSMUST0000010 3535	Immunoglobulin heavy chain V gene segment [Source:IMGT/GENE_DB;Acc:IGHV1S5] [ENSMUST00000103535]
A_51_P5159 85	U55685	Mus musculus anti-DNA immunoglobulin light chain IgG, antibody 452s.36, partial cds. [U55685]
A_52_P1054 013	AK041235	Mus musculus adult male aorta and vein cDNA, RIKEN full-length enriched library, clone:A530093J23 product:immunoglobulin heavy chain 4 (serum IgG1), full insert sequence. [AK041235]
A_52_P1390 27	Igh-VJ558	Mus musculus J558+ IgM heavy chain mRNA, hybridoma clone ME2B7, partial cds. [U39781]
A_52_P1462 6	Igk-V33	Mus musculus activated spleen cDNA, RIKEN full-length enriched library, clone:F830304C16 product:Ig kappa chain V-VI region XRPC 44 homolog [Mus musculus], full insert sequence [AK157689]
A_52_P1492 35	Mel13	Mouse anti-idiotypic antibody-resistant variant IgK (Vk-Ox1 gene family) mRNA, VJ5 region [M57586]
A_52_P1518 87	Igh-VJ558	Mus musculus adult male testis cDNA, RIKEN full-length enriched library, clone:1700110L11 product:immunoglobulin heavy chain, (J558 family), full insert sequence. [AK007163]
A_52_P1740 00	AB070542	Mus musculus VH186.2-D-J-IgG1 mRNA, partial cds, sequence:kec-5. [AB070542]
A_52_P2134 83	Ighv1-77	PREDICTED: Mus musculus similar to Ig heavy chain V region VH558 A1/A4 precursor (LOC619994), mRNA [XM_138377]
A_52_P2144 37	EG668544	PREDICTED: Mus musculus similar to Ig heavy chain V region VH558 A1/A4 precursor (LOC668544), mRNA [XM_001002167]
A_52_P2251 58	NAP113251-1	Unknown
A_52_P2382 30	AF152371	Mus musculus kappa light chain of Mab7 mRNA, partial cds. [AF152371]
A_52_P2462 48	AF240166	Mus musculus MRP3 mRNA, complete cds. [AF240166]
A_52_P2597 79	LOC631531	Immunoglobulin heavy chain V gene segment [Source:IMGT/GENE_DB;Acc:IGHV1S4] [ENSMUST00000103523]
A_52_P3064 1	Gm459	Immunoglobulin Kappa light chain V gene segment [Source:IMGT/GENE_DB;Acc:IGKV4-86] [ENSMUST00000103337]
A_52_P3584 06	ENSMUST0000010 3518	Immunoglobulin heavy chain V gene segment [Source:IMGT/GENE_DB;Acc:IGHV1-47] [ENSMUST00000103518]
A_52_P3831 14	Igl-V1	Mus musculus anti-deoxynivalenol scFv lambda light chain variable region mRNA, partial cds. [AY151141]
A_52_P3857 67	BC055911	Mus musculus cDNA clone MGC:68301 IMAGE:3662102, complete cds. [BC055911]

A_52_P4492 14	Gm1418	PREDICTED: Mus musculus gene model 1418, (NCBI) (Gm1418), mRNA [XM_357683]
A_52_P4502 76	Igl-V1	Mus musculus immunoglobulin lambda chain (IgL) mRNA, complete cds. [M94350]
A_52_P4636 37	AY895789	Mus musculus clone RLS1478F immunoglobulin heavy chain (Igh) mRNA, partial cds. [AY895789]
A_52_P4690 09	AY182513	Mus musculus clone BaFL-P40 immunoglobulin heavy chain variable region mRNA, partial cds. [AY182513]
A_52_P4769 89	AF210281	Mus musculus isolate B880 immunoglobulin heavy chain variable region mRNA, partial cds. [AF210281]
A_52_P4778 6	AB069910	Mus musculus V303-D-J-C mu mRNA, partial cds, sequence:R2-10. [AB069910]
A_52_P4791 63	NAP106724-1	Unknown
A_52_P4800 19	L48666	Mus musculus (cell line C3H/F2-15) chromosome 12 anti-DNA antibody heavy chain mRNA. [L48666]
A_52_P4904 70	NP614311	GB AF459850.1 AAO59848.1 immunoglobulin heavy chain VDJ region [Mus musculus] [NP614311]
A_52_P4925 32	Gm189	Mus musculus single chain Fv antibody (E4(Fv)) mRNA, partial cds [AF025535]
A_52_P5327 69	Igh	Mouse IgMk rearranged heavy-chain mRNA variable region (V-D-J) anti-DNA autoantibody [M20831]
A_52_P5440 90	AF218659	Mus musculus clone nMeV21 immunoglobulin heavy chain variable region mRNA, partial cds. [AF218659]
A_52_P5595 66	ENSMUST0000010 3527	Immunoglobulin heavy chain V gene segment [Source:IMGT/GENE_DB;Acc:IGHV1-56] [ENSMUST00000103527]
A_52_P5651 06	NAP107273-1	Unknown
A_52_P5656 36	AY172876	Mus musculus clone BApecB1a-P3 immunoglobulin heavy chain variable region mRNA, partial cds. [AY172876]
A_52_P5784 36	Gm1418	PREDICTED: Mus musculus gene model 1418, (NCBI) (Gm1418), mRNA [XM_357683]
A_52_P5820 68	ENSMUST0000010 3351	Immunoglobulin Kappa light chain V gene segment [Source:IMGT/GENE_DB;Acc:IGKV4-63] [ENSMUST00000103351]
A_52_P5854 3	Gm1524	AGENCOURT_10055965 NCI_CGAP_Co24 Mus musculus cDNA clone IMAGE:6479347 5', mRNA sequence [BQ937284]
A_52_P6142 07	BC080787	Mus musculus immunoglobulin kappa chain complex, mRNA (cDNA clone MGC:91220 IMAGE:4206216), complete cds. [BC080787]
A_52_P6223 55	Igl-V1	Mus musculus adult male small intestine cDNA, RIKEN full-length enriched library, clone:2010007E08 product:immunoglobulin lambda chain, variable 1, full insert sequence. [AK008145]
A_52_P6381 00	AB070552	Mus musculus V102-D-J-IgG1 mRNA, partial cds, sequence:lec-8. [AB070552]
A_52_P6488 24	X12388	Mouse hybridoma 10B10S mRNA for IgM(b) heavy chain variable region V(H)-J(H)2. [X12388]

A_52_P6729 03	Igl-V1	Mus musculus adult male small intestine cDNA, RIKEN full-length enriched library, clone:2010007E08 product:immunoglobulin lambda chain, variable 1, full insert sequence. [AK008145]
A_52_P6863 92	Igh-VJ558	Mus musculus adult male testis cDNA, RIKEN full-length enriched library, clone:1700110L11 product:immunoglobulin heavy chain, (J558 family), full insert sequence. [AK007163]
A_52_P8294 08	Igl-V1	Mus musculus adult male small intestine cDNA, RIKEN full-length enriched library, clone:2010007E08 product:immunoglobulin lambda chain, variable 1, full insert sequence. [AK008145]

CHAPTER 4: RELATIVE IMPACTS OF DIET INDUCED OBESITY AND GENETICS ON SUSCEPTIBILITY TO SARS-CoV INFECTION IN THE MOUSE

4.1 Introduction

The recent Severe Acute Respiratory Syndrome Coronavirus (SARS-CoV) and ongoing Middle East Respiratory Syndrome Coronavirus (MERS-CoV) outbreaks in 2003 and 2012, respectively, have caused high morbidity and mortality in patients. Severe SARS-CoV and MERS-CoV infection oftentimes progresses to acute respiratory distress syndrome (ARDS), a life-threatening, end stage lung condition in which alveolar damage, inflammation and edema oftentimes lead to death (7, 10, 16, 127). SARS-CoV and MERS-CoV cause ~14% and 36% mortality rates, respectively, according to the World Health Organization and several comorbidities like age, obesity and underlying lung disease predispose individuals to more severe disease outcomes (10, 16). Although these co-morbidities modulate severe disease outcomes, robust animal model development designed to phenocopy and study these disease-enhancing phenomena are lacking. To date, most studies have focused on the development of new animal models designed to identify the underlying immunologic mechanisms that regulate age-related disease enhancement or the impact of age on vaccine performance, leading to the discovery of serious deficiencies in our countermeasure design in these at risk populations. For example, the doubly-inactivated SARS-CoV vaccine (DIC) was developed and shown to be protective in 10 week old mice against a subsequent SARS-CoV infection. However, the DIC vaccine was shown to be ineffective, and alarmingly, induced a Th2 immune mediated immune pathology in aged

mice following homologous and heterologous SARS-like virus challenge (125, 221, 222). Because numerous SARS-CoV-like viruses are circulating in bats that are preprogrammed to replicate to high titer in primary human lung cells, future CoV outbreaks seem inevitable (8, 9). Thus, new model systems that mimic highly vulnerable populations and/or morbidity conditions are needed to evaluate pathogenic mechanisms and countermeasure performance.

Obesity is defined as an individual with a body-mass index ≥ 30 and is associated with increased risk of heart disease and diabetes. Obesity rates are conservatively expected to rise to 55% of US adults by 2030 and also are rapidly increasing around the world, with over 500 million adults and 43 million children under the age of 5 affected as of 2008 (223). In the Kingdom of Saudi Arabia (KSA) specifically, over 50% of adults are considered obese as of 2017 (132). Unfortunately, conditions in the KSA mirror the rapidly expanding problem of obesity throughout the Arabian Peninsula (224). Importantly, diabetes and heart disease are comorbidities associated with severe disease outcomes in SARS-CoV infected patients and obesity is a significant comorbidity for severe disease after MERS-CoV infection (126, 128, 130, 225, 226). Although other metabolic-related diseases were linked to increased SARS pathogenesis, obesity was not considered a comorbidity during the SARS-CoV outbreak. This difference might reflect the variation in obesity definitions used in Asian and European countries, coupled with the discovery that the European BMI cutoffs do not accurately reflect the health state associated with obesity in Asian countries. For example, it is likely that Asian countries would more accurately be defined as “obese” at a lower BMI than 30, potentially skewing comorbidity analyses in CoV outbreaks in Asian countries (226, 227). Thus, genetic variation between populations may also regulate obesity related disease enhancing phenotypes.

Obesity is associated with dysregulated cytokine signaling, poor wound healing, and dysfunctional cell-mediated immune responses, and has been linked to poor outcomes following infection (135, 228). Specifically, obesity is correlated with poor outcomes for respiratory disease and respiratory infection patients. Stapleton et. al. determined that obesity correlates with a greater risk of developing ARDS and other organ failure (229). Specific to ARDS, obesity reduces chest wall and lung compliance and leads to lower lung function via increased airway resistance (230, 231). Obesity increases systemic leptin levels, which is both proinflammatory and serves as a neutrophil attractant (133, 229). Both in mice and in humans, high fat diet and obesity correlate with a large influx of proinflammatory neutrophils into the lung prior to any disease or infection event (144, 229, 232). This persistent proinflammatory state can lead to a dysregulation of both the innate and adaptive immune responses associated with infection and disease. In the case of lung injury via asthma or allergic response, obesity correlates with increased lung fibrosis, endothelial collapse, airway hyper responsiveness, and proinflammatory cytokines associated with increased collagen deposition, rendering the lungs inflexible and impairing respiration (233-235).

Evidence of increased disease burden of obese patients in lung infection is born out through human and mouse studies of influenza as well. O'Brien et. al. found that obesity predisposes mice to increased morbidity and mortality in H1N1 and H3N2 influenza infection (139). Additionally, mice showed decreased epithelial cell proliferation and wound healing in the lung after primary influenza infection. Infected obese mice also displayed high levels of protein and albumin in bronchial alveolar lavage fluid (BALF), indicative of increased pulmonary barrier permeability and edema. In the days following infection, the lungs of obese mice retained

high levels of inflammatory cells such as neutrophils, monocytes, effector T cells, and NK cells, indicative of an extended illness and inflammatory period (139).

Evidence of obesity increasing respiratory disease burden as well as obesity comorbidity studies in MERS-CoV infections suggests a critical need to generate high fat diet induced obesity (DIO) models for emerging coronavirus infections. Although comorbidities are important determinants of SARS-CoV outcomes, host genetic variation also likely plays a vital role in obesity related comorbidities. Variability in SARS-CoV disease is seen in both human patients and in genetically distinct mouse models. A thorough study of SARS-CoV susceptibility loci in the Collaborative Cross (CC) by Gralinski et. al. showed the impact of genetic variability on SARS-CoV disease outcomes (117). The CC is a large panel of recombinant inbred (RI) mouse strains derived from both lab-inbred and wild-derived mouse lines. CC RI lines are diverse and mappable, intending to mimic the genetic diversity seen in human populations (112, 115). In this study, we not only develop new obese mouse models of severe emerging coronavirus lung disease, but also evaluate the impact of host genetic variation on obesity related comorbidities using genetically distinct CC lines before and after SARS-CoV infection. Our data demonstrate a clear association between genetics, obesity, and susceptibility and resistance to emerging coronavirus infection, providing a panel of new animal models for mechanistic studies, genetic susceptibility mapping studies, and countermeasure evaluation.

4.2 Results

4.2.1 Obesity Increases morbidity and mortality in the mouse model of SARS-CoV infection.

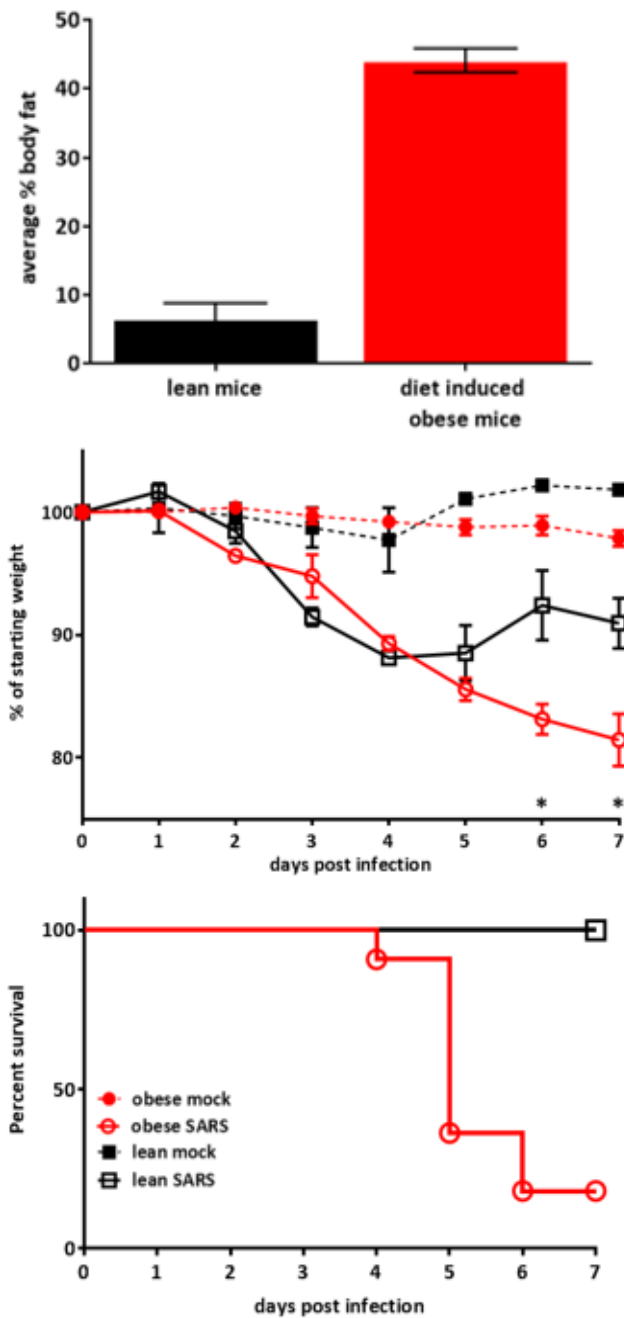


Fig. 4.1: Obesity increases morbidity and mortality in SARS-CoV infection. Obese mice failed to recover weight after infection, and showed markedly increased mortality compared to SARS-CoV infected mice. * $p < 0.005$

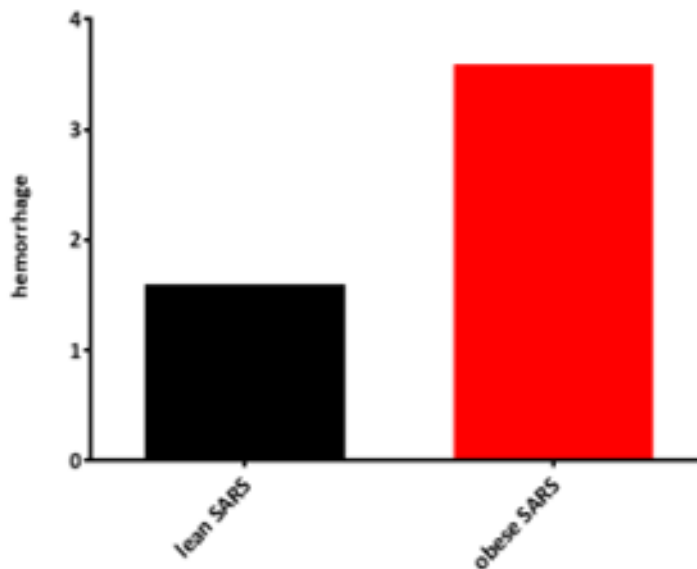
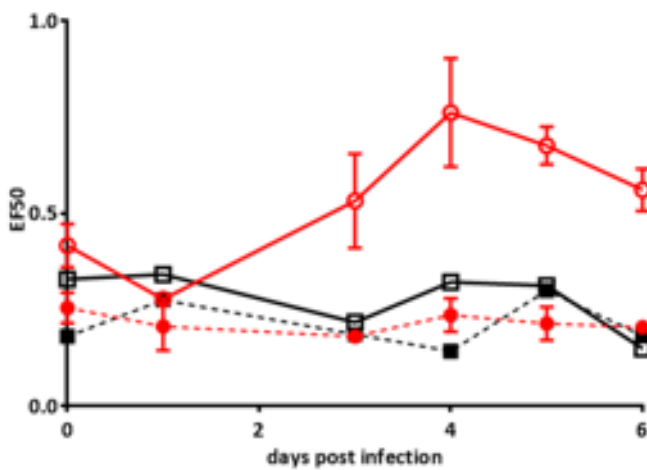
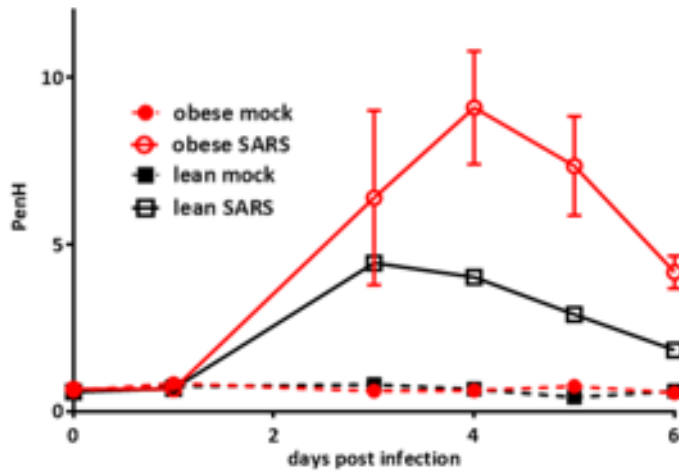


Fig. 4.2: Obesity impairs lung function and increases lung injury in SARS-CoV infection. Lung function measured using whole body plethysmography over the time course of infection. PenH is a derived measure indicating lung debris. EF50 indicates expiratory flow rate at 50% lung volume. Lung hemorrhage was measure at d7 with 4 indicating total hemorrhage and 0 indicating a healthy lung.

In order to determine the impact of diet induced obesity (DIO) on SARS-CoV infection, 4 week old C57BL/6J mice were weaned and maintained on a Research Diet high fat diet (HFD) chow, while control mice maintained a standard lean diet chow (CD). Animals were measured via magnetic resonance imaging (MRI) for body composition by MRI. At 20 weeks of age, the C57BL6 mice were infected with a sublethal dose of 10^4 PFU of mouse adapted SARS-CoV (MA15), intranasally (201). Only mice over 30% body fat were considered “obese” and used in the study (Fig 4.1). While lean mice displayed a normal ~10% weight loss phenotype and

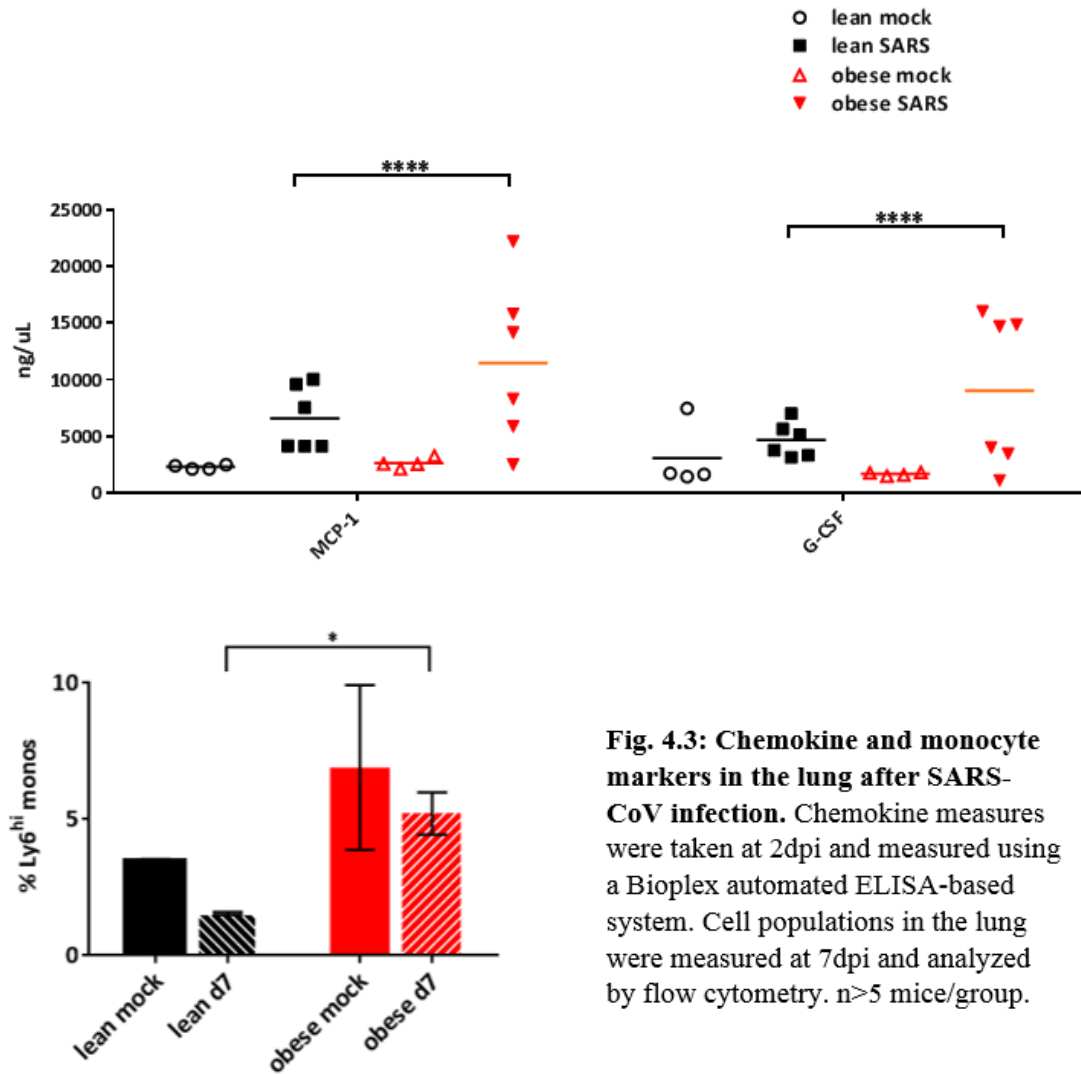


Fig. 4.3: Chemokine and monocyte markers in the lung after SARS-CoV infection. Chemokine measures were taken at 2dpi and measured using a Bioplex automated ELISA-based system. Cell populations in the lung were measured at 7dpi and analyzed by flow cytometry. $n > 5$ mice/group.

recovered quickly after infection, obese mice were significantly different in terms of increased weight loss and mortality (Fig 4.1), as about 80% of the obese animals died prior to 7 dpi.

4.2.2 Obesity impairs lung function and increases lung injury in SARS-CoV infection.

During the first week of infection, mice were measured daily for respiratory function using BUXCO plethysmography. For measurements, mice are moved into individual plethysmography chambers and allowed to acclimate for 30 minutes before a 5 minute recording time. A derived measurement of lung function is PenH, measuring airway resistance that is highly correlated with debris in the airway (236). Consonant with increased morbidity and mortality phenotypes, SARS-CoV infected obese mice displayed significantly higher levels of PenH during infection as compared to lean controls. In addition, EF50 measures respiratory flow at 50% of lung volume, indicative of a “wheeze” like state, or lung distress. SARS-CoV infected obese mice also showed significantly higher levels of EF50 during infection as well (Fig 4.2). At 7 days postinfection, surviving mice were assessed visually for hemorrhage on a 0-4 scale based on the totality of lung involvement. Obese mice displayed significantly higher levels of hemorrhage in the lung than infected controls, providing an additional marker of increased lung injury and/or reduced wound healing in the obese infected mice (Fig 4.2).

4.2.3 Obesity impacts immune responses to SARS-CoV infection.

After infection with 10^4 PFU of MA15, obese infected mice and controls were sacrificed on either 2 dpi for cytokine and chemokine analysis or 7 dpi for flow cytometry analysis (Fig 4.3, S4.3). SARS-CoV infected obese mice retained high levels of M1 precursors, Ly6Chi monocytes, at late timepoints after infection, indicating a prolonged proinflammatory response when compared to lean controls (Fig 4.3, S4.3). These findings are supported by Bioplex cytokine and chemokine analysis of homogenized lung tissue at 2dpi. The Bioplex 23-plex panel

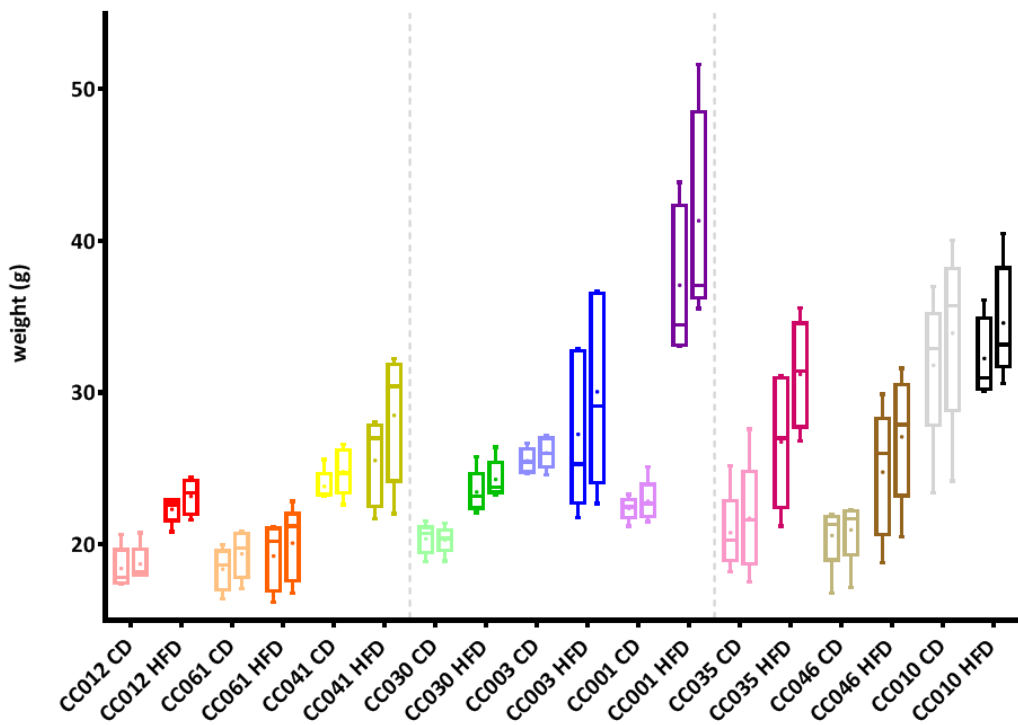
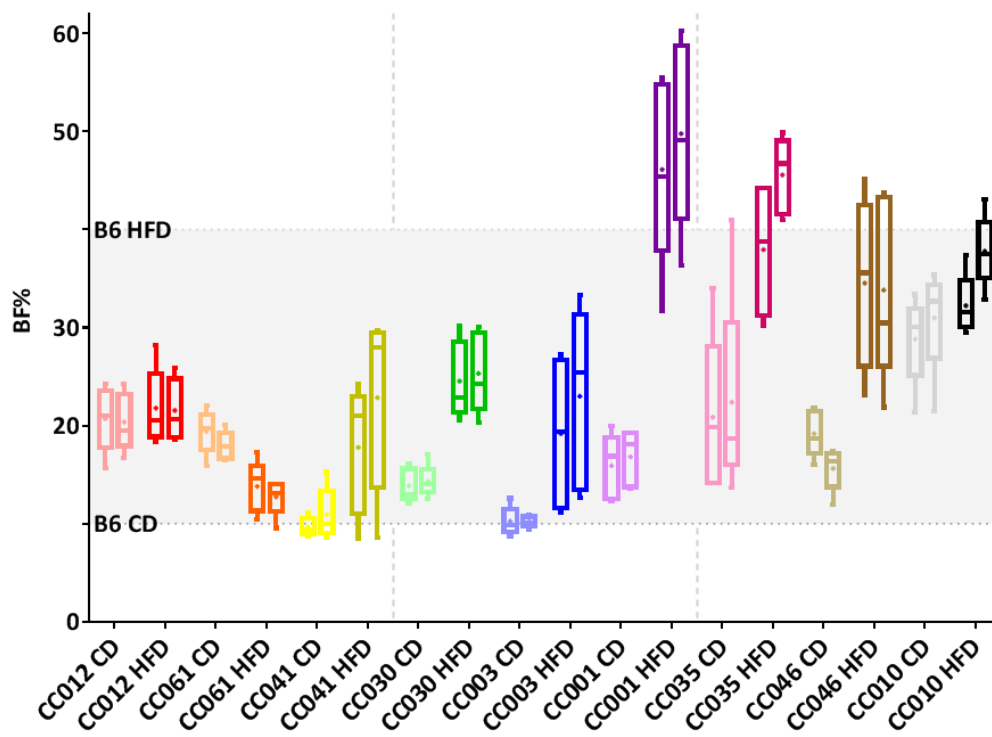
is an ELISA-based immunoassay measuring levels of 23 cytokines and chemokines (Eotaxin, G-CSF, GM-CSF, IFN- γ , IL-1 α , IL-1 β , IL-2, IL-3, IL-4, IL-5, IL-6, IL-9, IL-10, IL-12 (p40), IL-12 (p70), IL-13, IL-17A, KC, MCP-1 (MCAF), MIP-1 α , MIP-1 β , RANTES, TNF- α). As compared to controls, we saw elevated levels of several cytokines in both the obese and lean SARS-CoV infected animals (Fig 4.3, S4.1, S4.2).

4.2.4 Differential response in recombinant outbred mouse lines to high fat diet and SARS-CoV infection.

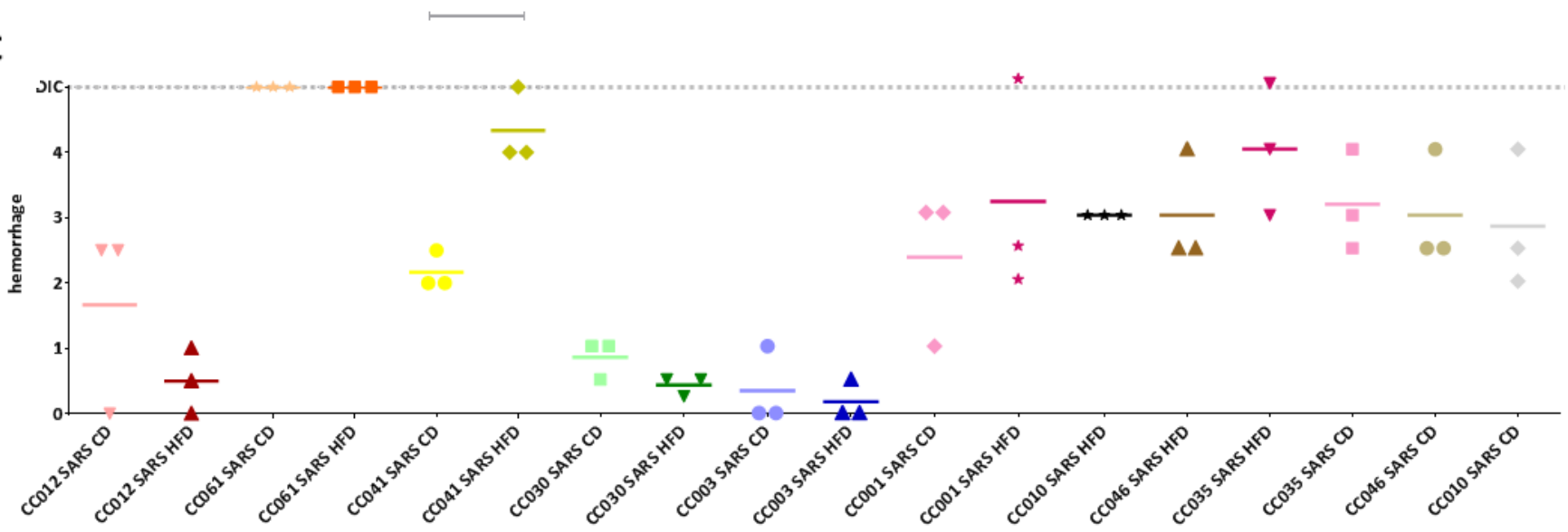
Underlying host genetics predispose individuals to obesity and obesity related comorbidities (237). To evaluate the impact of underlying host genetics on obesity and SARS-CoV disease severity, nine CC RI lines were divided into three groups of ten mice each. All groups underwent the same feeding and infection parameters, but were divided for experimental ease (Group A: CC012, CC061, CC041; Group B: CC030, CC003, CC001; Group C: CC035, CC046, CC010). Each line was divided into 5 mice per diet (HFD v CD), At weaning (appx. 4 weeks of age), each group of mice were maintained on the HFD or CD diets and evaluated for weight and body fat percentage using MRI (Fig 4.4). Lines CC041, CC030, CC003, CC001, CC035, and CC046 gained significantly more body fat on high fat diet when compared to their chow diet controls (Fig 4.4). Among these CC001 exceeded body fat percentages seen in the C57BL6 mice (Fig 4.1). Surprisingly, the remaining lines, CC012, CC061, and CC010 did not gain significantly more body fat when on the HFD diet. Among these, CC061 showed lower body fat on high fat diet compared to chow diet controls at 15 and 20 weeks of age – however, CC061 mice on high fat diet visibly moved high fat diet chow from the food holder to the cage litter and may have had putative intestinal distress as evidenced by soft stools. Measurements of food intake were not recorded in individual cages during this study. For all downstream studies,

all mice were used regardless of body fat percentage at the time of infection, as many lines did not meet the standard C57BL/6J criteria for obesity, >30% body fat (135, 140) (Fig. 4.4C).

At 20 weeks of age, each group of mice were then infected intranasally with 10^4 PFU of MA15 and the animals were monitored for weight loss and mortality through 7 dpi. (Fig 4.4). At 7 dpi, surviving mice were sacrificed assessed visually for hemorrhages previously described in Fig. 4.4C. Lines CC061, CC041, CC001, CC035, CC046, and CC010 continually lost weight or succumbed to illness during the study, showing high susceptibility to MA15 infection in both high fat and chow diet groups. While lines CC001, CC041 and CC046 had demonstrated significant BF gain under high fat diet conditions, CC001 HFD and CC046 HFD mice lost weight more slowly than controls fed on standard chow. More animals and repeat experiments will be needed to achieve statistical significance. All mice in Line CC061 succumbed to infection, with high fat diet mice succumbing 3 dpi, and chow diet mice succumbing 4 dpi. Lines CC010, CC012, and CC003 showed minimal weight loss followed by recovery of weight after MA15 infection, indicating low susceptibility to infection in both high fat and control groups. The only lines showing a significant difference in weight loss between high fat and control diet groups were CC012 at 4 dpi. However, both diet groups resolved infection similarly. Based on our data, pathogenesis as measured by weight loss and hemorrhage after infection was correlated highly with genetic line and did not directly correlate with diet.

A**B**

06 C



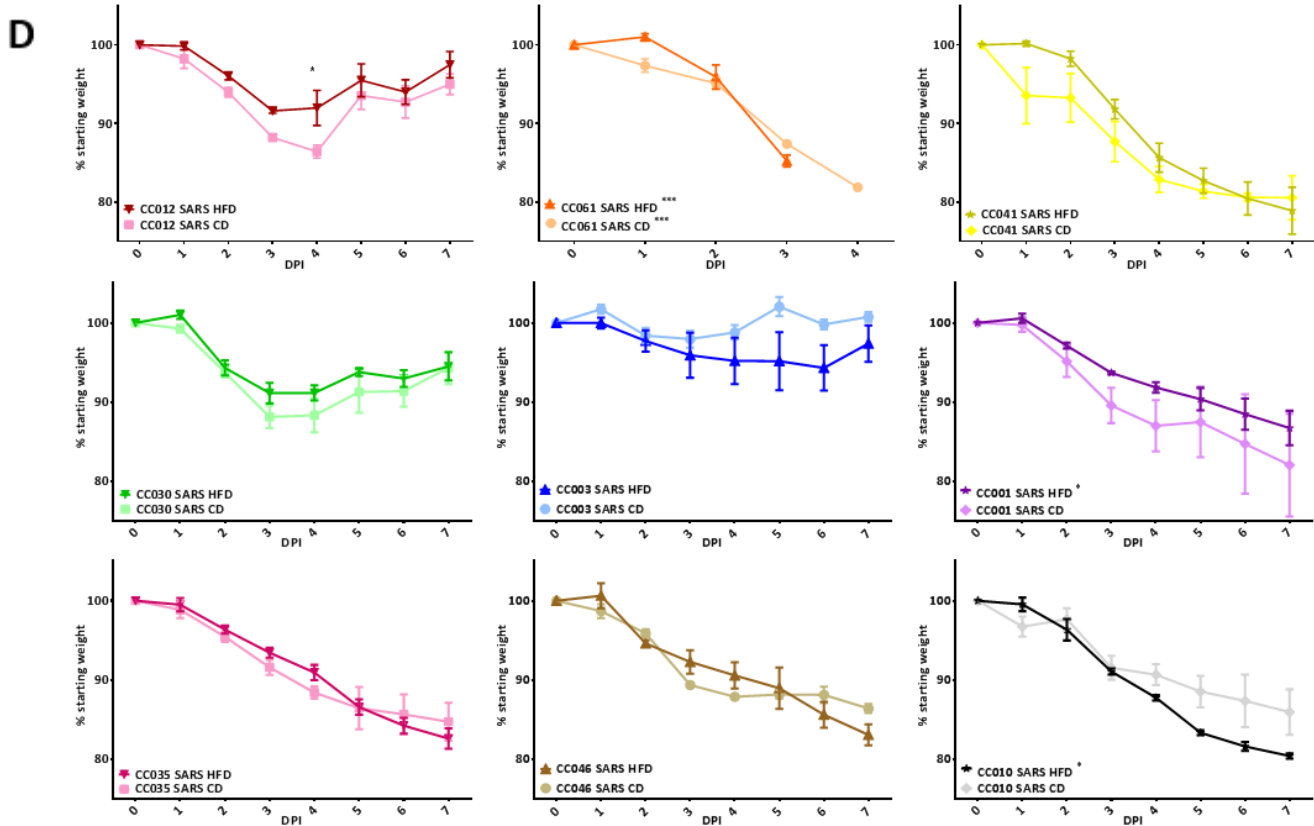


Fig. 4.4: SARS-CoV infection outcomes in 9 Collaborative Cross lines comparing high fat and control diets. (A) Weight and (B) body fat percentage were measured at 15 (left bar) and 20 weeks (right bar) of age, with high fat or control diet beginning at 4-5 weeks of age. Body fat percentage was determined by MRI designed for mouse body composition analysis. (C) Hemorrhage analysis was taken at 7dpi during sacrifice, and is measured visually as percentage of the lung hemorrhaged on a 0-4 scale. Mice succumbing to infection before harvest are denoted on the DIC line. (D) After infection, all animals were weighed daily to measure illness. n=5 mice per line per diet. In each group, 2 mice were mock infected and 3 were SARS-CoV infected at 10^4 PFU.

4.3 Discussion

Obesity is a disorder impacting over 500 million people globally. Obese populations have more than doubled since 1980, reaching 13% of adults worldwide(3). Obesity is associated with poor health outcomes in respiratory disease, including delayed and over-active inflammation, dysfunctional immune responses, and increased pathogenesis after virus emergence (128, 136-

140). Increasing obesity rates coupled with poor health outcomes in these patient populations justify the need for a better mechanistic understanding of the relationship between obesity, inflammation, adaptive immunity and the progression of infectious disease.

Obesity was shown to be a comorbidity and predictor of disease severity in human MERS cohorts. Additionally, obesity is known to increase the risk of developing ARDS during lung infection leading to longer hospital stays and increased pathology in obese patients (137, 232). Obesity was not been directly linked to SARS-CoV disease severity. One confounding factor is a low rate of obesity in the areas of SARS-CoV outbreaks, primarily in Asia. Secondly, the definitions of obesity and related metabolic syndromes apply primarily to western populations, whereas Asian populations most likely require an alternate criteria (226). Robust and highly reproducible small animal models are desperately needed to not only study the pathogenic mechanisms regulating increased disease severity but to provide a platform for evaluating vaccine and antiviral drug performance in extreme risk populations. Moreover, novel model platforms are desperately needed to map host genes and alleles which regulate increased disease severity after viral infection of the lung.

We developed a new mouse obesity model of SARS-CoV pathogenesis. Our model primarily replicates the research of the Beck lab, which identified that obesity results in increased morbidity and mortality in an influenza mouse model (140). Our obesity model relies on feeding animals on a high fat diet to C57BL/6 DIO mice for 15 weeks, starting at the time of weaning. At 20 weeks, any mice at or over 30% body fat are considered to be obese and can be included in our research cohorts. Lean control mice were taken from the same litters as obese mice and housed in the same room, but were fed a chow diet to retain low body fat percentage. Our SARS-CoV uses sublethal doses of mouse-adapted SARS-CoV (MA15) inoculated into 20

week aged mice (117). In this study, we show that C57BL/6 DIO mice are highly susceptible to SARS-CoV pathogenesis when compared to lean controls. DIO mice show increased weight loss, high levels of mortality, and decreased lung function throughout infection. Additionally, increased levels of proinflammatory markers MCP-1 and G-CSF were noted as compared to lean controls. During severe SARS-CoV infection in humans, IL-6 is significantly increased, while TGF-B and IL-8 are significantly decreased (238). In studies of obese patients, serum levels of IL-10, IL-6, and TNF α are significantly increased when compared to lean patients (239, 240). MCP-1, or monocyte chemoattractant protein, is implicated in pathogenesis of several diseases characterized by monocytic infiltrates (241). After SARS-CoV infection, activated monocyte infiltration is a hallmark of increased pathogenesis (242). GCS-F, or granulocyte-colony stimulating factor, is produced by endothelium, macrophages, and other immune cells. G-CSF stimulates the survival, proliferation, differentiation, and function of neutrophil precursors and mature neutrophils (243). Obesity and high fat diet were characterized by increased neutrophilia in the lungs and denotes a proinflammatory state in obese compared to lean mice (S4.3) (229, 233). Neutrophilia is a common marker of pathogenesis in viral respiratory disease and ARDS; neutrophils increase in the respiratory tract during influenza infection, and during severe influenza pneumonia, the number of neutrophils is positively correlated with disease severity (244). Together, immune regulators and infiltrating immune cells point toward a proinflammatory state in obese infected mice characterized by high levels of proinflammatory cytokines and a skew toward M1 proinflammatory monocytes. Surprisingly, other inflammatory factors associated with severe lung disease, such as TNF α , IFN-a, and IFN-b, were not significantly increased in high fat compared to control diet infected mice (S4.2). It is possible that these proinflammatory cytokines would be seen at varying levels at a different times after

infection not tested here. SARS-CoV pathogenesis is largely an issue of inflammation temporality; an early robust immune response or completely diminished immune response is associated with better survival in the mouse model, but a delayed immune response is associated with high morbidity and mortality (242). It is also possible that the dynamics of high fat diet MA15 infection display different cytokine patterning than other respiratory infections.

While the mechanism of increased pathogenesis is unknown, future studies will focus on a few likely pathways. For example, IFN- α/β functions to increase innate cellular defenses and activate immune cells to protect against infectious virus. IFN is secreted and recognized by secondary cells and, through a Jak/STAT signaling pathway, activates interferon stimulated gene (ISG) transcription, establishing an antiviral state in the host, and leads to the transcription of inflammatory cytokines including tumor necrosis factor alpha (TNF- α), interleukin-12 (IL-12), and IL-6 (76, 77, 245). However, increased adipose tissue in obesity secretes high levels of systemic leptin, which in turn upregulates suppressor of cytokine signaling 3 (SOCS3). SOCS3 is thought to inhibit IFN response by blocking the Jak/STAT signaling pathway, and thereby downregulating ISGs and inhibiting the host anti-viral response (133, 246). As an example, in DIO mice infected with the influenza virus, IFN- α/β transcripts were significantly reduced relative to lean mice 3 days post infection, suggesting dysfunctional viral sensing and IFN induction (136). IFN- α/β inhibits SARS-CoV replication both in vitro and in vivo (33, 63, 76, 77, 189, 247). Recent evidence has shown that a delayed IFN- α/β response early in infection will lead to increased lung injury and mortality in SARS-CoV infected mice (76). Therefore, altered IFN signaling and secretion via aberrant leptin signaling is a possible mechanism for increased SARS-CoV pathogenesis in obese mice. A second possible mechanism involves monocyte infiltration into the lung and resolution of infection. Macrophages play an important role in the

inflammatory response and resolution of ARDS (248). Transition from an M1 polarized “pro-inflammatory” to M2 polarized “anti-inflammatory” macrophage state is correlated with debris clearance and wound healing in the lung (76). During ARDS, M1 macrophages function in inflammatory cytokine secretion; monocyte, macrophage, and neutrophil recruitment; and tissue damage. M2 macrophages trigger tissue repair and a cessation of cell recruitment (249-252). One hallmark of poor outcomes in SARS-CoV infection in humans and mice is a high inflammatory monocyte count in the lung late in infection (76, 79).

Obesity is correlated with increased basal levels of inflammation, as well as an increase in M1 versus M2 polarization systemically. Increased SOCS3 is also thought to prevent M2 polarization (253). In influenza-infected mice, levels of monocytes in the lung are significantly increased though 13 days post infection in obese compared to lean mice (139). Our data shows that M1 precursors, Ly6Chi monocytes, are increased at late time points in obese SARS-CoV infected mice. Recently, high levels of M1 macrophages late in infection correlate with increased mortality after SARS-CoV infection, perhaps by prolonging lung injury due to and prolonged inflammatory immune state and an inability of the host to promote an anti-inflammatory, wound healing state (242). It is likely that this prolonged proinflammatory state in the obese lung may be responsible for increased morbidity and mortality in obese SARS-CoV infected mice, contributing to a dysfunctional immune responses to infection and dysregulated wound healing response seen in other respiratory disease models of obesity.

Currently, MERS-CoV is circulating on the Arabian Peninsula where over half of the population is obese. Several groups have developed mouse models for studying MERS-CoV pathogenesis, although none have evaluated the impact of obesity on viral infection. In our laboratory, gene editing was used to introduce two human codons into the mouse dipeptidyl

peptidase 4 receptor, converting it into a functional receptor for entry (45). Using the standard HFD described for C57BL/6 mice, this model should be readily available for evaluating the impact of HFD on MERS-CoV disease severity (128, 137). However, without understanding this mechanism, treatment approaches currently developed for controlling MERS-CoV infection in young mice may prove inappropriate or detrimental for the population. Moreover, obese patients often suffer from secondary ailments, including type II diabetes, metabolic syndrome, or hypertension (135, 254, 255). Diabetes as a comorbidity has been shown to enhance disease severity following MERS-CoV infection (256). Not only can these disease states add additional layers of risk, but the medications used to treat these symptoms come with unknown impacts on infectious disease outcomes. Various common medications have been shown to impact SARS-CoV disease in humans, such as use of corticosteroids (11, 257). However, most medications and disease states have not been studied as comorbidities. Research aims to model respiratory virus research on the human disease state in order to improve patient health and test patient treatments. In order to do this thoroughly, it is important to generate a disease model that mimics the complexity and common health states of patients.

Genetics also plays a vital role in disease response and outcomes. Obesity itself has a strong genetic link, with a 40-70% genetic component in body weight heritability, shown in both human studies and in the collaborative cross (237, 258, 259). Traditional studies of obesity genetics have focused on rare homozygous alterations in leptin pathway genes. However, the advent of genome-wide association studies (GWAS) and single nucleotide polymorphism (SNP) mapping have allowed for a more dynamic approach to human heritability studies. Genome wide complex trait analysis – analyzing the impact GWAS SNPs in aggregate rather than individually – has shown that 16% of obesity heritability in humans can be attributed to genetics (237).

Environment and diet also exerts a strong impact on the obesity phenotype. Diet and exercise have been associated with differential methylation of genes, providing a mechanism for gene-environment interactions, including the ability to counteract acquired or imprinted epigenomic patterns regulating obesity-related genes. Overall, genetics and heritability add complexity to obesity as a disease state. Atamni et. al. studied high fat diet in CC mice in conjunction with type II diabetes, finding that diet-induced type II diabetes is a complex trait controlled by multiple genetic factors and sex (260). This supports our finding wherein weight gain and body fat composition was highly dependent on genetic factors, and not primarily influenced by diet. Importantly, these findings mirror human studies of obesity genetics, both supporting our findings and supporting the hypothesis that CC genetic variability can be used to mimic human genetic variability. In particular, lines CC001 and CC061 show dramatically divergent responses under HFD, and an F1 cross study of these lines may provide a unique model system to map genes that regulate differential susceptibility to HFD in mice. Two other lines should be noted: CC012 and CC061, which remained at low weights in both the high fat and control diet cohorts. CC012 seemed to simply be incapable of gaining significant amounts of weight, as all animals remained a low body weight throughout the study. This points to a genetic involvement in weight gain, and would be an unusable line in high fat diet studies of obesity. CC061, alternately, showed low chow intake and putative gastric upset via loose stool and inflamed-looking rectum. This likely resulted from poor intestinal response to the high fat diet, and should be taken into consideration when interpreting their results.

Gralinski et. al. identified SARS-CoV susceptibility loci using the CC, finding various host genes that could be attributed to pathogenesis phenotypes in infection (116, 117). In our study of 9 divergent CC lines, genetics was far more predictive of disease outcome than diet.

Due to the importance of genetics in infectious disease susceptibility and the variation of SARS-CoV susceptibility seen in Gralinski et. al., it is not surprising that genetic lineage was an important arbiter of disease outcomes. However, the degree to which genetics as opposed to diet determined outcomes was surprising in light of the dramatic impact of diet and obesity on SARS morbidity and mortality seen in C57BL/6J mice. After HFD and infection, two potentially promising lines are a cross of CC041 and CC001 lines. CC041 did not gain significantly more weight or body fat on a high fat compared to control diet, with both high fat and control diet mice remaining within a “normal” weight range. CC001, alternately, showed close grouping of weights on control diet and a very high body fat percentage on high fat diet. An F2 cross of these lines with similar genetic profiles but opposing weight gain profiles might allow for a closer pinpointing of the genes responsible for differential fat gain on high fat diet. However, it is clear from studies in the CC that longer durations of HFD and larger cohorts of animals will be needed to circumvent the heterogeneous disease phenotypes seen in these animals.

As an alternate approach, because C57BL/6J mice reliably become obese on HFD, and are one of the eight founder lines of the CC, it is possible to map the relative impact of the C57BL/6J genome on weight gain and obesity in a larger panel of CC lines or crossed with HFD resistant lines to map disease regulating traits. The 9 CC lines study here cover approximately 80% of the B6 genome by SNP mapping, leaving approximately 34 areas of non-B6 coverage (Fig 1.2). Dr. Martin Ferris analyzed this coverage and queried the remaining CC lines in order to determine which lines could be best used to acquire complete coverage of the B6 genome, finding 9 additional lines (CC011, CC031, CC023, CC074, CC020, CC057, CC065, CC076, CC018, CC026, CC037, and CC075) that would effectively cover the remainder of the B6 genome.

The data described herein demonstrate a critical need for alternative animal model development allowing for detailed mapping of host susceptibility genes that regulate disease outcomes, when coupled with diet, obesity, host genetic variation and aging. Such model systems provide new opportunities for investigating vaccine and therapeutic interventions, while potentially revealing fundamental new insights into viral pathogenesis.

4.4 Methods

ETHICS STATEMENT AND BIOSAFETY

Mouse studies were carried out in accordance with the recommendations for the care and use of animals by the Office of Laboratory Animal Welfare at the NIH. IACUC at UNC-CH approved the animal studies performed under IACUC protocol 15-155. All virus work was performed in a certified biosafety level 3 (BSL3) laboratory containing redundant exhaust fans while wearing personal protective equipment including HEPA filtered powered air purifying respirators, Tyvek suits, hoods, and boots; work was additionally confined to a class II biological safety cabinet.

CELL CULTURE AND VIRUS

Recombinant mouse-adapted SARS-CoV (MA15) was generated, passaged once, and tittered on Vero E6 cells. For viral titering, the right bottom lobe of each mouse was homogenized then serially diluted to assess plaque forming units (PFU) in Vero E6 cells, with a detection limit of 100 PFU.

ANIMALS AND INFECTIONS

C57BL6/J mice were obtained from the Jackson labs (jax.org), housed and bred in pathogen free conditions in accordance with guidelines established by the Department of

Laboratory Animal Medicine at UNC-CH. Collaborative Cross (CC) strains were selected with the help of the CC and Dr. Martin Ferris, UNC, and were bred at UNC. At 5 weeks of age, CC mice were transferred to the Baric Lab and put on high fat or lean control diets. All mice were matched by age and litter in this study. All mice in this study were female unless otherwise stated. High fat diet mice were fed a 60% fat pellet diet (Research Diets) while control lean mice were fed a standard chow diet. Animals began their selective diets at 4-5 weeks of age and continued through their infection and harvest at 20 weeks of age. Prior to infection, they were monitored visually, by weight, and by MRI scan for body fat percentage. Only mice exceeding 30% body fat prior to infection were included in the “obese” cohorts for B6 mice. All mice on the 15 week high fat diet were included in the “high fat diet” cohort for all CC strains because standards have not been developed for these animals..

During infection, mice were maintained in SealSafe ventilated caging system in a BSL3 laboratory, equipped with redundant fans as previously described by our group. Before viral infection, mice were anesthetized using isoflurane. Mice were infected with 10^3 PFU MA15, 10^4 PFU MA15, 10^5 PFU MA15, or PBS for mock controls. Following sedation and infection, mice were monitored daily for weight loss and survival, as well as for signs that the animals were moribund (including labored breathing, lack of movement and lack of grooming). Mice that reached 20% weight loss were placed under exception and monitored at least twice daily. Mice that approached 30% weight loss were euthanized immediately. Mice deemed moribund were euthanized at the discretion of the researcher. Mice were euthanized with an isoflurane overdose followed by a secondary thoracotomy, at various time points, to collect lung tissues. In the absence of a thoracotomy, cervical dislocation was used as a secondary euthanasia method. All

are approved methods of the Institutional Animal Care and Use Committee (IACUC) at the UNC-CH.

HISTOLOGICAL ANALYSIS AND LUNG SCORING

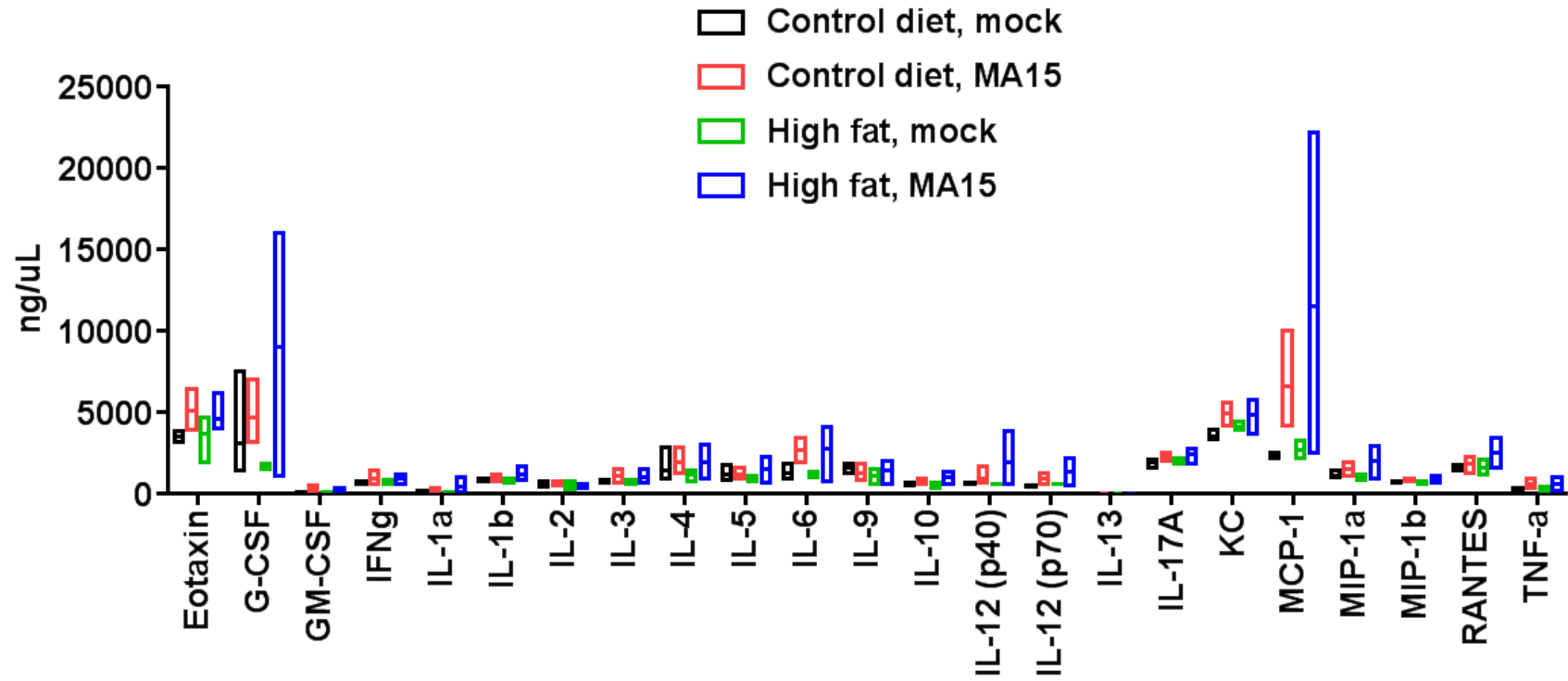
Lung samples were fixed in 10% phosphate-buffered formalin for >7 days, then moved to new formalin solution at 4°C before removal from BSL3. Fixed samples were then placed in cassettes, rehydrated, and moved to ethanol solution prior to submission to the Lineberger Comprehensive Cancer Center Animal Histopathology Core for processing and sectioning. Histopathology tissue sections were boiled in Tris-EDTA buffer for antigen retrieval, then SARS-CoV stained using anti-SARS-S antibody and HRP-conjugated secondary antibody. HRP was developed using DAB (Thermo Scientific Metal Enhanced DAB Substrate Kit), then counterstained. Gross hemorrhage of lung tissue was observed immediately after euthanasia and scored on a scale of 0 (no hemorrhage in any lobe) to 4 (extreme and complete hemorrhage in all lobes of the lung).

CYTOKINE PROFILING

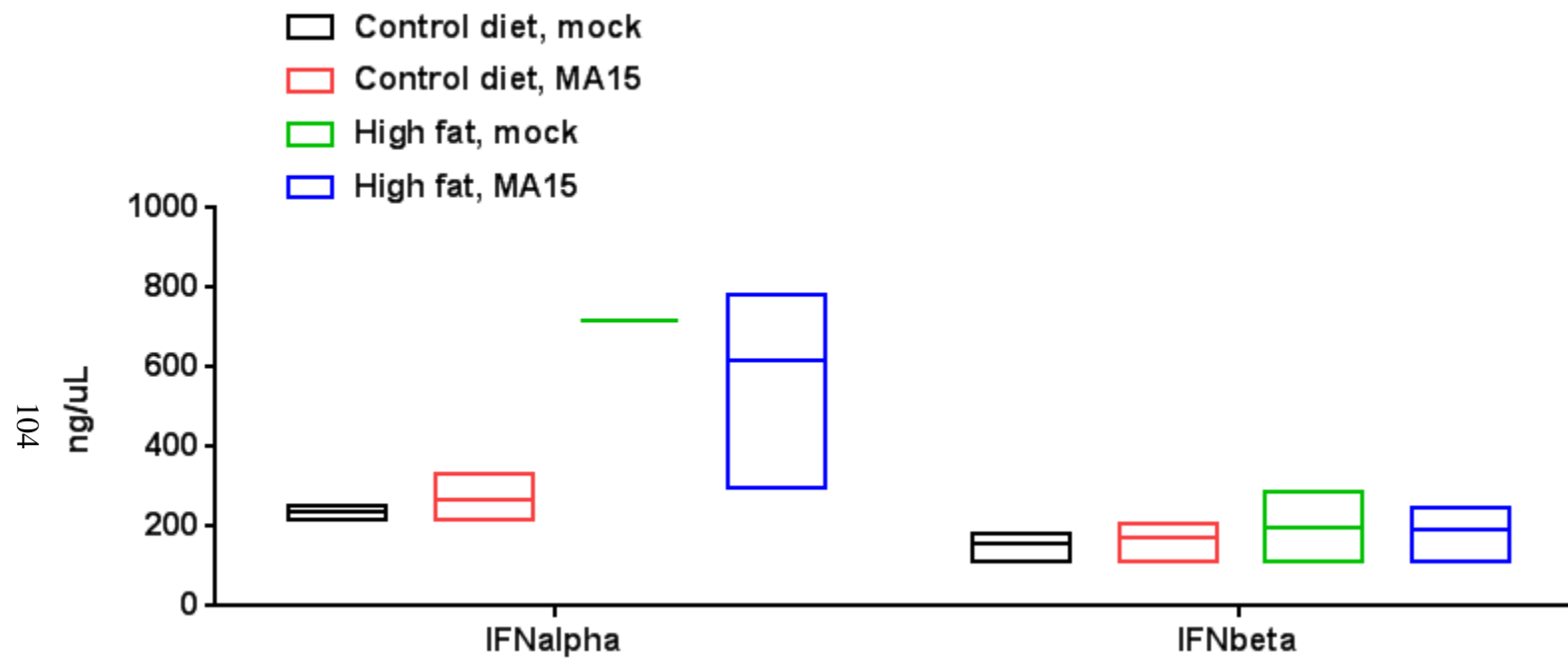
Sections of lung were frozen in PBS at -80°C until use. Sections were homogenized, then supernatant was used for cytokine profiling, assessed by the Bio-Plex Cytometric Bead Array 23-Plex (Bio-Rad), according to the manufacturer's instructions. Cytokines assayed were Eotaxin, G-CSF, GM-CSF, IFN- γ , IL-1 α , IL-1 β , IL-2, IL-3, IL-4, IL-5, IL-6, IL-9, IL-10, IL-12 (p40), IL-12 (p70), IL-13, IL-17A, KC, MCP-1 (MCAF), MIP-1 α , MIP-1 β , RANTES, and TNF- α . IFN-alpha and IFN-beta assays were run separately though Bio-Rad Bio-Plex arrays according to manufacturer instructions. The concentrations of individual cytokines were expressed as the mean \pm standard deviation (SD) from duplicate samples.

FLOW CYTOMETRY

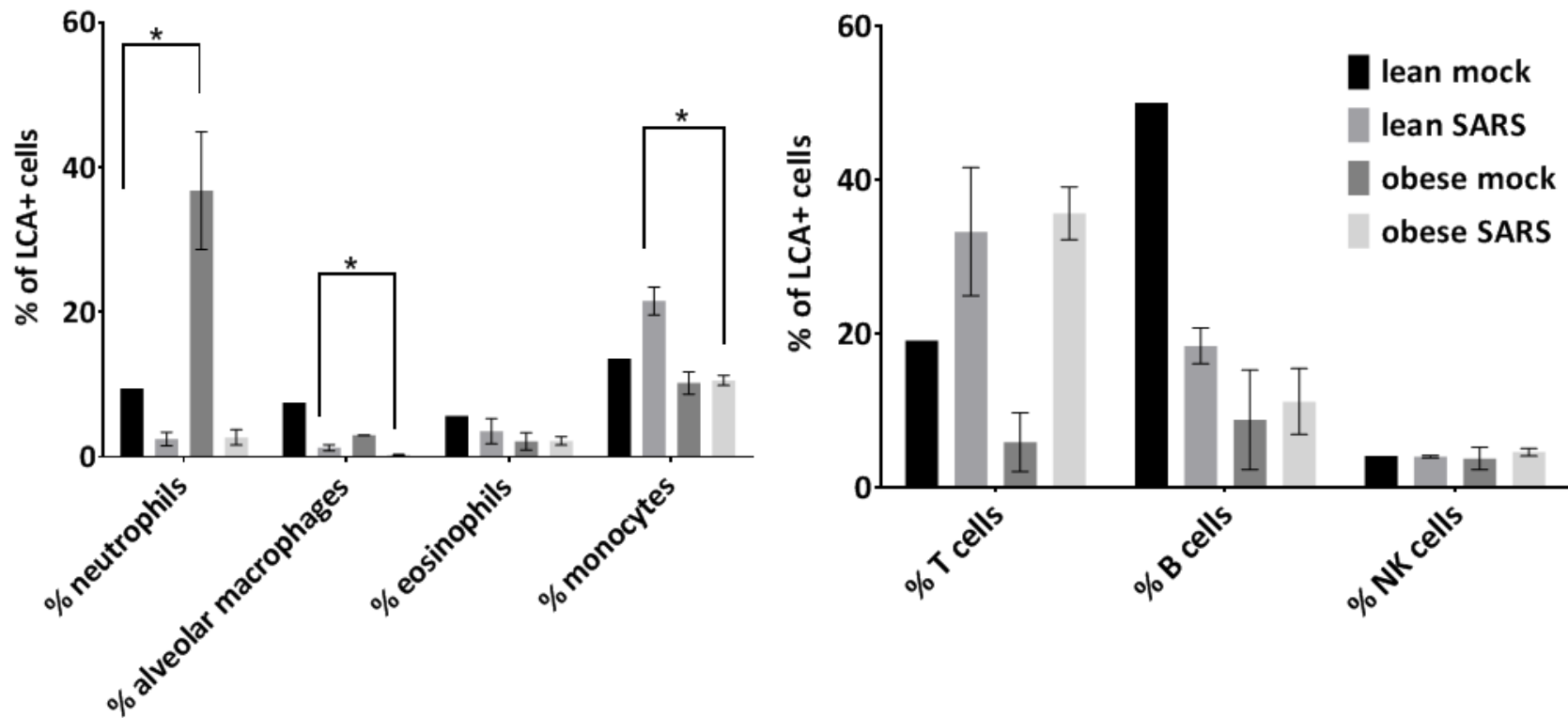
The right lung of selected mice were used for flow cytometric staining of inflammatory cells. Mice were perfused with PBS through the right ventricle before harvest, lung tissue was dissected and digested in RPMI (Gibco) supplemented with DNase and Collagenase (Roche). Samples were strained using a 70 micron filter (BD) and any residual red blood cells were lysed using ACK lysis buffer. Cells were stained in three separate panels using: (1) FITC anti-Ly-6C clone AL21 (BD), PE anti-SigLecF clone E50-2440 (BD), PETR anti-CD11c clone N418 (MP), PerCP anti-B220 clone RA3-6B2 (MP), PE-Cy7 anti-Gr-1 clone RB6-8C5 (eBio), eF450 anti-CD11b clone M1/70 (eBio), APC anti-LCA clone 30-F11 (eBio), APC-eF780 anti-MHC class II clone M5/114 (eBio) or (2) FITC anti-CD94 clone 18d3 (eBio), PE anti-CD3 ϵ clone 145-2C11 (eBio), PETR anti-CD4 clone RM4-5 (MP), PerCP anti-CD8 clone 53-6.7 (BD), PE-Cy7 anti-CD49b clone DX5 (eBio), eF450 anti-LCA clone 30-F11 (eBio), AF647 anti-CD19 clone 6D5 (Biolegend), APC-eF780 anti-B220 clone RA3-6B2 (eBio), (3) BB515 anti-CD19 (BD), APC-R700 CD45R (BD), BV606 anti-IgD (BD), BV421 anti-IgM (BD), PE anti-CD21 (BD), APC anti-CD138 (BD), BV737 anti-CD80 (BD), BV786 anti-CD5 (BD), APC-Cy7 anti-MHCII (BD). Samples were run in the UNC Flow Cytometry Core Facility on a Beckton Dickinson LSR II and analyzed in FlowJo.



Supplemental Fig 4.1. Full Bioplex 23-Plex Cytokine and Chemokine Panel Analysis of High Fat and Control Diet MA15 or mock Infected C57BL/6J mice. Samples taken at 2 dpi.



Supplemental Fig 4.2. Bioplex IFN Panel Analysis of High Fat and Control Diet MA15 or mock Infected C57BL/6J mice. Samples taken at 2 dpi.



Supplemental Fig 4.3. Lymphocyte and Monocyte flow cytometry panels of High Fat and Control Diet MA15 or mock infected C57BL/6J mice. Samples taken at 7 dpi.

CHAPTER 5: SUMMARY AND FUTURE DIRECTIONS

Coronaviruses are rapidly evolving, emerging viruses that cause considerable disease in humans, mammals and birds. Many of these viruses are pneumoenteric pathogens that cause severe disease in the lungs and gut of humans and animals. The genetic variation across coronaviruses is vast, leading to novel virus-host interaction networks. Research on emerging pathogens requires training in diverse techniques including reverse genetics, animal model development, virus-host interactions, pathogenesis, and immunity. My research program has spanned these diverse disciplines and sought to cover the disparate aspects of immunological response, disease comorbidities, and non-human and human emerging coronavirus. Therefore the discussion of each chapter and its larger significance to both this work and the field are discussed, separately, below.

5.1 The icPEDV system

Historically, reverse genetic systems for emerging animal coronaviruses have trailed far behind human studies. The primary goal of the studies in Chapter 2: *Characterization of a Pathogenic Full Length cDNA clone and Transmission Model of Porcine Epidemic Diarrhea Virus Strain PC22A*, was to develop a cDNA plasmid based cloning system for PEDV strain PC22A. By building recombinant viruses capable of replication and fluorescent protein expression *in vitro*, we developed a robust replication, disease, and transmission model *in vivo* using the gnotobiotic pig model. These studies pioneered new strategies and genetic approaches to study swine coronavirus pathogenesis and transmission *in vivo* (48), and were followed by the

development of molecular clones by other groups (168, 261-264). In more recent studies, the PEDV molecular clone was used to map attenuating mutations in the S glycoprotein and other genes, resulting in a genetically defined candidate live virus vaccine (265).

Will live attenuated, genetically defined recombinant viruses have a role in PEDV disease control? PEDV has been circulating throughout Europe and Asia for decades, but was not a serious concern for livestock in the U.S. until its outbreak in 2013. It quickly killed over 8 million piglets, or 10% of the U.S. farm pigs within the first year of outbreak (22, 26). In China, novel vaccine resistant PEDV strains have emerged, resulting in cyclic outbreaks of severe disease (266, 267). PEDV is plastic, highly virulent and transmissible, creating massive problems in farm isolation, procedural cleanliness, and piglet rearing in U.S. farms. In the years since the publication of our manuscript, treatments and better farming practices have been researched, and three vaccines are now available. In the US, the first vaccine conditionally licensed in 2013 was developed by Harrisvaccines, and is based on a truncated form of the PEDV spike in a Venezuelan Equine Encephalitis Virus (VEE) vector (152). This was used primarily to immunize weanling and weaned piglets intramuscularly. However, because newborn piglets are the most at-risk population, a series of immunizations for piglets is not practical. The second and third vaccines, developed by Zoetis and the Vaccine and Infectious Disease Organization (InterVac) in Canada, respectively, are instead administered to the pregnant or milking sow, and work via lactogenic immunity (27, 28). These both reduce mortality in infected piglets and open avenues to not only protect large losses of piglets, but also to prevent infection and therefore transmission in older animals. However, outbreaks generating massive loss of piglets are still occurring in the U.S. and Canada. Farmers must halt piglet influx into their farms, decontaminate facilities, and vaccinate animals. This is still a major burden on pork farming in the U.S. (268). Therefore, as a

pathogenic virus, PEDV is still an important disease to understand in the U.S. today. Our model of icPEDV allows for the genetic manipulation and study of PEDV, including analyses of candidate live attenuated viruses (265).

Beyond the disease state, PEDV and icPEDV offer aspects of research unique among coronaviruses. First, PEDV is one of the few coronaviruses with a transmission model of infection. Both wildtype and icPEDV are capable of transmitting between infected piglets while retaining high titer and mortality. For this reason, genetic studies of viral transmissibility can be conducted that have the potential to identify transmission factors for coronaviruses. Importantly, PEDV is a biosafety level 2 (BSL2) agent without a human host, meaning that transmission studies could be more readily performed on this coronavirus as opposed to human respiratory coronaviruses. Secondly, PEDV is distinct from other coronaviruses in its age dependency. While SARS-CoV and MERS-CoV show greater mortality in elderly populations, PEDV is primarily lethal in newborn populations. Therefore, icPEDV may additionally lend a tool for understanding the genetic mechanisms of age-dependent pathogenicity among coronaviruses.

Despite the benefits, there are various difficulties and drawbacks inherent in this study and the icPEDV system. First, while wildtype PEDV-PC22A replicates to high titer and is highly lethal *in vivo*, the virus does not replicate well *in vitro*. Because of this, generating and recovering icPEDV is difficult, time consuming, and frustrating. Infectious clone coronaviruses are distinctly difficult to generate due to their large genome that must be transcribed prior to electroporation into cells. Generation and electroporation of the full length RNA genome in a poorly-replicating virus proved to be problematic. A second difficulty in icPEDV is the expense and difficulty of the model. Gnotobiotic pig studies offer the advantage of studying PEDV in its host. However, the expense, time to raise and rear gnotobiotic piglets, and relatively small

animal cohorts make large genetic studies difficult to achieve. Despite this, the system has many advantages. Researchers in the Wang lab have passaged PEDV through cell culture in order to generate a better cell-adapted virus and have had some success. While this may reduce pathogenicity *in vivo*, passage experiments and acquired mutations can also allow for identification of SNPs and genetic mutations that attenuate PEDV. Ideally, a better tissue culture adapted model will abrogate the difficulties of the icPEDV system while retaining its benefits. For example, a passage 200 PEDV capable of high titer replication *in vitro* but incapable of transmission *in vivo* has the potential to lead to identification of genetic predictors of transmission. Because of the icPEDV clone, these mutations could be introduced into a wild-type genetic backbone and studied individually. This is one of the primary advantages of the infectious clone model, and we hope that it offers a tool to more easily research and manipulate PEDV genetics.

5.2 Humoral Immunity in primary SARS-CoV infections

Emerging coronavirus usually cause acute infections and in most individuals infectious virus is rapidly cleared, although viral genomic RNA may persist for months. In immunosuppressed individuals, however, MERS-CoV infections can persist for months in some individuals. Virus persistence in bats is common and critical for strain maintenance in natural populations. *Chapter 3: Critical role for B-cells in SARS-CoV clearance during acute infection* was initiated in order to study host genetic factors associated with early virus clearance and to follow up on curious results from *Rag*^{-/-} immune deficient mice in previously published studies of MA15 SARS-CoV infection. In one study, *Rag*^{-/-} mice lost no weight but retained high titer virus in the lung long term; in another, *Rag*^{-/-} mice lost weight equivalent to control mice but still retained titer in the lung (71, 119). Because *Rag*^{-/-} mice lack functional lymphocytes, this

pointed to a role for pathogenicity and/or clearance in either B or T cell populations. At this time, most of the field focused on the role of various T cell populations in virus clearance (76, 85, 86, 88-91, 93, 269). What began as research into minor T cell populations quickly became an interest in the role of early B cell responses in SARS-CoV infection. We concluded that B cells significantly contribute to SARS-CoV clearance during acute infection, and determined that adoptive transfer of serum from 7dpi mice was capable of preventing mortality when given prophylactically. These findings are novel to the SARS-CoV field and offer interesting applications for future coronavirus outbreaks.

Primarily, this work is a novel look into the role of B cells within the first week of SARS-CoV infection. B cells and humoral immunity has been well studied in the context of SARS-CoV infection memory and long term antibody generation. Surviving SARS-CoV patients generated robust IgG responses to SARS-CoV antigens that peaked in titer within the first year after infection (81, 97). However, B cells and antibodies have been rarely studied in the context of acute CoV infection. Primarily, T cells are thought to be responsible for viral clearance during acute infection. SARS-CoV infects the airway epithelium where dendritic cells are able to capture viral antigen via MHC-peptide complexes. These dendritic cells migrate to the draining lymph node where they activate effector T cells that can migrate to the lung (86). Once at the site of infection, effector T cells clear virus and stimulate immune response via cytokine, chemokine, and cytotoxic molecule excretion, direct cell killing, and secondary immune cell activation. During this time, helper T cells can activate B cells to begin antibody generation (270). In a sublethal C57BL/6 model, we were surprised to find that B cell activation early in infection is capable of producing high titers of SARS-CoV specific antibody capable of neutralization at 7 dpi similar to that seen at 15 and 30 dpi. This primarily serves the coronavirus community in

opening an avenue into the role of B cells in acute viral infection. The mechanisms of viral neutralization, specific Ig subtypes, and a thorough timeline of neutralizing antibody development are have yet to be described, and will ideally be addressed in future studies. Based on our findings, it is likely that a broadly neutralizing early IgM response is responsible for SARS-CoV neutralization by 7 dpi serum, due to the high titer of anti-SARS-CoV IgM present early infection. Future studies should isolate or ablate IgM function in order to confirm this finding. One option is the addition of 2-betamercaptoethanol into serum samples prior to *in vitro* neutralization assay to deplete IgM (271) in order to assess the relative neutralization of IgM versus IgG and other serum factors.

Similarly, confirmatory studies using alternate methods of B cell analysis would be useful to the field. Adoptive B cell transfer or serum transfer of isolated antibody subclasses would allow for a more thorough view of B cell function in acute infection. Similarly, the use of a CD40^{-/-} mouse model or T cell function analysis in the absence of B cells during acute infection would begin to elucidate the interactions of helper T cells, effector T cells, and B cells during the early days of SARS-CoV infection. Ideally, the use of CD40^{-/-} mice in conjunction with HELMET mice could provide a clearer image of the role of CD4T cells and B cell activation in early virus clearance. Based on the results here and ongoing studies in lab, HELMET mice, lacking the ability to generate robust antigen specific antibody, do not clear virus by 7dpi, but do clear by 15 dpi. OTII mice show a similar clearance dynamic, but lack the ability to develop a CD4TCR specific to antigen. Both of these results support a hypothesis of early clearance by B cells activated by CD4T helper cells – ie: viral infection initiates very early CD4T help to B cells, which upon activation can generate virus specific IgG antibodies. Though IgG is low early in infection, these results suggest that it is the IgG and not IgM that is

responsible for early viral clearance in the immune competent mouse model of MA15 infection. CD40^{-/-} mice lack CD40/CD40L, and as a result, CD4T cells are not able to activate B cells in response to antigen. A similar delay in clearance in this mouse line would lend further support to the idea that early IgG responses are responsible for early viral clearance in the immune intact model. Ideally, this would be followed up with isolation and adoptive transfer of 7dpi IgG sera isolate. However, our abilities to generate adequate amounts of sera, isolate IgG in adequate concentrations, and return this solution into mice safely in a BSL3 environment is likely beyond current capabilities. However, isolation of IgG and IgM at 2, 4, 7, and 15 dpi in tandem with neutralization assays would tell us whether IgG, even at low early concentrations *in vivo*, is the responsible party for clearance. Ig free serum should be run as a control for complement and other serum factors in these neutralization assays.

A more thorough understanding of these early lymphocytic processes is vital for future coronavirus outbreaks. For example, a surprising study from Ho et al. evaluated SARS patients for serum antibody titers within the first weeks of illness, finding that “early responder” patients who developed SARS-CoV neutralizing antibody within the first two weeks of infection were far less likely to have survived than those patients who seroconverted 3 or more weeks after infection (98). These findings point to a complex relationship of B cell activation, Ig subclass development and neutralization, and patient survival that might be better understood through both this and future work.

In this work, we show a protective potential for early serum transfer *in vivo*. Serum transfer from 7 dpi control mice to experimental mice one day prior to SARS-CoV infection conveyed protection from lethal disease in 12 and 20 week old mice. In previous research, patient polyclonal antibodies generated in the first year of infection or monoclonal antibodies

developed against SARS-CoV antigen were capable of protecting prophylactically in the mouse model and have been used in compassionate care cases of SARS-CoV infection in humans to successfully treat patients and clear virus (200, 272). Our studies have determined that, though transfer of convalescent serum from later days post infection better inhibited disease and weight loss in mice, serum antibody is capable of neutralizing virus even in the early days of SARS-CoV infection. However, it is unknown whether convalescent serum given therapeutically or during recovery would be equally beneficial. Previous studies have pointed toward a therapeutic use for antibody therapy in SARS-CoV infection (273), wherein Syrian hamsters infected with SARS-CoV recovered from illness after therapeutic treatment with monoclonal antibody. One possible benefit of early serum antibody transfer, as opposed to monoclonal antibody transfer, is mitigation of viral escape mutants. While SARS-CoV has been shown to “escape” from monoclonal antibody neutralization (274), neutralization via two non-competing monoclonal antibodies controls immune escape and extends the breadth of protection (275) – a similar outcome is likely with early polyclonal serum antibody therapy. However, both therapeutic use and viral escape in convalescent sera transfer should be addressed in future studies.

In the case of future coronavirus outbreaks, patient-derived convalescent serum antibody might be used to lower viral titers and prevent mortality in the case of compassionate care or infected patients not responding to treatment. These findings become particularly important in light of recent studies regarding pre-emergent SARS-like bat coronaviruses (31). SHC014-CoV, despite its genetic similarity to SARS-CoV, was not neutralized by monoclonal SARS-CoV antibodies (9). This suggests that future coronavirus outbreaks may not respond to current antibody therapy or vaccine models, and instead, quick patient serum-derived treatments may become significant. To expand on this idea, the use of outbreak convalescent patient sera may

not even be required. A recent publication by Gardner et. al. outlines a practical application for neutralizing polyclonal sera in patient treatment (276). Generally, antibody-based therapeutics fall into three categories: human polyclonal antibody, non-human derived polyclonal antibody, or monoclonal antibody made *in vitro* (276, 277). Human polyclonal antibody is ideal for protection against or treatment for infectious disease, however, this not readily available, and only then in small quantities (278). Non-human derived polyclonal antibody can be isolated in larger quantities and more easily, however immunoreactivity becomes a major problem.

Monoclonal antibodies can be “humanized” and generated en masse, but only bind a single target of a virion, making them less potent and creating a potential for escape mutants (274, 275).

Gardner et. al., however, developed a strategy to immunize transchromosomal bovines, which can produce potent neutralizing human antibodies in response to hyperimmunization, and have used the resultant purified polyclonal antibody effectively as a prophylactic and therapeutic treatment against high and low dose Venezuelan Equine Encephalitic Virus (276). This strategy may be applied similarly to coronavirus infection, and potentially in a more robust way. Using metagenomic data, diverse clusters of SARS- and MERS-like CoV have been identified (21, 198). Menachery et. al. exhibited the potential of generating these CoV using reverse genetics systems, effectively creating infectious CoV used in infection and neutralization assays (8, 198).

In preparation for emergent CoV outbreaks, it may be invaluable to create these phylogenetically diverse CoV to use as immunogens in the transchromosomal bovine model, effectively generating polyclonal antibody serum pools to treat novel CoV outbreaks. This method could additionally be applied during the early days of a novel outbreak in order to generate anti-CoV polyclonal antibody to use in the affected population both prophylactically and therapeutically. The possible applications for polyclonal antibody treatment are vast, but require that research

continues into antibody development and neutralization capacity. Of concern, at least three polyclonal and eight monoclonal antibody products have been evaluated in influenza virus clinical trials, yet efficacy results have been mixed and inconclusive (279)). Thus, early administration is likely key to product success.

5.3 Diet Induced Obesity in the SARS-CoV mouse model and collaborative cross

During both the SARS and MERS coronavirus outbreaks, comorbidities were an important determinant of patient outcomes. In the case of human respiratory coronaviruses, comorbidities which effected pathogenesis and survival included aging, chronic organ failure, diabetes, chronic obstructive pulmonary disorder, metabolic disease, and body mass index (12, 81, 126, 128). In the case of obesity, many metabolic, immunologic, and wound healing pathways are dysregulated prior to respiratory viral infection (255, 280). Obesity decreases respiratory function, gas exchange efficiency, and wound healing, while simultaneously increasing chronic inflammation (229, 231, 281). This chronic inflammation leads to dysregulated immune responses in the event that infection does occur. Notably, in respiratory disease, obesity increases both hospital stay and severity of illness in ARDS patients (137, 138). An important contribution herein is the development of new obese mouse models that enhance SARS-CoV pathogenesis. In other mouse models of respiratory disease, obesity causes increased vascular permeability in the lungs, poor T cell responses, higher mortality rates, and an extended duration of proinflammatory cells in the lungs after influenza virus infection (134, 136, 139, 140). Because of human comorbidity data and studies of respiratory disease and obesity, an obesity comorbidity model of SARS-CoV infection provides new insight into viral pathogenesis and vulnerable models for evaluating vaccine and antiviral drug performance.

As a model for the study in Chapter 4, we used C57BL/6J mice on a high fat diet for >15 weeks. This model has been established previously in both obesity models and comorbidity models of infectious disease. The high fat diet is advantageous in that the control, or lean diet mice, are genetically identical to the obese mice. Other mouse models of obesity include leptin knockout mice or other genetically distinct mouse lines. Previous research in the field of obesity and influenza by Milner et. al. compared leptin deficient mice, mice deficient in leptin only in the hypothalamic neurons, high fat diet mice, and two lean control diets to determine the impact of diet versus obesity on the model of infectious disease (135, 140). Importantly, they found that though diet may synergize with obesity to impact disease outcome, obesity alone was sufficient to increase susceptibility to influenza infection. Additionally, Kennedy et al. determined that while leptin knockout mice did become obese, the global lack of leptin, an important metabolic and immune regulator, confounds the effects of obesity and, presumably, viral infection .

We first found that high fat diet induced obesity dramatically increased morbidity and mortality in SARS-CoV infected mice. Obese mice showed poor respiratory function and failed to resolve illness. The value of this finding in coronavirology and infectious disease in general is an expansion of the field of comorbidity research. Obesity is a single variable that is studied here, however, research into the impact of diabetes or chronic respiratory distress syndrome on SARS or MERS outcomes can improve our understanding of coronavirus respiratory disease and patient health. Furthermore, research into the mechanisms of obesity-induced SARS-CoV susceptibility and mechanisms of alternate comorbidities may highlight new and novel pathways and targets for patient treatments that may otherwise be undiscovered. Future studies and retrospectives should consider addressing the impact of patient medication schedules on disease as well – the consequences of insulin injection, chronic corticosteroid use, or inhalers, for

example, are not well understood in the context of human coronavirus infection, despite being common medications for chronically ill patients.

In order to determine whether obesity consistently increased SARS-CoV pathogenesis, 9 lines of CC mice were fed a high fat diet, monitored for weight and body fat, then infected with a sublethal MA15 dose. While some research has been conducted on CC mice and metabolic outcomes, none have focused on these lines in the context of viral infection and diet. We observed that genetics were a major factor on the impact of high fat diet prior to infection. While some mouse lines (CC001, CC035, CC046, CC010) gained body fat and became obese on high fat diet, others did not show significant increases in body fat (CC012, CC041, CC030, CC003) or lost weight on HFD (CC061). In line with this finding, disease susceptibility followed with genetics as opposed to diet or obesity. Genetic lines, despite their diet, tracked in weight loss and mortality with their diet controls. These findings were surprising for various reasons. The genetic component of obesity in response to high fat diet was staggering. Whether this is attributable particularly to genetics or to the development of a high fat diet in classic inbred lab mouse strains is an important question for future work in both nutrition and obesity. It has been observed even in similar inbred lab strains that mice can exhibit highly differential susceptibility to SARS-CoV infection (unpublished observations). It follows that similar genetic determinants may impact susceptibility to obesity on a specific diet. Because of the scope of this study, it is not possible to track the specific metabolic outcomes of high fat versus control diet in each of the lines. However, future studies of diet in the CC mice should focus not only on obesity as an outcome but leptin levels, blood sugar, hormone signaling, and other metabolic markers. Similarly, the scope of the study does not allow for genetic mapping of obesity determinants. However, genetic

mapping of determinants of diet outcomes is likely to be a fascinating and illuminating study in the future.

The study of comorbidity in viral disease is relatively new. Virology research has been historically conducted in the least complex systems available, whether that be cell lines or inbred mice. This allows for targeted manipulation and control of viral genetics, host factors, or pathways of interest, and has been an invaluable tool to understand both virology and virus-host dynamics during infection. However, studying an infectious disease in an uncomplicated system also avoids the realities of human disease – patients are commonly affected by one or more additional diseases or medical issues, come from complex social and living environments, vary greatly in nutrition, and are genetically disparate. For any individual disease, these factors will impact outcomes to greater or lesser degrees, and are complicated to study. However, introducing dynamic host systems is important in order to better grasp the biological reality of a disease state and better address human medical needs.

5.4 Conclusion

Coronaviruses encompass a wide range of hosts, disease phenotypes, and outcomes. While some molecular coronavirology remains the same in each case, the dynamic between coronavirus and host is complicated and variable. Individual coronavirus species differ considerably in sequence, size, and non-structural gene makeup. Similarly, receptor binding, species (or even class), permissible cell type, disease state, and immune response vary massively between coronavirus hosts. Due to virus and host complexity, an interplay between viral evolution and host resilience refines and bolsters each in the push and pull of viral infection. Though this relationship is infinitely complex and difficult to grasp, small works such as these,

and great people such as our scientific leaders and PIs help us whittle away at the truth and come closer to understanding the elegance of life.

REFERENCES

1. **ICTV.** Coronaviridae - Positive Sense RNA Viruses - Positive Sense RNA Viruses (2011) - International Committee on Taxonomy of Viruses (ICTV). Accessed
2. **Woo PCY, Lau SKP, Lam CSF, Lau CCY, Tsang AKL, Lau JHN, Bai R, Teng JLL, Tsang CCC, Wang M, Zheng B-J, Chan K-H, Yuen K-Y.** 2012. Discovery of Seven Novel Mammalian and Avian Coronaviruses in the Genus Deltacoronavirus Supports Bat Coronaviruses as the Gene Source of Alphacoronavirus and Betacoronavirus and Avian Coronaviruses as the Gene Source of Gammacoronavirus and Deltacoronavirus. *Journal of Virology* **86**:3995-4008.
3. **Fehr AR, Perlman S.** 2015. Coronaviruses: An Overview of Their Replication and Pathogenesis. *Methods in molecular biology (Clifton, NJ)* **1282**:1-23.
4. **Sweileh WM.** 2017. Global research trends of World Health Organization's top eight emerging pathogens. *Globalization and Health* **13**:9.
5. **Peck KM, Burch CL, Heise MT, Baric RS.** 2015. Coronavirus Host Range Expansion and Middle East Respiratory Syndrome Coronavirus Emergence: Biochemical Mechanisms and Evolutionary Perspectives. *Annual Review of Virology* **2**:95-117.
6. **Gao H, Yao H, Yang S, Li L.** 2016. From SARS to MERS: evidence and speculation. *Frontiers of Medicine* **10**:377-382.
7. **De Wit E, Van Doremalen N, Falzarano D, Munster VJ.** 2016. SARS and MERS: recent insights into emerging coronaviruses. *Nature Reviews Microbiology*; London **14**:523-534.
8. **Menachery VD, Yount BL, Sims AC, Debbink K, Agnihothram SS, Gralinski LE, Graham RL, Scobey T, Plante JA, Royal SR, Swanstrom J, Sheahan TP, Pickles RJ, Corti D, Randell SH, Lanzavecchia A, Marasco WA, Baric RS.** 2016. SARS-like WIV1-CoV poised for human emergence. *Proceedings of the National Academy of Sciences* **113**:3048-3053.
9. **Menachery VD, Yount BL, Debbink K, Agnihothram S, Gralinski LE, Plante JA, Graham RL, Scobey T, Ge X-Y, Donaldson EF, Randell SH, Lanzavecchia A, Marasco WA, Shi Z-L, Baric RS.** 2015. A SARS-like cluster of circulating bat coronaviruses shows potential for human emergence. *Nature Medicine* **21**:1508-1513.
10. **Roberts A, Deming D, Paddock CD, Cheng A, Yount B, Vogel L, Herman BD, Sheahan T, Heise M, Genrich GL, Zaki SR, Baric R, Subbarao K.** 2007. A mouse-adapted SARS-coronavirus causes disease and mortality in BALB/c mice. *PLoS Pathog* **3**:e5.
11. **Wei M-T, de Vlas SJ, Yang Z, Borsboom GJJM, Wang L, Li H, Li Y, Zhang Z, Richardus JH, Wang S-X.** 2009. The SARS outbreak in a general hospital in Tianjin, China: clinical aspects and risk factors for disease outcome. *Tropical medicine & international health: TM & IH* **14 Suppl 1**:60-70.
12. **Booth CM, Matukas LM, Tomlinson GA, Rachlis AR, Rose DB, Dwosh HA, Walmsley SL, Mazzulli T, Avendano M, Derkach P, Ephtimios IE, Kitai I, Mederski BD, Shadowitz SB, Gold WL, Hawryluck LA, Rea E, Chenkin JS, Cescon DW, Poutanen SM, Detsky AS.** 2003. Clinical features and short-term outcomes of 144 patients with SARS in the greater Toronto area. *JAMA* **289**:2801-2809.

13. **Matthay MA, Zemans RL.** 2011. The acute respiratory distress syndrome: pathogenesis and treatment. *Annu Rev Pathol* **6**:147-163.
14. **Gossner C, Danielson N, Gervelmeyer A, Berthe F, Faye B, Kaasik Aaslav K, Adlhoch C, Zeller H, Penttinen P, Coulombier D.** 2014. Human-Dromedary Camel Interactions and the Risk of Acquiring Zoonotic Middle East Respiratory Syndrome Coronavirus Infection. *Zoonoses and Public Health* doi:10.1111/zph.12171.
15. **Zumla A, Hui DS, Perlman S.** 2015. Middle East respiratory syndrome. *The Lancet* **386**:995-1007.
16. **Frieman M, Heise M, Baric R.** 2008. SARS coronavirus and innate immunity. *Virus Res* **133**:101-112.
17. **Al-Abdallat MM, Payne DC, Alqasrawi S, Rha B, Tohme RA, Abedi GR, Al Nsour M, Iblan I, Jarour N, Farag NH, Haddadin A, Al-Sanouri T, Tamin A, Harcourt JL, Kuhar DT, Swerdlow DL, Erdman DD, Pallansch MA, Haynes LM, Gerber SI, Jordan M-CIT.** 2014. Hospital-associated outbreak of Middle East respiratory syndrome coronavirus: a serologic, epidemiologic, and clinical description. *Clinical Infectious Diseases: An Official Publication of the Infectious Diseases Society of America* **59**:1225-1233.
18. **Poletto C, Boëlle P-Y, Colizza V.** 2016. Risk of MERS importation and onward transmission: a systematic review and analysis of cases reported to WHO. *BMC infectious diseases* **16**:448.
19. **Al-Tawfiq JA, Perl TM.** 2015. Middle East respiratory syndrome coronavirus in healthcare settings. *Current Opinion in Infectious Diseases* **28**:392-396.
20. **Al Hammadi ZM, Chu DK, Eltahir YM, Al Hosani F, Al Mulla M, Tarnini W, Hall AJ, Perera RA, Abdelkhalek MM, Peiris JS, Al Muhairi SS, Poon LL.** 2015. Asymptomatic MERS-CoV Infection in Humans Possibly Linked to Infected Dromedaries Imported from Oman to United Arab Emirates, May 2015. *Emerg Infect Dis* **21**:2197-2200.
21. **Menachery VD, Graham RL, Baric RS.** 2017. Jumping species-a mechanism for coronavirus persistence and survival. *Current Opinion in Virology* **23**:1-7.
22. **Lee C.** 2015. Porcine epidemic diarrhea virus: An emerging and re-emerging epizootic swine virus. *Virol J* **12**:193.
23. **Ma Y, Zhang Y, Liang X, Lou F, Oglesbee M, Krakowka S, Li J.** 2015. Origin, Evolution, and Virulence of Porcine Deltacoronaviruses in the United States. *mBio* **6**:e00064-00015.
24. **Liu X, Lin C-M, Annamalai T, Gao X, Lu Z, Esseili MA, Jung K, El-Tholoth M, Saif LJ, Wang Q.** 2015. Determination of the infectious titer and virulence of an original US porcine epidemic diarrhea virus PC22A strain.
25. **Vlasova AN, Marthaler D, Wang Q, Culhane MR, Rossow KD, Rovira A, Collins J, Saif LJ.** 2014. Distinct characteristics and complex evolution of PEDV strains, North America, May 2013-February 2014. *Emerging Infectious Diseases* **20**:1620-1628.
26. **Schulz LL, Tonsor GT.** 2015. Assessment of the economic impacts of porcine epidemic diarrhea virus in the United States. *J Anim Sci* **93**:5111-5118.
27. **Gerdtts V, Zakhartchouk A.** 2017. Vaccines for porcine epidemic diarrhea virus and other swine coronaviruses. *Veterinary Microbiology* **206**:45-51.

28. **Langel SN, Paim FC, Lager KM, Vlasova AN, Saif LJ.** 2016. Lactogenic immunity and vaccines for porcine epidemic diarrhea virus (PEDV): Historical and current concepts. *Virus Res* **226**:93-107.
29. **Site. TP.** PEDv Impact on Pig Prices and Supply – A Look at 2015, 2016. Accessed
30. **Hu B, Zeng LP, Yang XL, Ge XY, Zhang W, Li B, Xie JZ, Shen XR, Zhang YZ, Wang N, Luo DS, Zheng XS, Wang MN, Daszak P, Wang LF, Cui J, Shi ZL.** 2017. Discovery of a rich gene pool of bat SARS-related coronaviruses provides new insights into the origin of SARS coronavirus. *PLoS Pathog* **13**:e1006698.
31. **Jeong J, Smith CS, Peel AJ, Plowright RK, Kerlin DH, McBroom J, McCallum H.** 2017. Persistent infections support maintenance of a coronavirus in a population of Australian bats (*Myotis macropus*). *Epidemiol Infect* **145**:2053-2061.
32. **Graham RL, Becker MM, Eckerle LD, Bolles M, Denison MR, Baric RS.** 2012. A live, impaired-fidelity coronavirus vaccine protects in an aged, immunocompromised mouse model of lethal disease. *Nat Med* **18**:1820-1826.
33. **Totura AL, Baric RS.** 2012. SARS coronavirus pathogenesis: host innate immune responses and viral antagonism of interferon. *Current Opinion in Virology* **2**:264-275.
34. **Vijay R, Perlman S.** 2016. Middle East respiratory syndrome and severe acute respiratory syndrome. *Current Opinion in Virology* **16**:70-76.
35. **Kim SH, Ko JH, Park GE, Cho SY, Ha YE, Kang JM, Kim YJ, Huh HJ, Ki CS, Jeong BH, Park J, Jang JH, Kim WS, Kang CI, Chung DR, Song JH, Peck KR.** 2017. Atypical presentations of MERS-CoV infection in immunocompromised hosts. *J Infect Chemother* **23**:769-773.
36. **Day CW, Baric R, Cai SX, Frieman M, Kumaki Y, Morrey JD, Smee DF, Barnard DL.** 2009. A new mouse-adapted strain of SARS-CoV as a lethal model for evaluating antiviral agents in vitro and in vivo. *Virology* **395**:210-222.
37. **Roberts A, Deming D, Paddock CD, Cheng A, Yount B, Vogel L, Herman BD, Sheahan T, Heise M, Genrich GL, Zaki SR, Baric R, Subbarao K.** 2007. A Mouse-Adapted SARS-Coronavirus Causes Disease and Mortality in BALB/c Mice. *PLoS Pathogens* **3**.
38. **Tseng C-TK, Huang C, Newman P, Wang N, Narayanan K, Watts DM, Makino S, Packard MM, Zaki SR, Chan T-S, Peters CJ.** 2007. Severe acute respiratory syndrome coronavirus infection of mice transgenic for the human Angiotensin-converting enzyme 2 virus receptor. *Journal of Virology* **81**:1162-1173.
39. **Vogel LN, Roberts A, Paddock CD, Genrich GL, Lamirande EW, Kapadia SU, Rose JK, Zaki SR, Subbarao K.** 2007. Utility of the aged BALB/c mouse model to demonstrate prevention and control strategies for severe acute respiratory syndrome coronavirus (SARS-CoV). *Vaccine* **25**:2173-2179.
40. **Gretebeck LM, Subbarao K.** 2015. Animal models for SARS and MERS coronaviruses. *Curr Opin Virol* **13**:123-129.
41. **Sutton TC, Subbarao K.** 2015. Development of animal models against emerging coronaviruses: From SARS to MERS coronavirus. *Virology* **479-480**:247-258.

42. **van Doremalen N, Munster VJ.** 2015. Animal models of Middle East respiratory syndrome coronavirus infection. *Antiviral Res* **122**:28-38.
43. **Peck KM, Scobey T, Swanstrom J, Jensen KL, Burch CL, Baric RS, Heise MT.** 2017. Permissivity of Dipeptidyl Peptidase 4 Orthologs to Middle East Respiratory Syndrome Coronavirus Is Governed by Glycosylation and Other Complex Determinants. *J Virol* **91**.
44. **Cockrell AS, Peck KM, Yount BL, Agnihothram SS, Scobey T, Curnes NR, Baric RS, Heise MT.** 2014. Mouse Dipeptidyl Peptidase 4 Is Not a Functional Receptor for Middle East Respiratory Syndrome Coronavirus Infection. *Journal of Virology* **88**:5195-5199.
45. **Cockrell AS, Yount BL, Scobey T, Jensen K, Douglas M, Beall A, Tang X-C, Marasco WA, Heise MT, Baric RS.** 2016. A mouse model for MERS coronavirus-induced acute respiratory distress syndrome. *Nature Microbiology* **2**:16226.
46. **Cockrell AS, Baric RS.** 2016. An effective DNA vaccine platform for Middle East respiratory syndrome coronavirus. *Ann Transl Med* **4**:499.
47. **Zhang N, Tang J, Lu L, Jiang S, Du L.** 2015. Receptor-binding domain-based subunit vaccines against MERS-CoV. *Virus Res* **202**:151-159.
48. **Beall A, Yount B, Lin C-M, Hou Y, Wang Q, Saif L, Baric R.** 2016. Characterization of a Pathogenic Full-Length cDNA Clone and Transmission Model for Porcine Epidemic Diarrhea Virus Strain PC22A. *mBio* **7**:e01451-01415.
49. **Scobey T, Yount BL, Sims AC, Donaldson EF, Agnihothram SS, Menachery VD, Graham RL, Swanstrom J, Bove PF, Kim JD, Grego S, Randell SH, Baric RS.** 2013. Reverse genetics with a full-length infectious cDNA of the Middle East respiratory syndrome coronavirus. *Proceedings of the National Academy of Sciences of the United States of America* **110**:16157-16162.
50. **Donaldson EF, Yount B, Sims AC, Burkett S, Pickles RJ, Baric RS.** 2008. Systematic assembly of a full-length infectious clone of human coronavirus NL63. *Journal of Virology* **82**:11948-11957.
51. **Yount B, Curtis KM, Fritz EA, Hensley LE, Jahrling PB, Prentice E, Denison MR, Geisbert TW, Baric RS.** 2003. Reverse genetics with a full-length infectious cDNA of severe acute respiratory syndrome coronavirus. *Proceedings of the National Academy of Sciences of the United States of America* **100**:12995-13000.
52. **Yount B, Denison MR, Weiss SR, Baric RS.** 2002. Systematic assembly of a full-length infectious cDNA of mouse hepatitis virus strain A59. *Journal of Virology* **76**:11065-11078.
53. **Yount B, Curtis KM, Baric RS.** 2000. Strategy for systematic assembly of large RNA and DNA genomes: transmissible gastroenteritis virus model. *Journal of Virology* **74**:10600-10611.
54. **Cockrell AS, Beall A, Yount B, Baric R.** 2017. Efficient Reverse Genetic Systems for Rapid Genetic Manipulation of Emergent and Preemergent Infectious Coronaviruses. *Methods in Molecular Biology (Clifton, NJ)* **1602**:59-81.
55. **Agnihothram S, Yount BL, Jr., Donaldson EF, Huynh J, Menachery VD, Gralinski LE, Graham RL, Becker MM, Tomar S, Scobey TD, Osswald HL, Whitmore A, Gopal R, Ghosh AK, Mesecar A, Zambon M, Heise M, Denison MR, Baric RS.** 2014. A mouse model for Betacoronavirus subgroup 2c using a bat coronavirus strain HKU5 variant. *MBio* **5**:e00047-00014.

56. **Baric RS, Sims AC.** 2005. Development of mouse hepatitis virus and SARS-CoV infectious cDNA constructs. *Current Topics in Microbiology and Immunology* **287**:229-252.
57. **Menachery VD, Gralinski LE, Mitchell HD, Dinnon KH, Leist SR, Yount BL, Graham RL, McAnarney ET, Stratton KG, Cockrell AS, Debbink K, Sims AC, Waters KM, Baric RS.** 2017. Middle East Respiratory Syndrome Coronavirus Nonstructural Protein 16 Is Necessary for Interferon Resistance and Viral Pathogenesis. *mSphere* **2**.
58. **Menachery VD, Mitchell HD, Cockrell AS, Gralinski LE, Yount BL, Jr., Graham RL, McAnarney ET, Douglas MG, Scobey T, Beall A, Dinnon K, 3rd, Kocher JF, Hale AE, Stratton KG, Waters KM, Baric RS.** 2017. MERS-CoV Accessory ORFs Play Key Role for Infection and Pathogenesis. *MBio* **8**.
59. **Cockrell AS, Yount BL, Scobey T, Jensen K, Douglas M, Beall A, Tang X-C, Marasco WA, Heise MT, Baric RS.** 2016. A Mouse Model for MERS Coronavirus Induced Acute Respiratory Distress Syndrome. *Nature microbiology* **2**:16226.
60. **Peck KM, Cockrell AS, Yount BL, Scobey T, Baric RS, Heise MT.** 2015. Glycosylation of Mouse DPP4 Plays a Role in Inhibiting Middle East Respiratory Syndrome Coronavirus Infection. *Journal of Virology* **89**:4696-4699.
61. **Menachery VD, Yount BL, Josset L, Gralinski LE, Scobey T, Agnihothram S, Katze MG, Baric RS.** 2014. Attenuation and restoration of severe acute respiratory syndrome coronavirus mutant lacking 2'-o-methyltransferase activity. *Journal of Virology* **88**:4251-4264.
62. **Freundt EC, Yu L, Goldsmith CS, Welsh S, Cheng A, Yount B, Liu W, Frieman MB, Buchholz UJ, Sreaton GR, Lippincott-Schwartz J, Zaki SR, Xu X-N, Baric RS, Subbarao K, Lenardo MJ.** 2010. The open reading frame 3a protein of severe acute respiratory syndrome-associated coronavirus promotes membrane rearrangement and cell death. *Journal of Virology* **84**:1097-1109.
63. **Frieman M, Yount B, Heise M, Kopecky-Bromberg SA, Palese P, Baric RS.** 2007. Severe acute respiratory syndrome coronavirus ORF6 antagonizes STAT1 function by sequestering nuclear import factors on the rough endoplasmic reticulum/Golgi membrane. *Journal of Virology* **81**:9812-9824.
64. **Deming D, Sheahan T, Heise M, Yount B, Davis N, Sims A, Suthar M, Harkema J, Whitmore A, Pickles R, West A, Donaldson E, Curtis K, Johnston R, Baric R.** 2006. Vaccine efficacy in senescent mice challenged with recombinant SARS-CoV bearing epidemic and zoonotic spike variants. *PLoS medicine* **3**:e525.
65. **Yount B, Roberts RS, Lindesmith L, Baric RS.** 2006. Rewiring the severe acute respiratory syndrome coronavirus (SARS-CoV) transcription circuit: engineering a recombination-resistant genome. *Proc Natl Acad Sci U S A* **103**:12546-12551.
66. **Sims AC, Baric RS, Yount B, Burkett SE, Collins PL, Pickles RJ.** 2005. Severe Acute Respiratory Syndrome Coronavirus Infection of Human Ciliated Airway Epithelia: Role of Ciliated Cells in Viral Spread in the Conducting Airways of the Lungs. *Journal of Virology* **79**:15511-15524.
67. **Curtis KM, Yount B, Baric RS.** 2001. A simple strategy to assemble infectious RNA and DNA clones. *Advances in Experimental Medicine and Biology* **494**:475-481.
68. **Loo Y-M, Fornek J, Crochet N, Bajwa G, Perwitasari O, Martinez-Sobrido L, Akira S, Gill MA, García-Sastre A, Katze MG, Gale M.** Distinct RIG-I and MDA5 Signaling by RNA Viruses in Innate Immunity. Accessed

69. **Reikine S, Nguyen JB, Modis Y.** 2014. Pattern Recognition and Signaling Mechanisms of RIG-I and MDA5. *Frontiers in Immunology* **5**.
70. **Kawai T, Akira S.** 2010. The role of pattern-recognition receptors in innate immunity: update on Toll-like receptors. *Nature Immunology* **11**:373-384.
71. **Sheahan T, Morrison TE, Funkhouser W, Uematsu S, Akira S, Baric RS, Heise MT.** 2008. MyD88 is required for protection from lethal infection with a mouse-adapted SARS-CoV. *PLoS Pathog* **4**:e1000240.
72. **Totura AL, Whitmore A, Agnihothram S, Schafer A, Katze MG, Heise MT, Baric RS.** 2015. Toll-Like Receptor 3 Signaling via TRIF Contributes to a Protective Innate Immune Response to Severe Acute Respiratory Syndrome Coronavirus Infection. *MBio* **6**:e00638-00615.
73. **Frieman MB, Chen J, Morrison TE, Whitmore A, Funkhouser W, Ward JM, Lamirande EW, Roberts A, Heise M, Subbarao K, Baric RS.** 2010. SARS-CoV pathogenesis is regulated by a STAT1 dependent but a type I, II and III interferon receptor independent mechanism. *PLoS Pathog* **6**:e1000849.
74. **Farcas GA, Poutanen SM, Mazzulli T, Willey BM, Butany J, Asa SL, Faure P, Akhavan P, Low DE, Kain KC.** 2005. Fatal severe acute respiratory syndrome is associated with multiorgan involvement by coronavirus. *J Infect Dis* **191**:193-197.
75. **Kopecky-Bromberg SA, Martinez-Sobrido L, Frieman M, Baric RA, Palese P.** 2007. Severe acute respiratory syndrome coronavirus open reading frame (ORF) 3b, ORF 6, and nucleocapsid proteins function as interferon antagonists. *J Virol* **81**:548-557.
76. **Channappanavar R, Fehr Anthony R, Vijay R, Mack M, Zhao J, Meyerholz David K, Perlman S.** 2016. Dysregulated Type I Interferon and Inflammatory Monocyte-Macrophage Responses Cause Lethal Pneumonia in SARS-CoV-Infected Mice. *Cell Host & Microbe* **19**:181-193.
77. **Cameron MJ, Ran L, Xu L, Danesh A, Bermejo-Martin JF, Cameron CM, Muller MP, Gold WL, Richardson SE, Poutanen SM, Willey BM, DeVries ME, Fang Y, Seneviratne C, Bosinger SE, Persad D, Wilkinson P, Greller LD, Somogyi R, Humar A, Keshavjee S, Louie M, Loeb MB, Brunton J, McGeer AJ, Kelvin DJ.** 2007. Interferon-Mediated Immunopathological Events Are Associated with Atypical Innate and Adaptive Immune Responses in Patients with Severe Acute Respiratory Syndrome. *Journal of Virology* **81**:8692-8706.
78. **Rockx B, Baas T, Zornetzer GA, Haagmans B, Sheahan T, Frieman M, Dyer MD, Teal TH, Proll S, van den Brand J, Baric R, Katze MG.** 2009. Early upregulation of acute respiratory distress syndrome-associated cytokines promotes lethal disease in an aged-mouse model of severe acute respiratory syndrome coronavirus infection. *Journal of Virology* **83**:7062-7074.
79. **Page C, Goicochea L, Matthews K, Zhang Y, Klover P, Holtzman MJ, Hennighausen L, Frieman M.** 2012. Induction of alternatively activated macrophages enhances pathogenesis during severe acute respiratory syndrome coronavirus infection. *Journal of Virology* **86**:13334-13349.
80. **Jia N, Feng D, Fang L-Q, Richardus JH, Han X-N, Cao W-C, de Vlas SJ.** 2009. Case fatality of SARS in mainland China and associated risk factors. *Tropical medicine & international health: TM & IH* **14 Suppl 1**:21-27.

81. **Xie L, Liu Y, Fan B, Xiao Y, Tian Q, Chen L, Zhao H, Chen W.** 2005. Dynamic changes of serum SARS-coronavirus IgG, pulmonary function and radiography in patients recovering from SARS after hospital discharge. *Respiratory Research* **6**:5.
82. **Nicholls JM, Poon LLM, Lee KC, Ng WF, Lai ST, Leung CY, Chu CM, Hui PK, Mak KL, Lim W, Yan KW, Chan KH, Tsang NC, Guan Y, Yuen KY, Peiris JSM.** 2003. Lung pathology of fatal severe acute respiratory syndrome. *Lancet (London, England)* **361**:1773-1778.
83. **Totura AL, Whitmore A, Agnihothram S, Schäfer A, Katze MG, Heise MT, Baric RS.** 2015. Toll-Like Receptor 3 Signaling via TRIF Contributes to a Protective Innate Immune Response to Severe Acute Respiratory Syndrome Coronavirus Infection. *mBio* **6**:e00638-00615.
84. **Gralinski LE, Baric RS.** 2015. Molecular pathology of emerging coronavirus infections. *The Journal of Pathology* **235**:185-195.
85. **Vijay R, Hua X, Meyerholz DK, Miki Y, Yamamoto K, Gelb M, Murakami M, Perlman S.** 2015. Critical role of phospholipase A2 group IID in age-related susceptibility to severe acute respiratory syndrome-CoV infection. *The Journal of Experimental Medicine* **212**:1851-1868.
86. **Channappanavar R, Zhao J, Perlman S.** 2014. T-cell-mediated immune response to respiratory coronaviruses. *Immunologic research* **59**:118-128.
87. **Chen J, Lau YF, Lamirande EW, Paddock CD, Bartlett JH, Zaki SR, Subbarao K.** 2010. Cellular immune responses to severe acute respiratory syndrome coronavirus (SARS-CoV) infection in senescent BALB/c mice: CD4+ T cells are important in control of SARS-CoV infection. *J Virol* **84**:1289-1301.
88. **Zhao J, Zhao J, Van Rooijen N, Perlman S.** 2009. Evasion by stealth: inefficient immune activation underlies poor T cell response and severe disease in SARS-CoV-infected mice. *PLoS Pathog* **5**:e1000636.
89. **Channappanavar R, Fett C, Zhao J, Meyerholz DK, Perlman S.** 2014. Virus-specific memory CD8 T cells provide substantial protection from lethal severe acute respiratory syndrome coronavirus infection. *Journal of Virology* **88**:11034-11044.
90. **Zhao J, Zhao J, Perlman S.** 2010. T cell responses are required for protection from clinical disease and for virus clearance in severe acute respiratory syndrome coronavirus-infected mice. *J Virol* **84**:9318-9325.
91. **Perlman S, Dandekar AA.** 2005. Immunopathogenesis of coronavirus infections: implications for SARS. *Nat Rev Immunol* **5**:917-927.
92. **Werner JL, Steele C.** 2014. Innate receptors and cellular defense against pulmonary infections. *Journal of immunology (Baltimore, Md : 1950)* **193**:3842-3850.
93. **Zhao J, Zhao J, Mangalam AK, Channappanavar R, Fett C, Meyerholz DK, Agnihothram S, Baric RS, David CS, Perlman S.** 2016. Airway Memory CD4(+) T Cells Mediate Protective Immunity against Emerging Respiratory Coronaviruses. *Immunity* **44**:1379-1391.
94. **Li CK, Wu H, Yan H, Ma S, Wang L, Zhang M, Tang X, Temperton NJ, Weiss RA, Brenchley JM, Douek DC, Mongkolsapaya J, Tran BH, Lin CL, Screaton GR, Hou JL, McMichael AJ, Xu XN.** 2008. T cell responses to whole SARS coronavirus in humans. *J Immunol* **181**:5490-5500.

95. **Janice Oh HL, Ken-En Gan S, Bertoletti A, Tan YJ.** 2012. Understanding the T cell immune response in SARS coronavirus infection. *Emerg Microbes Infect* **1**:e23.
96. **Zhao J, Alshukairi AN, Baharoon SA, Ahmed WA, Bokhari AA, Nehdi AM, Layqah LA, Alghamdi MG, Al Gethamy MM, Dada AM, Khalid I, Boujelal M, Al Johani SM, Vogel L, Subbarao K, Mangalam A, Wu C, Ten Eyck P, Perlman S, Zhao J.** 2017. Recovery from the Middle East respiratory syndrome is associated with antibody and T-cell responses. *Sci Immunol* **2**.
97. **Wu L-P, Wang N-C, Chang Y-H, Tian X-Y, Na D-Y, Zhang L-Y, Zheng L, Lan T, Wang L-F, Liang G-D.** 2007. Duration of Antibody Responses after Severe Acute Respiratory Syndrome. *Emerging Infectious Diseases* **13**:1562-1564.
98. **Ho M-S, Chen W-J, Chen H-Y, Lin S-F, Wang M-C, Di J, Lu Y-T, Liu C-L, Chang S-C, Chao C-L, King C-C, Chiou J-M, Su I-J, Yang J-Y.** 2005. Neutralizing Antibody Response and SARS Severity. *Emerging Infectious Diseases* **11**:1730-1737.
99. **Leung DTM, Hang C, Frankie T, Chun Hung M, Chan S, Kay P, Cheung JLK, Niu H, Tam JSL, Lim PL.** 2004. Antibody Response of Patients with Severe Acute Respiratory Syndrome (SARS) Targets the Viral Nucleocapsid. *The Journal of Infectious Diseases* **190**:379-386.
100. **Choe PG, Perera R, Park WB, Song KH, Bang JH, Kim ES, Kim HB, Ko LWR, Park SW, Kim NJ, Lau EHY, Poon LLM, Peiris M, Oh MD.** 2017. MERS-CoV Antibody Responses 1 Year after Symptom Onset, South Korea, 2015. *Emerg Infect Dis* **23**:1079-1084.
101. **Newton AH, Cardani A, Braciale TJ.** 2016. The host immune response in respiratory virus infection: balancing virus clearance and immunopathology. *Semin Immunopathol* **38**:471-482.
102. **Gordon JW, Scangos GA, Plotkin DJ, Barbosa JA, Ruddle FH.** 1980. Genetic transformation of mouse embryos by microinjection of purified DNA. *Proceedings of the National Academy of Sciences of the United States of America* **77**:7380-7384.
103. **Gordon JW, Ruddle FH.** 1981. Integration and stable germ line transmission of genes injected into mouse pronuclei. *Science (New York, NY)* **214**:1244-1246.
104. **Wade CM, Daly MJ.** 2005. Genetic variation in laboratory mice. *Nat Genet* **37**:1175-1180.
105. **Kitamura D, Roes J, Kuhn R, Rajewsky K.** 1991. A B cell-deficient mouse by targeted disruption of the membrane exon of the immunoglobulin mu chain gene. *Nature* **350**:423-426.
106. **Hogquist KA, Jameson SC, Heath WR, Howard JL, Bevan MJ, Carbone FR.** 1994. T cell receptor antagonist peptides induce positive selection. *Cell* **76**:17-27.
107. **Barnden MJ, Allison J, Heath WR, Carbone FR.** 1998. Defective TCR expression in transgenic mice constructed using cDNA-based alpha- and beta-chain genes under the control of heterologous regulatory elements. *Immunol Cell Biol* **76**:34-40.
108. **Mombaerts P, Iacomini J, Johnson RS, Herrup K, Tonegawa S, Papaioannou VE.** 1992. RAG-1-deficient mice have no mature B and T lymphocytes. *Cell* **68**:869-877.
109. **Goodnow CC, Crosbie J, Adelstein S, Lavoie TB, Smith-Gill SJ, Brink RA, Pritchard-Briscoe H, Wotherspoon JS, Loblay RH, Raphael K, et al.** 1988. Altered immunoglobulin expression and functional silencing of self-reactive B lymphocytes in transgenic mice. *Nature* **334**:676-682.

110. **Song HK, Hwang DY.** 2017. Use of C57BL/6N mice on the variety of immunological researches. *Lab Anim Res* **33**:119-123.
111. **Champy MF, Selloum M, Zeitler V, Caradec C, Jung B, Rousseau S, Pouilly L, Sorg T, Auwerx J.** 2008. Genetic background determines metabolic phenotypes in the mouse. *Mamm Genome* **19**:318-331.
112. **Chesler EJ, Miller DR, Branstetter LR, Galloway LD, Jackson BL, Philip VM, Voy BH, Culiati CT, Threadgill DW, Williams RW, Churchill GA, Johnson DK, Manly KF.** 2008. The Collaborative Cross at Oak Ridge National Laboratory: developing a powerful resource for systems genetics. *Mamm Genome* **19**:382-389.
113. **Consortium TCT, Churchill GA, Airey DC, Allayee H, Angel JM, Attie AD, Beatty J, Beavis WD, Belknap JK, Bennett B, Berrettini W, Bleich A, Bogue M, Broman KW, Buck KJ, Buckler E, Burmeister M, Chesler EJ, Cheverud JM, Clapcote S, Cook MN, Cox RD, Crabbe JC, Crusio WE, Darvasi A, Deschepper CF, Doerge RW, Farber CR, Forejt J, Gaile D, Garlow SJ, Geiger H, Gershenfeld H, Gordon T, Gu J, Gu W, Haan Gd, Hayes NL, Heller C, Himmelbauer H, Hitzemann R, Hunter K, Hsu H-C, Iraqi FA, Ivandic B, Jacob HJ, Jansen RC, Jepsen KJ, Johnson DK, Johnson TE, et al.** 2004-11-01 2004. The Collaborative Cross, a community resource for the genetic analysis of complex traits. Accessed
114. **Consortium CC.** 2012. The genome architecture of the Collaborative Cross mouse genetic reference population. *Genetics* **190**:389-401.
115. **Aylor DL, Valdar W, Foulds-Mathes W, Buus RJ, Verdugo RA, Baric RS, Ferris MT, Frelinger JA, Heise M, Frieman MB, Gralinski LE, Bell TA, Didion JD, Hua K, Nehrenberg DL, Powell CL, Steigerwalt J, Xie Y, Kelada SNP, Collins FS, Yang IV, Schwartz DA, Branstetter LA, Chesler EJ, Miller DR, Spence J, Liu EY, McMillan L, Sarkar A, Wang J, Wang W, Zhang Q, Broman KW, Korstanje R, Durrant C, Mott R, Iraqi FA, Pomp D, Threadgill D, de Villena FP-M, Churchill GA.** 2011. Genetic analysis of complex traits in the emerging Collaborative Cross. *Genome Research* **21**:1213-1222.
116. **Gralinski LE, Menachery VD, Morgan AP, Tatura AL, Beall A, Kocher J, Plante J, Harrison-Shostak DC, Schäfer A, Pardo-Manuel de Villena F, Ferris MT, Baric RS.** 2017. Allelic Variation in the Toll-Like Receptor Adaptor Protein Ticam2 Contributes to SARS-Coronavirus Pathogenesis in Mice. *G3 (Bethesda, Md)* **7**:1653-1663.
117. **Gralinski LE, Ferris MT, Aylor DL, Whitmore AC, Green R, Frieman MB, Deming D, Menachery VD, Miller DR, Buus RJ, Bell TA, Churchill GA, Threadgill DW, Katze MG, McMillan L, Valdar W, Heise MT, Pardo-Manuel de Villena F, Baric RS.** 2015. Genome Wide Identification of SARS-CoV Susceptibility Loci Using the Collaborative Cross. *PLoS genetics* **11**:e1005504.
118. **Frieman M, Yount B, Agnihothram S, Page C, Donaldson E, Roberts A, Vogel L, Woodruff B, Scorpio D, Subbarao K, Baric RS.** 2012. Molecular determinants of severe acute respiratory syndrome coronavirus pathogenesis and virulence in young and aged mouse models of human disease. *Journal of Virology* **86**:884-897.
119. **Graham RL, Becker MM, Eckerle LD, Bolles M, Denison MR, Baric RS.** 2012. A live, impaired-fidelity coronavirus vaccine protects in an aged, immunocompromised mouse model of lethal disease. *Nature Medicine* **18**:1820-1826.

120. **Baas T, Roberts A, Teal TH, Vogel L, Chen J, Tumpey TM, Katze MG, Subbarao K.** 2008. Genomic analysis reveals age-dependent innate immune responses to severe acute respiratory syndrome coronavirus. *Journal of Virology* **82**:9465-9476.
121. **Liu M, Liang W-N, Chen Q, Xie X-Q, Wu J, He X, Liu Z-J.** 2006. Risk factors for SARS-related deaths in 2003, Beijing. *Biomedical and environmental sciences: BES* **19**:336-339.
122. **Haq K, McElhaney JE.** 2014. Ageing and respiratory infections: the airway of ageing. *Immunol Lett* **162**:323-328.
123. **Baylis D, Bartlett DB, Patel HP, Roberts HC.** 2013. Understanding how we age: insights into inflammaging. *Longev Healthspan* **2**:8.
124. **Lee N, Shin MS, Kang I.** 2012. T-cell biology in aging, with a focus on lung disease. *J Gerontol A Biol Sci Med Sci* **67**:254-263.
125. **Bolles M, Deming D, Long K, Agnihothram S, Whitmore A, Ferris M, Funkhouser W, Gralinski L, Totura A, Heise M, Baric RS.** 2011. A double-inactivated severe acute respiratory syndrome coronavirus vaccine provides incomplete protection in mice and induces increased eosinophilic proinflammatory pulmonary response upon challenge. *J Virol* **85**:12201-12215.
126. **Moni MA, Liò P.** 2014. Network-based analysis of comorbidities risk during an infection: SARS and HIV case studies. *BMC Bioinformatics* **15**.
127. **Hui DS, Memish ZA, Zumla A.** 2014. Severe acute respiratory syndrome vs. the Middle East respiratory syndrome. *Current Opinion in Pulmonary Medicine* **20**:233-241.
128. **Badawi A, Ryoo SG.** 2016. Prevalence of comorbidities in the Middle East respiratory syndrome coronavirus (MERS-CoV): a systematic review and meta-analysis. *International journal of infectious diseases: IJID: official publication of the International Society for Infectious Diseases* **49**:129-133.
129. **Assiri A, McGeer A, Perl TM, Price CS, Al Rabeeah AA, Cummings DAT, Alabdullatif ZN, Assad M, Almulhim A, Makhdoom H, Madani H, Alhakeem R, Al-Tawfiq JA, Cotten M, Watson SJ, Kellam P, Zumla AI, Memish ZA.** 2013. Hospital Outbreak of Middle East Respiratory Syndrome Coronavirus. *New England Journal of Medicine* **369**:407-416.
130. **Assiri A, Al-Tawfiq JA, Al-Rabeeah AA, Al-Rabiah FA, Al-Hajjar S, Al-Barrak A, Flemban H, Al-Nassir WN, Balkhy HH, Al-Hakeem RF, Makhdoom HQ, Zumla AI, Memish ZA.** 2013. Epidemiological, demographic, and clinical characteristics of 47 cases of Middle East respiratory syndrome coronavirus disease from Saudi Arabia: a descriptive study. *The Lancet Infectious Diseases* **13**:752-761.
131. **Al-Tawfiq JA, Hinedi K, Ghandour J, Khairalla H, Musleh S, Ujayli A, Memish ZA.** 2014. Middle East Respiratory Syndrome Coronavirus: A Case-Control Study of Hospitalized Patients. *Clinical Infectious Diseases* **59**:160-165.
132. **Alqarni SSM.** 2016. A Review of Prevalence of Obesity in Saudi Arabia. *Journal of Obesity & Eating Disorders* **2**.
133. **Almond MH, Edwards MR, Barclay WS, Johnston SL.** 2013. Obesity and susceptibility to severe outcomes following respiratory viral infection. *Thorax* **68**:684-686.

134. **Zhang AJ, To KK, Li C, Lau CC, Poon VK, Chan CC, Zheng BJ, Hung IF, Lam KS, Xu A, Yuen KY.** 2013. Leptin mediates the pathogenesis of severe 2009 pandemic influenza A(H1N1) infection associated with cytokine dysregulation in mice with diet-induced obesity. *J Infect Dis* **207**:1270-1280.
135. **Milner JJ, Beck MA.** 2012. The impact of obesity on the immune response to infection. *The Proceedings of the Nutrition Society* **71**:298-306.
136. **Smith AG, Sheridan PA, Harp JB, Beck MA.** 2007. Diet-Induced Obese Mice Have Increased Mortality and Altered Immune Responses When Infected with Influenza Virus. *The Journal of Nutrition* **137**:1236-1243.
137. **Cocoros NM, Lash TL, DeMaria A, Jr., Klompas M.** 2014. Obesity as a risk factor for severe influenza-like illness. *Influenza Other Respir Viruses* **8**:25-32.
138. **Charland KM, Buckeridge DL, Hoen AG, Berry JG, Elixhauser A, Melton F, Brownstein JS.** 2013. Relationship between community prevalence of obesity and associated behavioral factors and community rates of influenza-related hospitalizations in the United States. *Influenza Other Respir Viruses* **7**:718-728.
139. **O'Brien KB, Vogel P, Duan S, Govorkova EA, Webby RJ, McCullers JA, Schultz-Cherry S.** 2012. Impaired wound healing predisposes obese mice to severe influenza virus infection. *J Infect Dis* **205**:252-261.
140. **Milner JJ, Rebeles J, Dhungana S, Stewart DA, Sumner SC, Meyers MH, Mancuso P, Beck MA.** 2015. Obesity Increases Mortality and Modulates the Lung Metabolome during Pandemic H1N1 Influenza Virus Infection in Mice. *J Immunol* **194**:4846-4859.
141. **Berry M, Gamielidien J, Fielding BC.** 2015. Identification of new respiratory viruses in the new millennium. *Viruses* **7**:996-1019.
142. **Stevenson GW, Hoang H, Schwartz KJ, Burrough ER, Sun D, Madson D, Cooper VL, Pillatzki A, Gauger P, Schmitt BJ, Koster LG, Killian ML, Yoon KJ.** 2013. Emergence of Porcine epidemic diarrhea virus in the United States: clinical signs, lesions, and viral genomic sequences. *Journal of Veterinary Diagnostic Investigation: Official Publication of the American Association of Veterinary Laboratory Diagnosticians, Inc* **25**:649-654.
143. **Madson DM, Magstadt DR, Arruda PHE, Hoang H, Sun D, Bower LP, Bhandari M, Burrough ER, Gauger PC, Pillatzki AE, Stevenson GW, Wilberts BL, Brodie J, Harmon KM, Wang C, Main RG, Zhang J, Yoon KJ.** 2014. Pathogenesis of porcine epidemic diarrhea virus isolate (US/Iowa/18984/2013) in 3-week-old weaned pigs. *Veterinary Microbiology* **174**:60-68.
144. **Jung K, Annamalai T, Lu Z, Saif LJ.** 2015. Comparative pathogenesis of US porcine epidemic diarrhea virus (PEDV) strain PC21A in conventional 9-day-old nursing piglets vs. 26-day-old weaned pigs. *Veterinary Microbiology* **178**:31-40.
145. **Ma Y, Zhang Y, Liang X, Lou F, Oglesbee M, Krakowka S, Li J.** 2015. Origin, evolution, and virulence of porcine deltacoronaviruses in the United States. *MBio* **6**:e00064.
146. **Thimmasandra Narayanappa A, Sooryanarain H, Deventhiran J, Cao D, Ammayappan Venkatachalam B, Kambiranda D, LeRoith T, Heffron CL, Lindstrom N, Hall K, Jobst P, Sexton C, Meng XJ, Elankumaran S.** 2015. A novel pathogenic Mammalian orthoreovirus from diarrhetic pigs and Swine blood meal in the United States. *MBio* **6**:e00593-00515.

147. **Abdul-Rasool S, Fielding BC.** 2010. Understanding Human Coronavirus HCoV-NL63. *Open Virol J* **4**:76-84.
148. **Song D, Park B.** 2012. Porcine epidemic diarrhoea virus: a comprehensive review of molecular epidemiology, diagnosis, and vaccines. *Virus Genes* **44**:167-175.
149. **Sun R-Q, Cai R-J, Chen Y-Q, Liang P-S, Chen D-K, Song C-X.** 2012. Outbreak of porcine epidemic diarrhea in suckling piglets, China. *Emerging Infectious Diseases* **18**:161-163.
150. **Huang Y-W, Dickerman AW, Piñeyro P, Li L, Fang L, Kiehne R, Opriessnig T, Meng X-J.** 2013. Origin, evolution, and genotyping of emergent porcine epidemic diarrhea virus strains in the United States. *mBio* **4**:e00737-00713.
151. **Lin C-N, Chung W-B, Chang S-W, Wen C-C, Liu H, Chien C-H, Chiou M-T.** 2014. US-like strain of porcine epidemic diarrhea virus outbreaks in Taiwan, 2013-2014. *The Journal of Veterinary Medical Science / the Japanese Society of Veterinary Science* **76**:1297-1299.
152. **Song D, Moon H, Kang B.** 2015. Porcine epidemic diarrhea: a review of current epidemiology and available vaccines. *Clin Exp Vaccine Res* **4**:166-176.
153. **Liu C, Tang J, Ma Y, Liang X, Yang Y, Peng G, Qi Q, Jiang S, Li J, Du L, Li F.** 2015. Receptor usage and cell entry of porcine epidemic diarrhea coronavirus. *J Virol* **89**:6121-6125.
154. **Huan C-c, Wang Y, Ni B, Wang R, Huang L, Ren X-f, Tong G-z, Ding C, Fan H-j, Mao X.** 2015. Porcine epidemic diarrhea virus uses cell-surface heparan sulfate as an attachment factor. *Archives of Virology* **160**:1621-1628.
155. **Duarte M, Gelfi J, Lambert P, Rasschaert D, Laude H.** 1993. Genome organization of porcine epidemic diarrhoea virus. *Advances in Experimental Medicine and Biology* **342**:55-60.
156. **Sato T, Takeyama N, Katsumata A, Tuchiya K, Kodama T, Kusanagi K-i.** 2011. Mutations in the spike gene of porcine epidemic diarrhea virus associated with growth adaptation in vitro and attenuation of virulence in vivo. *Virus Genes* **43**:72-78.
157. **Park J-E, Cruz DJM, Shin H-J.** 2011. Receptor-bound porcine epidemic diarrhea virus spike protein cleaved by trypsin induces membrane fusion. *Archives of Virology* **156**:1749-1756.
158. **Xu X, Zhang H, Zhang Q, Dong J, Liang Y, Huang Y, Liu H-J, Tong D.** 2013. Porcine epidemic diarrhea virus E protein causes endoplasmic reticulum stress and up-regulates interleukin-8 expression. *Virology Journal* **10**:26.
159. **Xu X, Zhang H, Zhang Q, Huang Y, Dong J, Liang Y, Liu H-J, Tong D.** 2013. Porcine epidemic diarrhea virus N protein prolongs S-phase cell cycle, induces endoplasmic reticulum stress, and up-regulates interleukin-8 expression. *Veterinary Microbiology* **164**:212-221.
160. **Kocherhans R, Bridgen A, Ackermann M, Tobler K.** 2001. Completion of the porcine epidemic diarrhoea coronavirus (PEDV) genome sequence. *Virus Genes* **23**:137-144.
161. **Wang K, Lu W, Chen J, Xie S, Shi H, Hsu H, Yu W, Xu K, Bian C, Fischer WB, Schwarz W, Feng L, Sun B.** 2012. PEDV ORF3 encodes an ion channel protein and regulates virus production. *FEBS letters* **586**:384-391.
162. **Li C, Li Z, Zou Y, Wicht O, van Kuppeveld FJM, Rottier PJM, Bosch BJ.** 2013. Manipulation of the porcine epidemic diarrhea virus genome using targeted RNA recombination. *PLoS One* **8**:e69997.

163. **Oka T, Saif LJ, Marthaler D, Esseili MA, Meulia T, Lin C-M, Vlasova AN, Jung K, Zhang Y, Wang Q.** 2014. Cell culture isolation and sequence analysis of genetically diverse US porcine epidemic diarrhea virus strains including a novel strain with a large deletion in the spike gene. *Veterinary Microbiology* **173**:258-269.
164. **Renukaradhya GJ, Meng X-J, Calvert JG, Roof M, Lager KM.** 2015. Live porcine reproductive and respiratory syndrome virus vaccines: Current status and future direction. *Vaccine* **33**:4069-4080.
165. **Schwegmann-Wessels C, Herrler G.** 2006. Transmissible gastroenteritis virus infection: a vanishing specter. *Dtsch Tierarztl Wochenschr* **113**:157-159.
166. **Pensaert M.** 1990. Background paper. The appearance of the porcine respiratory coronavirus has created new problems and perspectives. *Adv Exp Med Biol* **276**:419-420.
167. **Wang L, Byrum B, Zhang Y.** 2014. Detection and genetic characterization of deltacoronavirus in pigs, Ohio, USA, 2014. *Emerging Infectious Diseases* **20**:1227-1230.
168. **Jengarn J, Wongthida P, Wanasen N, Frantz PN, Wanitchang A, Jongkaewwattana A.** 2015. Genetic manipulation of porcine epidemic diarrhea virus (PEDV) recovered from a full-length infectious cDNA clone. *J Gen Virol* doi:10.1099/vir.0.000184.
169. **Herfst S, Imai M, Kawaoka Y, Fouchier RA.** 2014. Avian influenza virus transmission to mammals. *Curr Top Microbiol Immunol* **385**:137-155.
170. **Liu L, Lear Z, Hughes DJ, Wu W, Zhou EM, Whitehouse A, Chen H, Hiscox JA.** 2015. Resolution of the cellular proteome of the nucleocapsid protein from a highly pathogenic isolate of porcine reproductive and respiratory syndrome virus identifies PARP-1 as a cellular target whose interaction is critical for virus biology. *Vet Microbiol* **176**:109-119.
171. **USDA-APHIS.** 2014. USDA Licenses First Vaccine for Porcine Epidemic Diarrhea. Service UAaPHI,
172. **Hart MK, Caswell-Stephan K, Bakken R, Tammariello R, Pratt W, Davis N, Johnston RE, Smith J, Steele K.** 2000. Improved mucosal protection against Venezuelan equine encephalitis virus is induced by the molecularly defined, live-attenuated V3526 vaccine candidate. *Vaccine* **18**:3067-3075.
173. **Fine DL, Roberts BA, Teehee ML, Terpening SJ, Kelly CL, Raetz JL, Baker DC, Powers AM, Bowen RA.** 2007. Venezuelan equine encephalitis virus vaccine candidate (V3526) safety, immunogenicity and efficacy in horses. *Vaccine* **25**:1868-1876.
174. **Rao V, Hinz ME, Roberts BA, Fine D.** 2004. Environmental hazard assessment of Venezuelan equine encephalitis virus vaccine candidate strain V3526. *Vaccine* **22**:2667-2673.
175. **Tonkin DR, Whitmore A, Johnston RE, Barro M.** 2012. Infected dendritic cells are sufficient to mediate the adjuvant activity generated by Venezuelan equine encephalitis virus replicon particles. *Vaccine* **30**:4532-4542.
176. **MacDonald GH, Johnston RE.** 2000. Role of dendritic cell targeting in Venezuelan equine encephalitis virus pathogenesis. *J Virol* **74**:914-922.
177. **Zhao J, Li K, Wohlford-Lenane C, Agnihothram SS, Fett C, Zhao J, Gale MJ, Jr., Baric RS, Enjuanes L, Gallagher T, McCray PB, Jr., Perlman S.** 2014. Rapid generation of a mouse model for Middle East respiratory syndrome. *Proc Natl Acad Sci U S A* **111**:4970-4975.

178. **Sheahan T, Whitmore A, Long K, Ferris M, Rockx B, Funkhouser W, Donaldson E, Gralinski L, Collier M, Heise M, Davis N, Johnston R, Baric RS.** 2011. Successful vaccination strategies that protect aged mice from lethal challenge from influenza virus and heterologous severe acute respiratory syndrome coronavirus. *J Virol* **85**:217-230.
179. **Menachery VD, Yount BL, Jr., Josset L, Gralinski LE, Scobey T, Agnihothram S, Katze MG, Baric RS.** 2014. Attenuation and restoration of severe acute respiratory syndrome coronavirus mutant lacking 2'-o-methyltransferase activity. *J Virol* **88**:4251-4264.
180. **Regla-Nava JA, Nieto-Torres JL, Jimenez-Guardeno JM, Fernandez-Delgado R, Fett C, Castano-Rodriguez C, Perlman S, Enjuanes L, DeDiego ML.** 2015. Severe acute respiratory syndrome coronaviruses with mutations in the E protein are attenuated and promising vaccine candidates. *J Virol* **89**:3870-3887.
181. **Graham RL, Baric RS.** 2010. Recombination, reservoirs, and the modular spike: mechanisms of coronavirus cross-species transmission. *J Virol* **84**:3134-3146.
182. **Denison MR, Graham RL, Donaldson EF, Eckerle LD, Baric RS.** 2011. Coronaviruses: an RNA proofreading machine regulates replication fidelity and diversity. *RNA Biol* **8**:270-279.
183. **Gralinski LE, Baric RS.** 2015. Molecular pathology of emerging coronavirus infections. *J Pathol* **235**:185-195.
184. **Jung K, Wang Q, Scheuer KA, Lu Z, Zhang Y, Saif LJ.** 2014. Pathology of US Porcine Epidemic Diarrhea Virus Strain PC21A in Gnotobiotic Pigs. *Emerging Infectious Diseases* **20**:668-671.
185. **Anonymous.** WHO | Update 49 - SARS case fatality ratio, incubation period. Accessed
186. **Cameron MJ, Ran L, Xu L, Danesh A, Bermejo-Martin JF, Cameron CM, Muller MP, Gold WL, Richardson SE, Poutanen SM, Willey BM, DeVries ME, Fang Y, Seneviratne C, Bosinger SE, Persad D, Wilkinson P, Greller LD, Somogyi R, Humar A, Keshavjee S, Louie M, Loeb MB, Brunton J, McGeer AJ, Canadian SRN, Kelvin DJ.** 2007. Interferon-mediated immunopathological events are associated with atypical innate and adaptive immune responses in patients with severe acute respiratory syndrome. *J Virol* **81**:8692-8706.
187. **Chan KH, Poon LL, Cheng VC, Guan Y, Hung IF, Kong J, Yam LY, Seto WH, Yuen KY, Peiris JS.** 2004. Detection of SARS coronavirus in patients with suspected SARS. *Emerg Infect Dis* **10**:294-299.
188. **Frieman M, Baric R.** 2008. Mechanisms of severe acute respiratory syndrome pathogenesis and innate immunomodulation. *Microbiol Mol Biol Rev* **72**:672-685, Table of Contents.
189. **Frieman M, Ratia K, Johnston RE, Mesecar AD, Baric RS.** 2009. Severe acute respiratory syndrome coronavirus papain-like protease ubiquitin-like domain and catalytic domain regulate antagonism of IRF3 and NF-kappaB signaling. *J Virol* **83**:6689-6705.
190. **Frieman M, Yount B, Heise M, Kopecky-Bromberg SA, Palese P, Baric RS.** 2007. Severe acute respiratory syndrome coronavirus ORF6 antagonizes STAT1 function by sequestering nuclear import factors on the rough endoplasmic reticulum/Golgi membrane. *J Virol* **81**:9812-9824.
191. **Rockx B, Baas T, Zornetzer GA, Haagmans B, Sheahan T, Frieman M, Dyer MD, Teal TH, Proll S, van den Brand J, Baric R, Katze MG.** 2009. Early upregulation of acute respiratory distress

- syndrome-associated cytokines promotes lethal disease in an aged-mouse model of severe acute respiratory syndrome coronavirus infection. *J Virol* **83**:7062-7074.
192. **Totura AL, Baric RS.** 2012. SARS coronavirus pathogenesis: host innate immune responses and viral antagonism of interferon. *Curr Opin Virol* **2**:264-275.
 193. **Venkataraman T, Coleman CM, Frieman MB.** 2017. Overactive Epidermal Growth Factor Receptor Signaling Leads to Increased Fibrosis after Severe Acute Respiratory Syndrome Coronavirus Infection. *J Virol* **91**.
 194. **Nie Y, Wang G, Shi X, Zhang H, Qiu Y, He Z, Wang W, Lian G, Yin X, Du L, Ren L, Wang J, He X, Li T, Deng H, Ding M.** 2004. Neutralizing antibodies in patients with severe acute respiratory syndrome-associated coronavirus infection. *J Infect Dis* **190**:1119-1126.
 195. **Zhu Z, Chakraborti S, He Y, Roberts A, Sheahan T, Xiao X, Hensley LE, Prabakaran P, Rockx B, Sidorov IA, Corti D, Vogel L, Feng Y, Kim JO, Wang LF, Baric R, Lanzavecchia A, Curtis KM, Nabel GJ, Subbarao K, Jiang S, Dimitrov DS.** 2007. Potent cross-reactive neutralization of SARS coronavirus isolates by human monoclonal antibodies. *Proc Natl Acad Sci U S A* **104**:12123-12128.
 196. **Tang F, Quan Y, Xin ZT, Wrammert J, Ma MJ, Lv H, Wang TB, Yang H, Richardus JH, Liu W, Cao WC.** 2011. Lack of peripheral memory B cell responses in recovered patients with severe acute respiratory syndrome: a six-year follow-up study. *J Immunol* **186**:7264-7268.
 197. **Rockx B, Corti D, Donaldson E, Sheahan T, Stadler K, Lanzavecchia A, Baric R.** 2008. Structural basis for potent cross-neutralizing human monoclonal antibody protection against lethal human and zoonotic severe acute respiratory syndrome coronavirus challenge. *J Virol* **82**:3220-3235.
 198. **Menachery VD, Yount BL, Jr., Debbink K, Agnihothram S, Gralinski LE, Plante JA, Graham RL, Scobey T, Ge XY, Donaldson EF, Randell SH, Lanzavecchia A, Marasco WA, Shi ZL, Baric RS.** 2015. A SARS-like cluster of circulating bat coronaviruses shows potential for human emergence. *Nat Med* **21**:1508-1513.
 199. **Menachery VD, Yount BL, Jr., Sims AC, Debbink K, Agnihothram SS, Gralinski LE, Graham RL, Scobey T, Plante JA, Royal SR, Swanstrom J, Sheahan TP, Pickles RJ, Corti D, Randell SH, Lanzavecchia A, Marasco WA, Baric RS.** 2016. SARS-like WIV1-CoV poised for human emergence. *Proc Natl Acad Sci U S A* **113**:3048-3053.
 200. **Yeh K-M, Chiueh T-S, Siu LK, Lin J-C, Chan PKS, Peng M-Y, Wan H-L, Chen J-H, Hu B-S, Perng C-L, Lu J-J, Chang F-Y.** 2005. Experience of using convalescent plasma for severe acute respiratory syndrome among healthcare workers in a Taiwan hospital. *Journal of Antimicrobial Chemotherapy* **56**:919-922.
 201. **Gralinski LE, Bankhead A, 3rd, Jeng S, Menachery VD, Proll S, Belisle SE, Matzke M, Webb-Robertson BJ, Luna ML, Shukla AK, Ferris MT, Bolles M, Chang J, Aicher L, Waters KM, Smith RD, Metz TO, Law GL, Katze MG, McWeeney S, Baric RS.** 2013. Mechanisms of severe acute respiratory syndrome coronavirus-induced acute lung injury. *MBio* **4**.
 202. **Clarke SR, Barnden M, Kurts C, Carbone FR, Miller JF, Heath WR.** 2000. Characterization of the ovalbumin-specific TCR transgenic line OT-I: MHC elements for positive and negative selection. *Immunol Cell Biol* **78**:110-117.
 203. **Crotty S.** 2015. A brief history of T cell help to B cells. *Nat Rev Immunol* **15**:185-189.

204. **Topham DJ, Doherty PC.** 1998. Clearance of an influenza A virus by CD4+ T cells is inefficient in the absence of B cells. *J Virol* **72**:882-885.
205. **Prince HE, Lape-Nixon M.** 2014. Role of cytomegalovirus (CMV) IgG avidity testing in diagnosing primary CMV infection during pregnancy. *Clin Vaccine Immunol* **21**:1377-1384.
206. **Menachery VD, Baric RS.** 2013. Bugs in the system. *Immunol Rev* **255**:256-274.
207. **Menachery VD, Einfeld AJ, Schafer A, Josset L, Sims AC, Proll S, Fan S, Li C, Neumann G, Tilton SC, Chang J, Gralinski LE, Long C, Green R, Williams CM, Weiss J, Matzke MM, Webb-Robertson BJ, Schepmoes AA, Shukla AK, Metz TO, Smith RD, Waters KM, Katze MG, Kawaoka Y, Baric RS.** 2014. Pathogenic influenza viruses and coronaviruses utilize similar and contrasting approaches to control interferon-stimulated gene responses. *MBio* **5**:e01174-01114.
208. **Channappanavar R, Zhao J, Perlman S.** 2014. T cell-mediated immune response to respiratory coronaviruses. *Immunologic Research* **59**:118-128.
209. **Khanolkar A, Hartwig SM, Haag BA, Meyerholz DK, Epping LL, Haring JS, Varga SM, Harty JT.** 2009. Protective and pathologic roles of the immune response to mouse hepatitis virus type 1: implications for severe acute respiratory syndrome. *J Virol* **83**:9258-9272.
210. **Chachu KA, Strong DW, LoBue AD, Wobus CE, Baric RS, Virgin HWt.** 2008. Antibody is critical for the clearance of murine norovirus infection. *J Virol* **82**:6610-6617.
211. **Chachu KA, LoBue AD, Strong DW, Baric RS, Virgin HW.** 2008. Immune mechanisms responsible for vaccination against and clearance of mucosal and lymphatic norovirus infection. *PLoS Pathog* **4**:e1000236.
212. **Hasan M, Polic B, Bralic M, Jonjic S, Rajewsky K.** 2002. Incomplete block of B cell development and immunoglobulin production in mice carrying the muMT mutation on the BALB/c background. *Eur J Immunol* **32**:3463-3471.
213. **Ghosh S, Hoselton SA, Schuh JM.** 2012. mu-chain-deficient mice possess B-1 cells and produce IgG and IgE, but not IgA, following systemic sensitization and inhalational challenge in a fungal asthma model. *J Immunol* **189**:1322-1329.
214. **Armitage RJ, Fanslow WC, Strockbine L, Sato TA, Clifford KN, Macduff BM, Anderson DM, Gimpel SD, Davis-Smith T, Maliszewski CR, et al.** 1992. Molecular and biological characterization of a murine ligand for CD40. *Nature* **357**:80-82.
215. **Nutt SL, Hodgkin PD, Tarlinton DM, Corcoran LM.** 2015. The generation of antibody-secreting plasma cells. *Nat Rev Immunol* **15**:160-171.
216. **Beigel JH, Voell J, Kumar P, Raviprakash K, Wu H, Jiao JA, Sullivan E, Luke T, Davey RT, Jr.** 2018. Safety and tolerability of a novel, polyclonal human anti-MERS coronavirus antibody produced from transchromosomal cattle: a phase 1 randomised, double-blind, single-dose-escalation study. *Lancet Infect Dis* **18**:410-418.
217. **Arabi YM, Hajeer AH, Luke T, Raviprakash K, Balkhy H, Johani S, Al-Dawood A, Al-Qahtani S, Al-Omari A, Al-Hameed F, Hayden FG, Fowler R, Bouchama A, Shindo N, Al-Khairy K, Carson G, Taha Y, Sadat M, Alahmadi M.** 2016. Feasibility of Using Convalescent Plasma Immunotherapy for MERS-CoV Infection, Saudi Arabia. *Emerg Infect Dis* **22**:1554-1561.

218. **Anthony SJ, Gilardi K, Menachery VD, Goldstein T, Ssebide B, Mbabazi R, Navarrete-Macias I, Liang E, Wells H, Hicks A, Petrosov A, Byarugaba DK, Debbink K, Dinnon KH, Scobey T, Randell SH, Yount BL, Cranfield M, Johnson CK, Baric RS, Lipkin WI, Mazet JA.** 2017. Further Evidence for Bats as the Evolutionary Source of Middle East Respiratory Syndrome Coronavirus. *MBio* **8**.
219. **Menachery VD, Graham RL, Baric RS.** 2017. Jumping species-a mechanism for coronavirus persistence and survival. *Curr Opin Virol* **23**:1-7.
220. **Gralinski LE, Sheahan TP, Morrison TE, Menachery VD, Jensen K, Leist SR, Whitmore A, Heise MT, Baric RS.** 2018. Complement Activation Contributes to Severe Acute Respiratory Syndrome Coronavirus Pathogenesis. *MBio* **9**.
221. **Sheahan TP, Sims AC, Graham RL, Menachery VD, Gralinski LE, Case JB, Leist SR, Pirc K, Feng JY, Trantcheva I, Bannister R, Park Y, Babusis D, Clarke MO, Mackman RL, Spahn JE, Palmiotti CA, Siegel D, Ray AS, Cihlar T, Jordan R, Denison MR, Baric RS.** 2017. Broad-spectrum antiviral GS-5734 inhibits both epidemic and zoonotic coronaviruses. *Sci Transl Med* **9**.
222. **Sheahan T, Whitmore A, Long K, Ferris M, Rockx B, Funkhouser W, Donaldson E, Gralinski L, Collier M, Heise M, Davis N, Johnston R, Baric RS.** 2011. Successful vaccination strategies that protect aged mice from lethal challenge from influenza virus and heterologous severe acute respiratory syndrome coronavirus. *Journal of Virology* **85**:217-230.
223. **Organization WH.** WHO | Obesity and overweight. Accessed
224. **ALNohair S.** 2014. Obesity in Gulf Countries. *International Journal of Health Sciences* **8**:79-83.
225. **Cabeça TK, Granato C, Bellei N.** 2013. Epidemiological and clinical features of human coronavirus infections among different subsets of patients. *Influenza and Other Respiratory Viruses* **7**:1040-1047.
226. **Consultation WHOE.** 2004. Appropriate body-mass index for Asian populations and its implications for policy and intervention strategies. *Lancet* **363**:157-163.
227. **Yi SS, Kwon SC, Wyatt L, Islam N, Trinh-Shevrin C.** 2015. Weighing in on the hidden Asian American obesity epidemic. *Prev Med* **73**:6-9.
228. **Karlsson EA, Beck MA.** 2010. The burden of obesity on infectious disease. *Exp Biol Med (Maywood)* **235**:1412-1424.
229. **Stapleton RD, Suratt BT.** 2014. Obesity and nutrition in acute respiratory distress syndrome. *Clin Chest Med* **35**:655-671.
230. **Arena R, Cahalin LP.** 2014. Evaluation of cardiorespiratory fitness and respiratory muscle function in the obese population. *Prog Cardiovasc Dis* **56**:457-464.
231. **Lin CK, Lin CC.** 2012. Work of breathing and respiratory drive in obesity. *Respirology* **17**:402-411.
232. **Mancuso P.** 2013. Obesity and respiratory infections: Does excess adiposity weigh down host defense? *Pulmonary Pharmacology & Therapeutics* **26**:412-419.
233. **Jung SH, Kwon JM, Shim JW, Kim DS, Jung HL, Park MS, Park SH, Lee J, Lee WY, Shim JY.** 2013. Effects of diet-induced mild obesity on airway hyperreactivity and lung inflammation in mice. *Yonsei Med J* **54**:1430-1437.

234. **Calixto M, Lintomen L, Schenka A, Saad M, Zanesco A, Antunes E.** 2010. Obesity enhances eosinophilic inflammation in a murine model of allergic asthma. *British Journal of Pharmacology* **159**:617-625.
235. **Ge XN, Greenberg Y, Hosseinkhani MR, Long EK, Bahaie NS, Rao A, Ha SG, Rao SP, Bernlohr DA, Sriramarao P.** 2013. High-fat diet promotes lung fibrosis and attenuates airway eosinophilia after exposure to cockroach allergen in mice. *Exp Lung Res* **39**:365-378.
236. **Menachery VD, Gralinski LE, Baric RS, Ferris MT.** 2015. New Metrics for Evaluating Viral Respiratory Pathogenesis. *PLoS One* **10**:e0131451.
237. **Waalén J.** 2014. The genetics of human obesity. *Transl Res* **164**:293-301.
238. **Zhang Y, Li J, Zhan Y, Wu L, Yu X, Zhang W, Ye L, Xu S, Sun R, Wang Y, Lou J.** 2004. Analysis of serum cytokines in patients with severe acute respiratory syndrome. *Infect Immun* **72**:4410-4415.
239. **Nikseresht M.** 2017. Comparison of serum cytokine levels in obese and lean men: effects of nonlinear periodized resistance training and obesity. *J Strength Cond Res* doi:10.1519/JSC.0000000000002039.
240. **Ciftci TU, Kakturk O, Bukan N, Bilgihan A.** 2004. The relationship between serum cytokine levels with obesity and obstructive sleep apnea syndrome. *Cytokine* **28**:87-91.
241. **Panee J.** 2012. Monocyte Chemoattractant Protein 1 (MCP-1) in obesity and diabetes. *Cytokine* **60**:1-12.
242. **Channappanavar R, Fehr AR, Vijay R, Mack M, Zhao J, Meyerholz DK, Perlman S.** 2016. Dysregulated Type I Interferon and Inflammatory Monocyte-Macrophage Responses Cause Lethal Pneumonia in SARS-CoV-Infected Mice. *Cell Host Microbe* **19**:181-193.
243. **Page AV, Liles WC.** 2011. Colony-stimulating factors in the prevention and management of infectious diseases. *Infect Dis Clin North Am* **25**:803-817.
244. **Camp JV, Jonsson CB.** 2017. A Role for Neutrophils in Viral Respiratory Disease. *Front Immunol* **8**:550.
245. **Perry AK, Chen G, Zheng D, Tang H, Cheng G.** 2005. The host type I interferon response to viral and bacterial infections. *Cell Research* **15**:407-422.
246. **Wunderlich CM, Hövelmeyer N, Wunderlich FT.** 2013. Mechanisms of chronic JAK-STAT3-SOCS3 signaling in obesity. *JAK-STAT* **2**.
247. **Kopecky-Bromberg SA, Martínez-Sobrido L, Frieman M, Baric RA, Palese P.** 2007. Severe Acute Respiratory Syndrome Coronavirus Open Reading Frame (ORF) 3b, ORF 6, and Nucleocapsid Proteins Function as Interferon Antagonists. *Journal of Virology* **81**:548-557.
248. **Neil R Aggarwal LSK.** 2014. Diverse macrophage populations mediate acute lung inflammation and resolution. *American journal of physiology Lung cellular and molecular physiology* **306**.
249. **Kraakman MJ, Murphy AJ, Jandeleit-Dahm K, Kammoun HL.** 2014. Macrophage Polarization in Obesity and Type 2 Diabetes: Weighing Down Our Understanding of Macrophage Function? *Frontiers in Immunology* **5**.

250. **Lumeng CN, Bodzin JL, Saltiel AR.** 2007. Obesity induces a phenotypic switch in adipose tissue macrophage polarization. *Journal of Clinical Investigation* **117**:175-184.
251. **Liu YC, Zou XB, Chai YF, Yao YM.** 2014. Macrophage polarization in inflammatory diseases. *Int J Biol Sci* **10**:520-529.
252. **Labonte AC, Tosello-Trampont AC, Hahn YS.** 2014. The role of macrophage polarization in infectious and inflammatory diseases. *Mol Cells* **37**:275-285.
253. **Papatriantafyllou M.** 2013. Macrophages: SOCS2 and SOCS3 in macrophage polarization. *Nature Reviews Immunology* **13**:7-7.
254. **de Heredia FP, Gómez-Martínez S, Marcos A.** 2012. Obesity, inflammation and the immune system. *The Proceedings of the Nutrition Society* **71**:332-338.
255. **Fresno M, Alvarez R, Cuesta N.** 2011. Toll-like receptors, inflammation, metabolism and obesity. *Arch Physiol Biochem* **117**:151-164.
256. **Kulcsar KA, Coleman CM, Beck SE, Frieman MB.** 2019. Comorbid diabetes results in immune dysregulation and enhanced disease severity following MERS-CoV infection. *JCI Insight* **4**.
257. **Auyeung TW, Lee JSW, Lai WK, Choi CH, Lee HK, Lee JS, Li PC, Lok KH, Ng YY, Wong WM, Yeung YM.** 2005. The use of corticosteroid as treatment in SARS was associated with adverse outcomes: a retrospective cohort study. *The Journal of Infection* **51**:98-102.
258. **Albuquerque D, Stice E, Rodriguez-Lopez R, Manco L, Nobrega C.** 2015. Current review of genetics of human obesity: from molecular mechanisms to an evolutionary perspective. *Mol Genet Genomics* **290**:1191-1221.
259. **Mao JH, Langley SA, Huang Y, Hang M, Bouchard KE, Celniker SE, Brown JB, Jansson JK, Karpen GH, Snijders AM.** 2015. Identification of genetic factors that modify motor performance and body weight using Collaborative Cross mice. *Sci Rep* **5**:16247.
260. **Atamni HJ, Mott R, Soller M, Iraqi FA.** 2016. High-fat-diet induced development of increased fasting glucose levels and impaired response to intraperitoneal glucose challenge in the collaborative cross mouse genetic reference population. *BMC Genet* **17**:10.
261. **Li J, Jin Z, Gao Y, Zhou L, Ge X, Guo X, Han J, Yang H.** 2017. Development of the full-length cDNA clones of two porcine epidemic diarrhea disease virus isolates with different virulence. *PLoS One* **12**:e0173998.
262. **Jengarn J, Wongthida P, Wanasen N, Frantz PN, Wanitchang A, Jongkaewwattana A.** 2015. Genetic manipulation of porcine epidemic diarrhoea virus recovered from a full-length infectious cDNA clone. *J Gen Virol* **96**:2206-2218.
263. **Fan B, Yu Z, Pang F, Xu X, Zhang B, Guo R, He K, Li B.** 2017. Characterization of a pathogenic full-length cDNA clone of a virulent porcine epidemic diarrhea virus strain AH2012/12 in China. *Virology* **500**:50-61.
264. **Li C, Li Z, Zou Y, Wicht O, van Kuppeveld FJ, Rottier PJ, Bosch BJ.** 2013. Manipulation of the porcine epidemic diarrhea virus genome using targeted RNA recombination. *PLoS One* **8**:e69997.

265. **Hou Y, Lin CM, Yokoyama M, Yount BL, Marthaler D, Douglas AL, Ghimire S, Qin Y, Baric RS, Saif LJ, Wang Q.** 2017. Deletion of a 197-Amino-Acid Region in the N-Terminal Domain of Spike Protein Attenuates Porcine Epidemic Diarrhea Virus in Piglets. *J Virol* **91**.
266. **Zhang Q, Liu X, Fang Y, Zhou P, Wang Y, Zhang Y.** 2017. Detection and phylogenetic analyses of spike genes in porcine epidemic diarrhea virus strains circulating in China in 2016-2017. *Virology* **14**:194.
267. **Zhao Y, Wang C, Qiu B, Li C, Wang H, Jin H, Gai W, Zheng X, Wang T, Sun W, Yan F, Gao Y, Wang Q, Yan J, Chen L, Perlman S, Zhong N, Zhao J, Yang S, Xia X.** 2017. Passive immunotherapy for Middle East Respiratory Syndrome coronavirus infection with equine immunoglobulin or immunoglobulin fragments in a mouse model. *Antiviral Research* **137**:125-130.
268. **Scherba G BC, Jarrell VL, et al.** Evaluation of responses to both oral and parenteral immunization modalities for porcine epidemic diarrhea virus in production units. *J Swine Health Prod.* **2016;24(1):29–35**.
269. **de Aquino MT, Puntambekar SS, Savarin C, Bergmann CC, Phares TW, Hinton DR, Stohlman SA.** 2013. Role of CD25(+) CD4(+) T cells in acute and persistent coronavirus infection of the central nervous system. *Virology* **447**:112-120.
270. **Heyman B.** 2000. Regulation of antibody responses via antibodies, complement, and Fc receptors. *Annual Review of Immunology* **18**:709-737.
271. **Hosono M, Muramatsu S.** 1972. Use of 2-Mercaptoethanol for Distinguishing Between IgM and IgG Antibody-Producing Cells of Mice Immunized with Bovine γ Globulin. *The Journal of Immunology* **109**:857-863.
272. **Subbarao K, McAuliffe J, Vogel L, Fahle G, Fischer S, Tatti K, Packard M, Shieh WJ, Zaki S, Murphy B.** 2004. Prior infection and passive transfer of neutralizing antibody prevent replication of severe acute respiratory syndrome coronavirus in the respiratory tract of mice. *J Virol* **78**:3572-3577.
273. **Roberts A, Thomas WD, Guarner J, Lamirande EW, Babcock GJ, Greenough TC, Vogel L, Hayes N, Sullivan JL, Zaki S, Subbarao K, Ambrosino DM.** 2006. Therapy with a severe acute respiratory syndrome-associated coronavirus-neutralizing human monoclonal antibody reduces disease severity and viral burden in golden Syrian hamsters. *J Infect Dis* **193**:685-692.
274. **Rockx B, Donaldson E, Frieman M, Sheahan T, Corti D, Lanzavecchia A, Baric RS.** 2010. Escape from human monoclonal antibody neutralization affects in vitro and in vivo fitness of severe acute respiratory syndrome coronavirus. *J Infect Dis* **201**:946-955.
275. **ter Meulen J, van den Brink EN, Poon LL, Marissen WE, Leung CS, Cox F, Cheung CY, Bakker AQ, Bogaards JA, van Deventer E, Preiser W, Doerr HW, Chow VT, de Kruif J, Peiris JS, Goudsmit J.** 2006. Human monoclonal antibody combination against SARS coronavirus: synergy and coverage of escape mutants. *PLoS Med* **3**:e237.
276. **Gardner CL, Sun C, Luke T, Raviprakash K, Wu H, Jiao JA, Sullivan E, Reed DS, Ryman KD, Klimstra WB.** 2017. Antibody Preparations from Human Transchromosomal Cows Exhibit Prophylactic and Therapeutic Efficacy against Venezuelan Equine Encephalitis Virus. *J Virol* **91**.

277. **Casadevall A, Pirofski LA.** 2005. The potential of antibody-mediated immunity in the defence against biological weapons. *Expert Opin Biol Ther* **5**:1359-1372.
278. **Luke TC, Casadevall A, Watowich SJ, Hoffman SL, Beigel JH, Burgess TH.** 2010. Hark back: passive immunotherapy for influenza and other serious infections. *Crit Care Med* **38**:e66-73.
279. **Beigel JH.** 2018. Polyclonal and monoclonal antibodies for the treatment of influenza. *Curr Opin Infect Dis* **31**:527-534.
280. **Calabro P, Yeh ET.** 2007. Obesity, inflammation, and vascular disease: the role of the adipose tissue as an endocrine organ. *Subcell Biochem* **42**:63-91.
281. **Konter J, Baez E, Summer RS.** 2013. Obesity: "priming" the lung for injury. *Pulm Pharmacol Ther* **26**:427-429.